EFFECT OF THE SURFACE PROPERTIES ON BACTERIAL ADHESION AND NOVEL APPROACHES FOR PREVENTION

A Dissertation

by

JUN KYUN OH

Submitted to the Office of Graduate and Professional Studies of
Texas A&M University
in partial fulfillment of the requirements for the degree of

DOCTOR OF PHILOSOPHY

Chair of Committee,	Mustafa Akbulut
Co-Chair of Committee,	Luis Cisneros-Zevallos
Committee Members,	Zhengdong Cheng
	Mike McShane
Head of Department,	Ibrahim Karaman

December 2016

Major Subject: Materials Science and Engineering

ABSTRACT

The aim of this research was to investigate the potential of silica-based surface modification methods to prevent bacterial attachment to material surfaces. This dissertation presents the sol-gel method, reactive-ion etching (RIE) method, and dip-coating method to fabricate bacteria repelling hygienic materials.

The bacterial antiadhesion properties of hydrophobically-modified silica aerogels, with other distinctive characteristics including superior thermal insulation and ultra-light weight, make these aerogels attractive candidates for novel food-contact surfaces to improve food safety. Moreover, healthcare-associated infections (HAIs) caused by pathogenic bacteria are a worldwide problem and are responsible for numerous cases of morbidity and mortality. Findings from the study also showed that hydrophobic nanoporous silica aerogel (HNSA) has potential as an antiadhesive hygienic material that can inhibit exogenous bacterial contamination. The results suggest that the use of HNSA as surfaces that come into contact with bacterial pathogens in the healthcare environment can improve bacterial hygiene, and therefore, may reduce the rate of HAIs.

Because of the growing prevalence of antimicrobial-resistant strains, there is an increasing need to develop material surfaces that prevent bacteria in the absence of antibiotic agents. Herein, we present a self-masking reactive-ion etching (SM-RIE) approach for bacterial antiadhesive “rice leaf-like surfaces” (RLLS). RLLS surfaces showed exceptional bacterial antiadhesion properties with a >99.9% adhesion inhibition efficiency, as well as demonstrated optical-grade transparency (i.e., ≥92% transmission).

We anticipate that the combination of bacterial antiadhesion efficiency, optical-grade transparency, and convenient single-step method of preparation makes RLLS a very attractive candidate surface for biosensors, endoscopes, microfluidic and bio-optical instruments, lab-on-a-chip, and touchscreen devices.

Gloves made of materials such as latex, nitrile, and polyethylene are the most common types of protective equipment used to prevent cross-contamination and transmission of pathogenic bacteria in the food industry. In this study, we report a surface modification by dip-coating method involving “fluorinated silica nanoparticles” (FSNs) to improve the protective ability against bacterial contamination of disposable glove surfaces. The bacterial populations on FSN-coated latex, nitrile and polyethylene gloves was reduced by 1–2 log units in comparison to bare gloves, which already reduce the bacterial attachment to some extent.

DEDICATION

This dissertation is dedicated to my parents, Dr. Hee Mock Oh and Mrs. Sam Yeon Cho.

ACKNOWLEDGEMENTS

First of all, I would like to thank my advisor, Dr. Mustafa Akbulut, whose guidance, patience, and encouragement are invaluable. He has been an amazing mentor to me and I am grateful for the many opportunities he provided. I would also like to thank my co-advisor, Dr. Luis Cisneros-Zevallos, for his advice and support throughout the course of my studies. Sincere thanks to my committee members, Dr. Zhengdong Cheng and Dr. Mike McShane, for their kind and generous support.

I extend my heartfelt thanks to my current and former colleagues in Dr. Mustafa Akbulut's research group. Additionally, I would like to thank the staff of the Materials Characterization Facility (MCF) at Texas A&M University.

Special thanks to the following funding sources that made my research possible: the Agriculture and Food Research Initiative (AFRI) (Grant No. 2011-67017-30028) from the National Institute of Food and Agriculture (NIFA) of the United States Department of Agriculture (USDA), and the National Science Foundation (NSF) (Grant No. 1434421).

Finally, I would like to thank my father and mother for their unconditional love and support throughout the course of my academic career.

NOMENCLATURE

AFM	Atomic force microscopy
AMR	Antimicrobial resistance
ANOVA	Analysis of variance
ATCC	American Type Culture Collection
ATR-FTIR	Attenuated total reflection-Fourier transform infrared
BET	Brunauer-Emmett-Teller
BJH	Barret-Joyner-Halenda
CDC	Centers for Disease Control and Prevention
CFU	Colony-forming unit
DIC	Differential interference contrast
DLVO	Derjaguin-Landau-Verwey-Overbeek
ECDC	European Centre for Disease Prevention and Control
EPS	Extracellular polymeric substance
FDTS	Trichloro(1H,1H,2H,2H-perfluorooctyl)silane
FSN	Fluorinated silica nanoparticle
GFP	Green fluorescent protein
HAI	Healthcare-associated infection
HNSA	Hydrophobic nanoporous silica aerogel
KOH	Potassium hydroxide
LBADSA	Low-bond axisymmetric drop shape analysis

NIH	National Institutes of Health
PDMS	Polydimethylsiloxane
PEG	Polyethylene glycol
PMMA	Poly(methyl methacrylate)
PTFE	Polytetrafluoroethylene
PVA	Polyvinyl alcohol
QCM-D	Quartz crystal microbalance with dissipation monitoring
RIE	Reactive-ion etching
RLLS	Rice leaf-like surfaces
RMS	Root-mean-square
SAM	Self-assembled monolayer
SEM	Scanning electron microscope
SIMS	Secondary ion mass spectrometry
SM-RIE	Self-masking reactive-ion etching
TMCS	Trimethylsilyl chloride
TSA	Tryptic soy agar
TSB	Tryptic soy broth
XPS	X-ray photoelectron spectroscopy

TABLE OF CONTENTS

Page

LIST OF FIGURES

Page

LIST OF TABLES

Page

CHAPTER I

INTRODUCTION

1.1. Objectives

The primary objectives of the proposed work are to generate an enhanced understanding of bacterial adhesion while developing new bacterial antiadhesive materials. As part of this objective, we seek to determine the effect of the surface topography and the effect of surface chemistry on bacterial attachment to material surfaces. For accomplishing this task, we have fabricated materials that can prevent bacterial attachment effectively without generating any antimicrobial activity. Studies of bacterial adhesion behavior are important because of their relevance to human health and diseases. Food safety related bacteria (i.e., *Salmonella* and *Listeria*) and healthcare-associated infections (HAIs) related bacteria (i.e., *Escherichia coli* and *Staphylococcus aureus*) were selected for the studies.

Foodborne disease cases arising from the bacterial cross-contamination of food-contact surfaces and the subsequent cross-contamination of food products represent a significant concern for public health and have emerged as a global challenge.[1] The sources of pathogenic bacteria contaminating food-contact surfaces are typically soil, water, contaminated foods, equipment, animals, humans, and aerosols.[2] *Salmonella* spp., *Escherichia coli* O157:H7, *Listeria monocytogenes, Campylobacter* spp., *Shigella* spp., and *Bacillus cereus* are bacterial pathogens that can exist on food and food-contact surfaces.[3] Currently, there are a number of studies reporting the mechanisms for

interaction of these microorganisms with common materials of food-contact surfaces such as stainless steel, glass, polyethylene, polycarbonate, polyurethane, and polytetrafluoroethylene (PTFE).[4]

Moreover, bacterial contamination is one of the major causes of HAIs. *E. coli*, *S. aureus*, and *Pseudomonas aeruginosa* are known as the most common pathogens involved in hospital infections.[5] The Centers for Disease Control and Prevention (CDC) estimates that there were 721,800 HAIs from all kinds of bacteria in the United States in 2011.[6] The sources of pathogenic bacteria are typically equipment, packaging materials, and storage facilities.[7,8] Hospital supplies and equipment that gets contaminated and is not properly cleaned is a major concern. When bacterial adhesion and subsequent biofilm formation has occurred on a surface, it is difficult to remove microorganisms by post-treatment such as physical washing (e.g., rubbing, brushing, and sonication) and chemical washing (e.g., chlorine-based sanitizer, hydrogen peroxide solution, and alcohol-based disinfectant). One of the main reasons is that microorganisms are protected by extracellular polymeric substances (EPSs), which guard against external physical and chemical attack.[2] Also, it has been reported that pathogenic bacteria can survive on inanimate surfaces for several months.[9] Thus, contaminated surfaces have the ability to transfer microorganisms to equipment resulting in myriad of potential health risks.

Developing bacterial antiadhesive materials are important because of microorganisms that are resistant (i.e., antimicrobial-resistant bacteria and thermo-resistant bacteria) to disinfectants are important issues.[10,11] Also, the integration of bacterial antiadhesion properties and transparency within a single surface is one of the key

challenges. With the increasing number of emerging biomedical applications and optical devices requiring high levels of transparency and operations in bacterial media,[12,13] the need for overcoming this challenge has intensified. The ultimate goal of this research will be to fabricate bacterial antiadhesive materials with optical-grade transparent properties. Therefore, we plan to pursue the following specific aims to meet the demands required for bacterial antiadhesive materials: (i) fabricate nanoporous hydrophobic silica aerogel and compare bacterial adhesion behavior with other silica-based materials,[14,15] (ii) fabricate bioinspired "rice leaf-like surfaces" (RLLS) with bacterial antiadhesion properties and transparency within a single surface,[16] and (iii) develop bacterial antiadhesive dip-coating method involving "fluorinated silica nanoparticles" (FSNs).[17]

1.2. Background and Significance

1.2.1. Influence of Material Surface Physical Properties on Bacterial Adhesion

Many factors such as material properties, biological factors, and environmental factors contribute to bacterial antiadhesion on surfaces. Surface topography related to roughness and porosity can be considered as material properties.[18] Biological factors include, for instance, gene transfer, quorum sensing, cell surface hydrophobicity, and surface charge of cells.[19] Environmental factors include the effect of the pH and temperature. However there are limits to change intrinsic properties, i.e., biological and environmental conditions. Thus, understanding the effect of the surface topography is important to control fouling behavior. It is known that surface roughness and texture can greatly influence bacterial adhesion.[20] Taylor et al.[21] used poly(methyl methacrylate)

(PMMA) surfaces of varying roughness to investigate the effect of the substratum roughness on the adhesion of *Pseudomonas aeruginosa* and *Staphylococcus epidermidis*. They found that for the range of 0.04 μm to 1.24 μm a small increase in roughness resulted in a significant increase in bacterial attachment.

1.2.2. Influence of Material Surface Chemical Properties on Bacterial Adhesion

Hydrophilic materials tend to aggregate on hydrophilic surfaces.[22] While bacteria can adhere on both hydrophobic and hydrophilic surfaces, bacterial attachment tends to occur significantly more on hydrophilic surfaces due to their hydrophilic nature.[23] Therefore, it is necessary to investigate the surface chemistry characteristics of the developed surfaces to gain insight into their bacterial adhesion behaviors. However, most past studies have focused on the effect of the surface properties on the thermodynamical aspects of bacterial adhesion, i.e., experiments were performed under a fixed time period of bacterial exposure. There exists a limited number of studies on the initial behavior and kinetics of bacterial adhesion to surfaces. This is especially important for the situations where the adsorption is not limited by diffusion.

1.2.3. Fabrication of Antifouling Materials: Antimicrobial Approach

Previous work reported surface pre-treatment methods focused on the antimicrobial surface modification. For example, antimicrobial polymer coating and surface functionalization with antibiotic agents are appropriate method to avoid initial contact to prevent bacterial attachment.[24,25] Moreover, a number of studies on mechanisms for interaction of microorganisms with antimicrobial agents and active release of antibiotics facilitate the development of new antifouling materials that can prevent

bacterial attachment effectively.[26] However, using antimicrobial agents involves limitations such as sustainability of antibiotic release over long period,[27] toxicity to human tissues,[28] effectiveness against antimicrobial-resistant bacteria,[10,29] and lower long-term antimicrobial activity.[30] In summary, there is a need to develop antifouling materials that robustly inhibit the attachment of pathogens in the absence of antimicrobial agents.

1.2.4. Fabrication of Antifouling Materials: Antiadhesion Approach

Many studies have shown that bacterial antiadhesion properties of materials have great potential for biological applications. For example, polyethylene glycol (PEG)-based coating and zwitterionic polymer coating to minimize the intermolecular interactions between bacteria and surfaces,[31,32] changing surface properties, i.e., wetting behavior and topography, by using stimuli-responsive polymer materials that response to changes in stimuli such as heat and shear force,[33,34] and surface coating containing heparin as an antiadhesive agent by layer-by-layer assembly.[35] However, the above-mentioned methods are based on nonporous materials, thus, the effect of bacterial adhesion behavior on nanoporous materials has been investigated far less. To design bacterial antiadhesive surfaces more profitably, nanoporous materials can be utilized. This can be achieved by applying concept that repulsive force between bacteria and surfaces can be enhanced by nanoporous structured surfaces.[36]

1.3. Dissertation Outline

This dissertation is divided into seven chapters, including this introduction (Chapter I). Chapter II of this dissertation provides a general overview and relevant

information about the effect of the surface properties on bacterial adhesion. Chapter III describes sol-gel synthesis and functionalization methods to fabricate hydrophobically-modified silica aerogels and its potential application for food safety. Chapter IV describes another competitive advantage of hydrophobically-modified silica aerogels, i.e., nanoporous silica aerogel (HNSA), hygienic surfaces for healthcare-related applications. In Chapter V, by using self-masking reactive-ion etching (SM-RIE) technique, "rice leaf-like surfaces" (RLLS) were fabricated. A synergistic combination of bacterial antiadhesion properties and optical-grade transparency of RLLS are confirmed for a broad set of biomedical applications. Chapter VI describes disposable gloves coated with "fluorinated silica nanoparticles" (FSNs) by dip-coating method. FSN coating provided gloves a superhydrophobic character and demonstrated bacterial antiadhesion properties. Finally, in Chapter VII, the conclusions drawn from this dissertation are presented and possible future work is discussed.

CHAPTER II

EFFECT OF THE SURFACE PROPERTIES ON BACTERIAL ADHESION

2.1. Bacteria Preparation, Inoculation, and Enumeration

2.1.1. Bacterial Growth

Working cultures of *Salmonella enterica* subsp. *enterica* serovar Typhimurium str. LT2, *Escherichia coli* O157:H7, and *Staphylococcus aureus* were obtained by transferring a loopful of culture from tryptic soy agar (TSA) slant to 9.0 mL of tryptic soy broth (TSB) and working cultures of *Listeria innocua* NADC 2841 was obtained by transferring a loopful of culture from a TSA slant containing 0.6% yeast extract to 9.0 mL of TSB containing 0.6% yeast extract. The tubes for all strains were incubated aerobically without agitation at 37 °C for 24 h. After 24 h, a loopful of culture was transferred to fresh TSB (or TSB containing 0.6% yeast extract for *L. innocua*), and incubated aerobically for 24 h at 37 °C twice consecutively. In order to utilize fluorescent microscope for visualization of the microorganisms on the surfaces, *Salmonella enterica* subsp. *enterica* serovar Typhimurium 14028s and enterohemorrhagic *Escherichia coli* O157:H7 str. EDL933 strains were transformed with a green fluorescent protein (GFP) expressing plasmid pCM18.[37] The final concentration reached by all strains in the growth medium ranged from 8.7 to 9.1 log CFU/mL.

2.1.2. Inoculation of Surfaces with Bacteria

For bacterial inoculation purpose under static conditions, samples were immersed in 9.0 mL bacterial suspensions (8.7–9.1 1og CFU/mL), and incubated for 4 h at room

temperature. The treated samples were then gently removed from the bacterial suspensions to count attached bacteria on surfaces. When removing the samples, they were drawn in a single vertical motion from the bacterial suspension and held vertically for 3 min to allow remaining droplets to slide away so that drying effects were not superimposed on the results of adhesion. All inoculation experiments were replicated four times.

For bacterial inoculation purpose under dynamic conditions, flow experiments were carried out using custom flow chamber with 1 cm × 1 cm window made out of the material of interest. Bacterial adhesion behavior on developed window (i.e., RLLS) was compared with pristine quartz window (uncoated) and hydrophobic quartz window (methylated) by replacing chamber window in each experiment. For all surfaces, the flow rate of bacterial suspension inside chamber was controlled to be 2.5 µL/s.

2.1.3. Bacterial Adhesion Assay

SEM was employed to quantify the attachment of bacteria strains on surfaces. To ensure electrical conductivity required by SEM technique, 10 nm of gold coating was applied to sample surfaces. For quantitative analysis, 100 µm × 100 µm of SEM images from at least nine different areas were analyzed to count the number of attached bacteria. Experiments were repeated three times for each sample.

Images of flowing bacteria were visualized using differential interference contrast (DIC) microscopy at a frame rate of 0.5 fps. Movies created by stacking images obtained at various time points were analyzed manually with ImageJ (National Institutes of Health (NIH), Bethesda, MD, USA) software to count attached bacteria on surfaces.

Fluorescent *S.* Typhimurium 14028s and *E. coli* O157:H7 EDL933 strains were

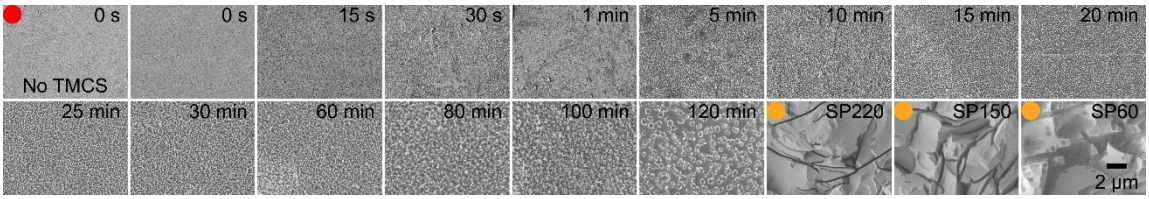

Figure 1. SEM micrographs of 18 different surface roughness of quartz surfaces. Smooth pristine quartz surface (red dot), TMCS-functionalized nanorough quartz surfaces, and TMCS-functionalized microrough quartz surfaces (yellow dot) were present.

determined by using an Axiovert 200M inverted fluorescent microscope. Micrographs obtained with fluorescent microscope were analyzed with ImageJ software.

We also enumerated bacteria on material surfaces by using pour plating method. Briefly, samples inoculated by bacteria were vortex-mixed in sterile water for 10 min to detach bacteria from surfaces. Then, serial dilutions of the suspension containing detached bacteria were made and plated on TSA. Bacterial densities were determined after 24 h of aerobic incubation at 37 °C. The plating experiments were replicated six times.

Screening of antimicrobial activity was carried out to determine if antimicrobial activity or bacterial antiadhesion is responsible for the observed results in each specific study. All strains were grown in the presence of TMCS-functionalized materials and in the presence of 1% (v/v) bleach solution for 4 h at room temperature. Bacteria in the absence of any treatment were used as negative controls. The results are reported as colony-forming units per milliliter (CFU/mL) and replicated least three times.

2.2. Effect of the Surface Topography

2.2.1. Nano/Mircorough Quartz Surfaces

The effect of the nano/microscale roughness on bacterial adhesion behavior were

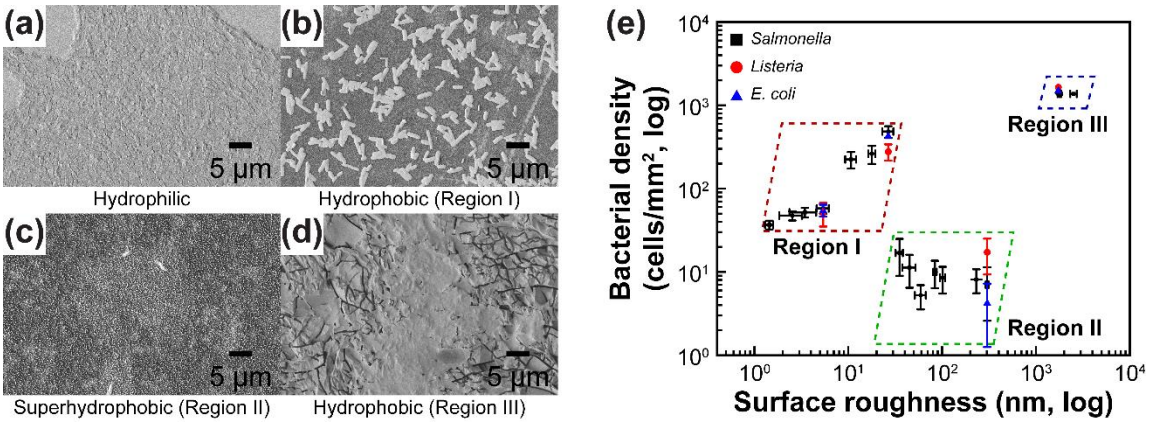

Figure 2. SEM micrographs of (a) pristine quartz surface (hydrophilic), (b) nanorough quartz surface (hydrophobic, region I), (c) nanorough quartz surface (superhydrophobic, region II), and (d) microrough quartz surface (hydrophobic, region III) after inoculated with *S.* Typhimurium LT2. (e) Graph shows the density of attached bacteria on surfaces with different roughness and hydrophobicity (x-axis and y-axis has logarithmic scales).

studied on controlled surfaces with 18 different surface roughness (Figure 1) to distinguish how bacterial attachment decrease or increase on the basis of surface nano/microroughness. For sample preparation, reactive-ion etching (RIE) process using tetrafluoromethane (CF_4)/oxygen (O_2) gas mixture has enabled to fabricate nanoscale precise control of nanorough quartz (SiO_2) surfaces by varying etching time. Microrough quartz surfaces were obtained by surface roughening using different grit size of sandpaper and followed by etching with 30% potassium hydroxide (KOH) solution to remove scraps. In addition, nano/microrough quartz slides were functionalized with trimethylsilyl chloride (TMCS) by placing the slides in solution of 6% TMCS in hexane for 24 h. Surface properties were investigated using attenuated total reflectance-Fourier transform infrared (ATR-FTIR) spectroscopy, X-ray photoelectron spectroscopy (XPS), atomic force microscopy (AFM), and contact angle measurement.

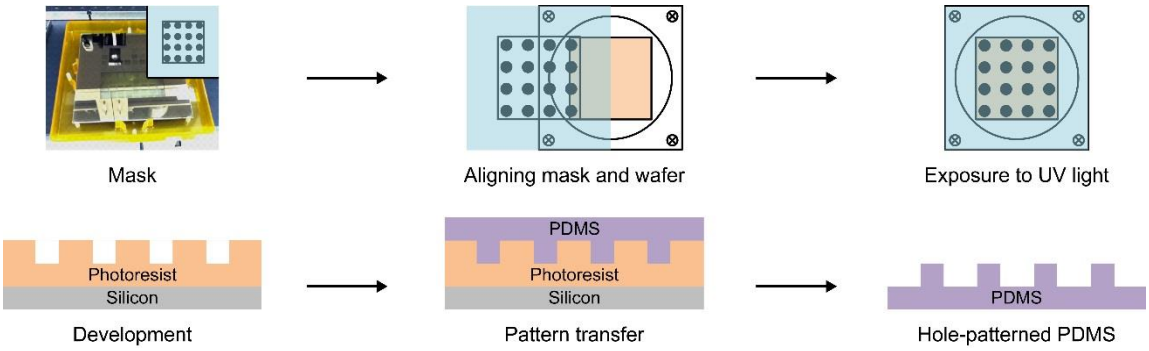

Figure 3. Schematic illustration of photolithography process using photoresist patterns on silicon wafer (stamp) for transferring patterns onto PDMS.

By modifying surface nano/microroughness, we are able to vary contact angle of water on surfaces from 90° to 150° or higher. Comparing 18 different surfaces of roughness within this regime shows full range of nano/microroughness effects on bacteria adhesion, as shown in Figure 2. Results can be explained in two points of view based on previously reported results tendency. Bacteria adhesion increase by microscale hummock and hollow structures on surfaces.[38] On the other hand, mostly decrease on nanoscale roughness surfaces with reducing possibility of bacterial to adhere on wavy surfaces.[39] Until water contact angle reach to plateau state (~150°), behavior follows Wenzel model. In contrast, non-wetting state follows Cassie-Baxter model.[40] Bacteria adhesion increase until roughness reach around 35 nm, which is also critical point to change to superhydrophobic regime. Results show similar trend reported by Singh et al. on titania thin films; bacteria attachment increased as roughness up to 20 nm, decreased above 20 nm.[41] Microbes entrapped on microrough surfaces. Surface topography feature size bigger than bacteria size makes easier to bacteria trapped.

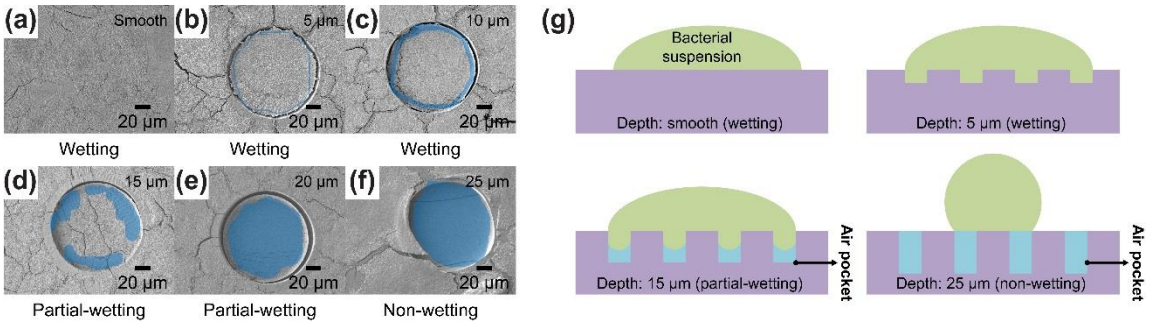

Figure 4. (a)–(f) SEM micrographs of bacteria remain after dry on smooth and hole-patterned PDMS surfaces with different depths (5–25 μm). Empty regions are highlighted with blue. (g) Schematic illustration of three different possible wetting states (i.e., wetting, partial-wetting, and non-wetting) of bacterial suspension associated with air pocket.

2.2.2. Hole-Patterned PDMS Surfaces

Hole-patterned polydimethylsiloxane (PDMS) surfaces with different depth ranges were prepared to study the effect of the trapped air pockets on bacterial adhesion. Photolithography technique was used to make photoresist master to transfer pattern onto PDMS substrates (Figure 3). Thickness of photoresist was controlled by spin coating speed and time, which makes pattern height different after development process. As a result, depth range of 5 μm to 25 μm with diameter of 128 μm and spacing between each pattern of 100 μm patterns were fabricated. Static contact angle of a water droplet was measured to determine wetting characteristics of surfaces. The pattern depth was measured by using stylus contact profilometry.

Surface structure provides air pocket formation, leading to increase in hydrophobicity as air pocket volume increase. Liquid drying effect induced by a passing air-liquid interface. Non-wetting state is proposed by hydrophobic microstructures by gas lubricated surfaces.[42] Also, some researcher find air retained air-grid surface which

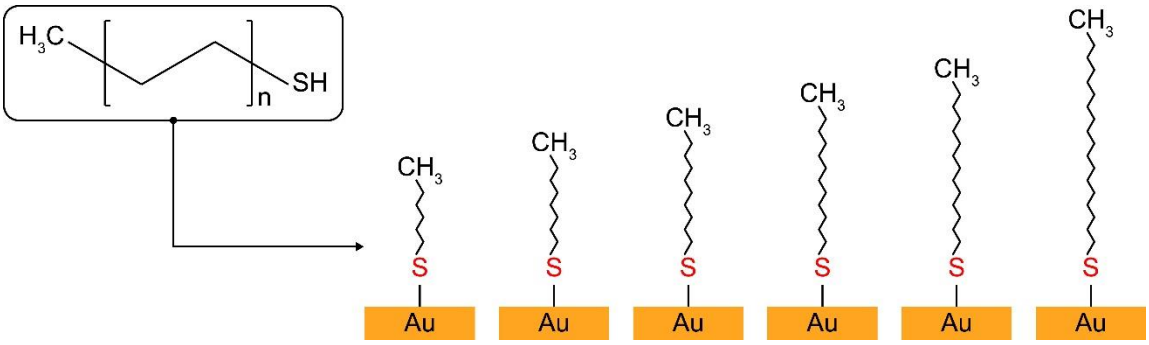

Figure 5. Schematic representation of alkanethiol self-assembled monolayers (SAMs) on gold (Au) substrate used in this work.

prevent liquid from contact area.[43] Increase of trapped air volume lead to increase of hydrophobicity which is expressed by Cassie-Baxter equation.[44] Yoshimitsu et al.[45] reported surfaces structure that can trap more air show high hydrophobicity. Bacteria suspension will be detached by passing through air-liquid interface by inducing shear force. This can be support explaining our results shown in Figure 4, deep hole-patterned surfaces present less bacteria attachment after drying process. There is more possibility to form air bubble which will lead to increase shear force to make drying process more effective to prevent bacterial attachment to surfaces. Hydrodynamic shear force can be determined by Derjaguin-Landau-Verwey-Overbeek (DLVO) interactions. Forming air pockets are making three phase interaction; air-liquid-surface instead of two phase; liquid-surface interaction.[46]

2.3. Effect of the Surface Chemistry

2.3.1. Thiol Coatings on Gold Sensor Surfaces

For studying the effect of the surface chemistry on smooth surfaces were carried

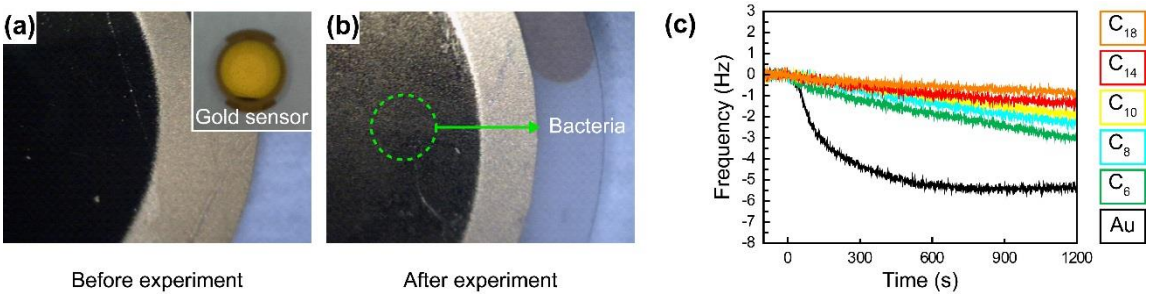

Figure 6. Light micrographs of gold sensor surfaces (a) before and (b) after QCM-D experiment (green dashed circle indicates attached bacteria on sensor surfaces). (c) QCM-D results show the change in the frequency upon exposing thiol surfaces to bacterial suspension with a flow rate of 2.5 μL/s.

out using quartz crystal microbalance with dissipation monitoring (QCM-D) which enable to measure nanoscale mass change. Linear alkanethiols were used to prepare hydrophobic surfaces with systematically varying hydrophobicities (Figure 5). Self-assembly solution was prepared by dissolving thiol in ethanol at a concentration of 5 mM. Then, a smooth gold (Au) sensor (root-mean-square (RMS) roughness < 2 nm) was placed in thiol solution for 24 h at room temperature (23 °C) to yield monolayer formation on the sensor. Surface coverage of alkanethiol functionalized gold surfaces were analyzed by secondary ion mass spectrometry (SIMS).

We have investigated initial bacterial adhesion behavior as a function of time via QCM-D. Figure 6 shows a typical QCM-D frequency data for adsorption of *S.* Typhimurium LT2 onto the alkanethiol surfaces as a function of time. The adhering bacteria gave rise to a decrease in resonant frequency as they adsorb to the QCM-D electrode, due to the increased effective mass on the electrode. In general, a larger frequency shifts corresponds to a larger mass change for a given rigidity and density of the adsorbate. Hence, the frequency response suggests that for a given time, the more

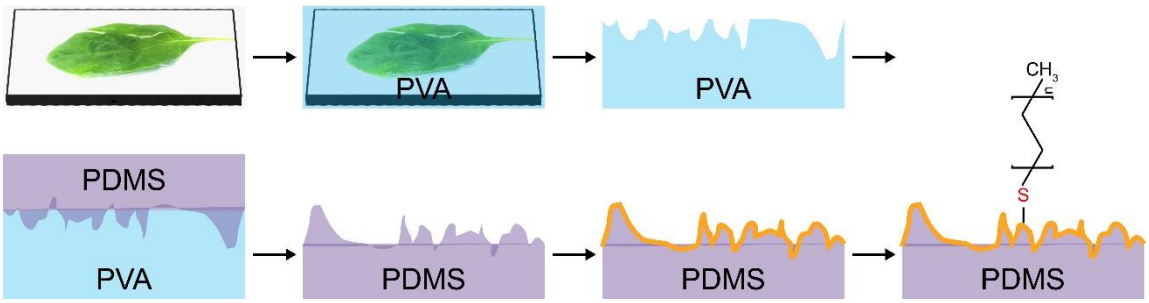

Figure 7. Schematic illustration of fabrication process for obtaining PVA spinach mold and PDMS spinach replica. After 20 nm thickness of gold (yellow layer) coating, substrates were modified by alkanethiols.

hydrophobic surfaces are, the less favorable bacterial attachment becomes. For all surfaces, while, at early times (<350 s), the frequency data followed an exponential trend while at later times (>350 s), the exponential trend evolved into a steady-state, linear regime.

2.3.2. Thiol Coatings on PDMS Spinach Replica Surfaces

Polydimethylsiloxane (PDMS) spinach replica surfaces were used to study the effect of the surface chemistry on microrough surfaces. The first step in fabricating PDMS spinach replica is rinsing spinach with water to remove dirt and other residues from surfaces. After, a solution of 10 wt% polyvinyl alcohol (PVA) in water was prepared to cast spinach mold. PVA solution was poured over spinach surfaces and left to dry at room temperature for 3 days before peeling. When PVA mold is prepared, PDMS was poured into a PVA mold and placed in oven to cure PDMS at 60 °C for 24 h before peeling. Subsequently, 20 nm gold sputter coating was applied on PDMS spinach replica surfaces for thiol-functionalization (Figure 7). Thiol-functionalized surfaces were characterized by measuring contact angle of water and diiodomethane to calculate surface tension (σ) of each surface.

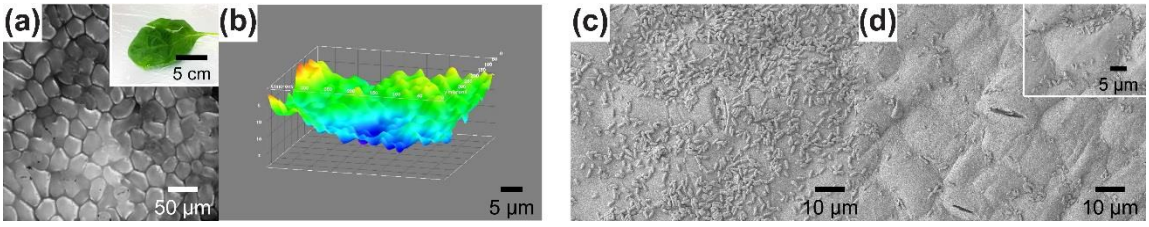

Figure 8. (a) Confocal microscope image of fresh spinach surfaces. Inset: photograph of fresh spinach leaf. (b) 3D projection of fresh spinach by using z-stacked confocal microscope images. SEM micrographs of (c) hydrophilic PDMS spinach replica and (d) hydrophobic PDMS spinach replica surfaces. Inset: detail view of bacterial attachment to valleys.

As surface hydrophobicity increase, bacterial attachment to microrough PDMS spinach replica surfaces reduced. However, SEM micrograph results from PDMS spinach replica surfaces indicate not only surface chemistry but also microscale surface texture effects on bacterial adhesion and makes slightly different trends. As shown in Figure 8, bacteria tend to stay more at the valleys of rough surfaces. This behavior can be explained by previous research report that scale of surface roughness larger than bacteria size (dimensions ranging from 700 nm to 4000 nm) enhanced bacterial colonization, because bacteria prefer surfaces that can increase surface-bacteria total contact area such as valleys, depressions, pits, and edges.[47]

CHAPTER III

HYDROPHOBICALLY-MODIFIED SILICA AEROGELS: NOVEL FOOD-CONTACT SURFACES WITH BACTERIAL ANTIADHESION PROPERTIES*

3.1. Introduction

Foodborne disease cases arising from the bacterial cross-contamination of food-contact surfaces and the subsequent cross-contamination of food products represent a significant concern for public health and have emerged as a global challenge.[1,48,49] The sources of pathogenic bacteria contaminating food-contact surfaces are typically soil, water, contaminated foods, equipment, animals, humans, and aerosols.[2] *Salmonella* spp., *Escherichia coli* O157:H7, *Listeria monocytogenes*, *Campylobacter* spp., *Shigella* spp., and *Bacillus cereus* are bacterial pathogens that can exist on food and food-contact surfaces.[3,50,51] Currently, there are a number of studies reporting the mechanisms for interaction of these microorganisms with common materials of food-contact surfaces such as stainless steel, glass, paper, high density polyethylene, polycarbonate, polyurethane, and polytetrafluoroethylene (PTFE).[52–60]

After attachment, pathogenic bacteria can survive on food-contact surfaces such as stainless steel for hours or days after initial contact.[61] Thus, contaminated food-contact surfaces have the ability to transfer microorganisms to raw foods resulting in the potential

*Reprinted with permission from "Hydrophobically-modified silica aerogels: Novel food-contact surfaces with bacterial anti-adhesion properties" by Jun Kyun Oh, Keila Perez, Nandita Kohli, Veli Kara, Jingyu Li, Younjin Min, Alejandro Castillo, Matthew Taylor, Arul Jayaraman, Luis Cisneros-Zevallos, Mustafa Akbulut, 2015. *Food Control*, 52, 132–141, Copyright 2014 by Elsevier Ltd.

for foodborne illnesses.[62,63] When good hygienic practices are applied, such as washing with hot water and soap, it is possible to reduce the number of viable pathogens on food-contact surfaces.[64] However, if cleaning and sanitizing procedures are inadequate, multiple scenarios for bacterial contamination where food safety and quality is compromised emerge.[65] Furthermore, as food-contact surfaces are used and abraded with time, cleaning and sanitizing may be even more difficult due to the development of crevices and other rough surfaces on them, thereby resulting in bacterial attachment and potential cross-contamination of foods.[66] In summary, there is a need to develop novel food-contact surfaces that robustly inhibit the attachment of pathogens.

Mérian and Goddard[67] have recently reviewed the emerging classes of non-fouling materials that have a potential for food applications. To this end, protein-repellent surfaces,[68,69] zwitterionic surfaces,[70] stimuli-responsive polymers,[34] biomimetic materials (e.g., lotus leaf, rice leaf, butterfly wing, fish scale, and shark skin),[71] and amphiphilic surfaces[72] have been considered. In this study, we investigated the feasibility of hydrophobically-modified silica aerogels, an advanced material that can be prepared in an economical fashion, as a food-contact surfaces that could have antiadherent activity against bacteria. Silica aerogel was selected based on reports on the use of functionalized silica mesoporous structures in several biomedical applications such as antifouling surfaces against proteins and cells. For instance, poly(carboxybetaine methacrylate) functionalized silica hydrogel was shown to resist protein (fibrinogen) adsorption.[73] In another study, fluoroalkoxysilane coated structures involving silica colloids were found to reduce adhesion of *Staphylococcus aureus* and *Pseudomonas aeruginosa*.[74] Hu et al.[75]

showed that composite structures involving poly(L-lactide) and silica nanoparticles exhibited antiadhesion behavior towards bacteria and cells. In addition, silica aerogels are very good thermal insulators.[76,77] Such a property can be useful for some food-contact surfaces or process environment (e.g., post-lethality environment for the handling/packaging of fully cooked meats, produce cooling chambers, or other chilled food storage environment).

Gram-negative *Salmonella* Typhimurium LT2 and *Salmonella* Typhimurium 14082s, and Gram-positive *Listeria innocua* NADC 2841 were utilized for studying the interactions of the developed food-contact surfaces with bacteria through dip-inoculation. The bacterial adhesion behavior was evaluated using conventional plating and scanning electron microscopy (SEM). The surface and porosity properties of the silica aerogel were characterized using attenuated total reflectance-Fourier transform infrared (ATR-FTIR) spectroscopy, atomic force microscopy (AFM), contact angle measurements, Brunauer-Emmett-Teller (BET) analysis, and ellipsometry techniques.

3.2. Materials and Methods

3.2.1. Preparation of Quartz and Silica Aerogel and their Methylated Versions

1 cm × 1 cm quartz (SiO_2) slides (Ted Pella, Inc., Redding, CA, USA) were first rinsed with Milli-Q water (resistivity ≥ 18.2 MΩ·cm) produced by an ultrapure water purification system (Milli-Q Advantage A10; EMD Millipore Corp., Billerica, MA, USA), and left dry at room temperature (23 °C). Subsequently, oxygen (O_2; Brazos Valley Welding Supply, Inc., Bryan, TX, USA) plasma treatment by CS-1701 reactive-ion etcher

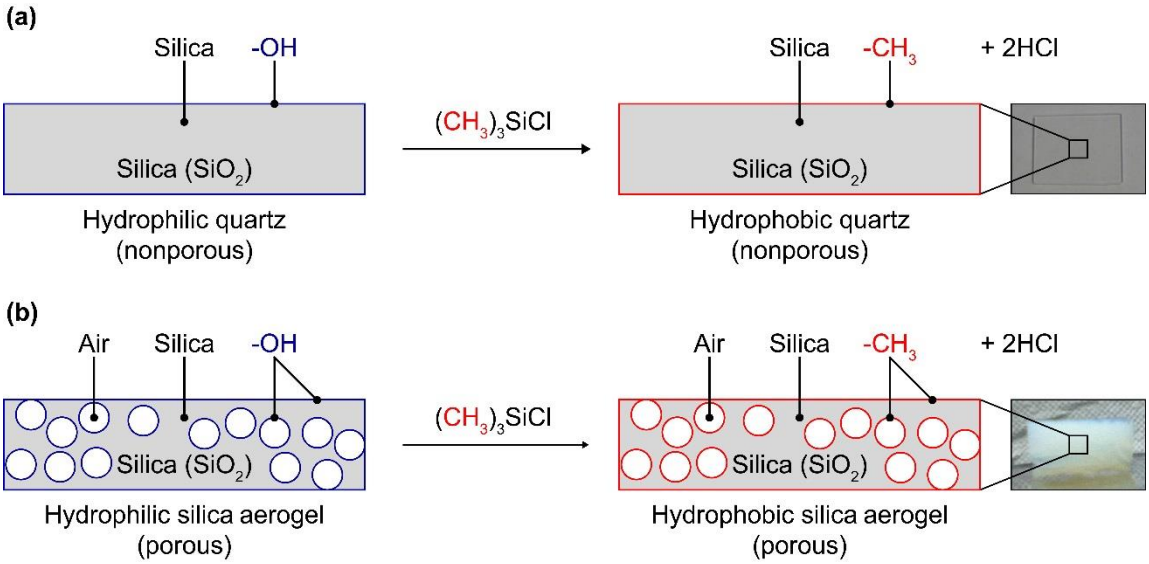

Figure 9. Schematic of hydrophobization of silica (SiO_2) materials (a) quartz and (b) silica aerogel via methylation reaction using TMCS.

(RIE; Nordson March, Concord, CA, USA) was applied to remove organic adsorbates on surfaces and further clean the surfaces. In addition, plasma treatment is known to be an effective method for sanitizing surfaces from bacteria,[78,79] and can eliminate pre-existing bacteria, if any, present on surfaces.

After rinsing with sterile Milli-Q water again, these slides were used as the negative controls. In addition, some of the quartz slides were functionalized with trimethylsilyl chloride (TMCS; Sigma-Aldrich Co., St. Louis, MO, USA) by placing the clean slides in 6% TMCS solution. The silanation reaction was allowed to take place for 24 h (Figure 9). The slides were then rinsed with ethanol (200 proof; Koptec, King of Prussia, PA, USA) and purged with a stream of nitrogen (N_2; Brazos Valley Welding Supply, Inc., Bryan, TX, USA) for 10 min and left dry at room temperature (23 °C) before use (positive controls).

Silica (SiO_2) aerogel was synthesized by the sol-gel polymerization of tetraethyl orthosilicate (TEOS; Sigma-Aldrich Co., St. Louis, MO, USA) via hydrolysis and condensation reaction.[80] Ammonium fluoride (NH_4F; Sigma-Aldrich Co., St. Louis, MO, USA) was used as a hydrolysis catalyst, and ammonium hydroxide (NH_4OH; Sigma-Aldrich Co., St. Louis, MO, USA) as a condensation catalyst. TEOS was dissolved in ethanol and the resultant solution was mixed with NH_4F, NH_4OH, and water to initiate the gelation. The reaction was allowed to take place for 24 h and the silica aerogel formed was dried using supercritical carbon dioxide (CO_2; Brazos Valley Welding Supply, Inc., Bryan, TX, USA) at the critical point (31.1 °C, 72.9 bar). This resulted in hydrophilic silica aerogel which was submerged in 6% TMCS solution for 24 h to functionalize silica surfaces with TMCS. Next, the functionalized silica aerogel was rinsed with hexane (Avantor Performance Materials, Inc., Center Valley, PA, USA) to eliminate excess TMCS and byproducts, and dried at 60 °C until hexane evaporated completely.

3.2.2. Characterization of Quartz and Aerogel

The chemical interactions of TMCS with silica materials (i.e., quartz and silica aerogel) were characterized by attenuated total reflectance-Fourier transform infrared (ATR-FTIR) spectroscopy. ATR-FTIR spectra were measured using an IRPrestige-21 (Shimadzu Corp., Kyoto, Japan) system and analyzed using IRsolution version 1.40 (Shimadzu Corp., Kyoto, Japan) software.

Surface topography of the samples was characterized using atomic force microscopy (AFM, Dimension Icon; Bruker, Santa Barbara, CA, USA). For AFM sample preparation, a stream of nitrogen gas was gently directed downward onto the surface of

the samples to remove any potential dust, and then fixed on the stage with a super glue to decrease data noise due to its extremely light weight. Topographical micrographs were obtained by using ScanAsyst™ mode in air. The silicon tip had the nominal spring constant 0.4 N/m, nominal tip radius 2 nm, and the nominal resonant frequency of 70 kHz.

In order to determine the surface hydrophobicity, static water contact angles were measured for different types of surfaces using the sessile drop technique.[81,82] Reported contact angles on each surface were obtained by averaging six measurements at room temperature (23 °C). The contact angles were analyzed by ImageJ (National Institutes of Health (NIH), Bethesda, MD, USA) software via contact angle plug-in.

The Brunauer-Emmett-Teller (BET) method was used to determine surface area, average pore diameter, and pore volume distribution of the hydrophobic silica aerogel. This was achieved by nitrogen adsorption isotherms at a temperature of 77 K by using ASAP2010 (Micromeritics Instrument Co., Norcross, GA, USA). The surface area was computed from N_2 adsorption curves following the Barret-Joyner-Halenda (BJH) method.[83]

The refractive index of silica aerogel was measured using an angle dependent ellipsometer (Nanofilm EP^3-SE; Nanofilm Technology GmbH, Göttingen, Germany) under dry and wet conditions to calculate what fraction of nanopores of silica aerogel was filled with water upon water contact.

3.2.3. Chemical Stability Tests

Chemical stability of hydrophobic silica aerogel was monitored in deionized (DI) water (H_2O) and in 10% hydrogen peroxide (H_2O_2, 30% solution; Avantor Performance

Materials, Inc., Center Valley, PA, USA), a commonly used sanitizer in food industry, as a function of time. This was achieved through analysing aliquots collected from solutions containing submerged hydrophobic silica aerogel pieces using ATR-FTIR. These measurements were conducted at immersion times of 4 h, 3 days, 1 week, and 2 weeks for both DI water (H_2O) and 10% hydrogen peroxide (H_2O_2) solutions.

3.2.4. Growth and Maintenance of Microorganisms

Salmonella enterica subsp. *enterica* serovar Typhimurium str. LT2 (ATCC 700720; American Type Culture Collection, Manassas, VA, USA) and *L. innocua* NADC 2841 (NADC 2841; National Animal Disease Center, Ames, IA, USA) were obtained from the Center for Food Safety Culture Collection in the Department of Animal Science (Texas A&M University, College Station, TX, USA). Working cultures of *S.* Typhimurium LT2 were obtained by transferring a loopful of culture from tryptic soy agar (TSA; Becton, Dickinson and Co., Sparks, MD, USA) slant to 9.0 mL of tryptic soy broth (TSB; Becton, Dickinson and Co., Sparks, MD, USA) and working cultures of *L. innocua* NADC 2841 was obtained by transferring a loopful of culture from a TSA slant containing 0.6% yeast extract (Becton, Dickinson and Co., Sparks, MD, USA) to 9.0 mL of TSB containing 0.6% yeast extract. The tubes for all strains were incubated aerobically without agitation at 37 °C for 24 h. After 24 h, a loopful of culture was transferred to fresh TSB (or TSB containing 0.6% yeast extract for *L. innocua* NADC 2841), and incubated aerobically for 24 h at 37 °C twice consecutively. The final concentration reached by *S.* Typhimurium LT2 and *L. innocua* NADC 2841 in the growth medium ranged from 8.8 to 9.1 log CFU/mL.

3.2.5. Inoculation of Surfaces with Bacterial Organisms

For sterilization purpose, each sample i.e., hydrophilic nonporous silica (negative control), hydrophobic nonporous silica (positive control), and hydrophobic silica aerogel (nanoporous) was washed in 70% ethanol for 5 min and then rinsed in sterile Milli-Q water. After completion of the sterilization process, the absence of microorganisms was confirmed by SEM. Next, the samples were immersed in 9.0 mL bacterial suspensions (8.8–9.1 log CFU/mL) for 4 h at room temperature (23 °C). Then, the samples were gently removed from the bacterial suspension in a single vertical motion, and held vertically for 5 min to eliminate the remaining droplet so that drying effects were not superimposed on the adhesion effects. Finally, nitrogen gas was gently blown on the sample to further remove the thin liquid film. The treated samples were then isolated for counting attached bacterial cells. All of these experiments were carried out under sterile conditions in biological safety cabinet to prevent any contamination.

For the comparison purposes, the above mentioned dipping inoculation assay was also utilized for common food-contact materials such as polytetrafluoroethylene (PTFE), polycarbonate, stainless steel, and glass. The disk shape samples (10 mm in diameter and 5 mm in height) were sterilized and inoculated as described above. All inoculation experiments were replicated four times.

3.2.6. Enumeration of Attached Bacteria

As a direct counting approach, a scanning electron microscope (SEM, JSM-7500F; JEOL, Tokyo, Japan) was used to observe *S.* Typhimurium LT2 and *L. innocua* NADC 2841 on surfaces to quantify bacterial adhesion on various types of silica surfaces. In SEM

experiments, a thin layer (15 nm) gold (Au) film was deposited on the bacteria adhered surfaces to ensure the scattering contrast and electrical conductivity required by SEM technique. The SEM micrographs were analyzed by ImageJ to quantify *S.* Typhimurium LT2 and *L. innocua* NADC 2841 attachments. For statistical reliability, at least nine different areas of 100 μm × 100 μm from three different samples were observed to count number of attached bacteria.

We also enumerated bacteria on silica aerogel using pour plating approach. Briefly, silica aerogel samples (5 mm × 5 mm) inoculated by bacteria were vortex-mixed in sterile water for 10 min to detach bacteria from surfaces. Then, serial dilutions of the suspension containing detached bacteria were made and plated on TSA containing 0.1 g/mL of rifampicin (Sigma-Aldrich Co., St. Louis, MO, USA) for *S.* Typhimurium LT2 and TSA containing 6.0 μg/mL yeast extract for *L. innocua* NADC 2841. Bacterial densities were determined after 24 h of aerobic incubation at 37 °C. The plating experiments were replicated six times.

3.2.7. Bacterial Proliferation Assay

After observing significant reductions in bacterial attachment on silica aerogel, we performed an additional assay to determine if bacterial antiadhesion or antimicrobial activity is responsible for the observed trends. Briefly, bacterial (*S.* Typhimurium LT2 and *L. innocua* NADC 2841) suspensions (8.8–9.1 log CFU/mL) were exposed to TMCS-functionalized silica aerogel through immersion or to 1% (v/v) bleach solution through mixing (positive control) for 4 h at room temperature (23 °C). Bacterial suspension without any exposure step was used as the negative control. Then, pour plating method

was utilized by taking 1.0 mL of bacterial suspension from each solution to make serial dilutions and then by counting the total number of bacteria. These experiments were replicated three times for each condition.

3.2.8. Characterization of Thermal Properties

The thermal insulation behavior was evaluated using a thermochromic film placed directly on top of the surface of interest (see Appendix A: Supplemental Information, Section A1 for further details). The prepared thermochromic film was found to change its color from blue to red at temperatures 40 °C or above. PTFE, polycarbonate, stainless steel, and glass samples having similar shape and dimensions to hydrophobic silica aerogel sample (10 mm in diameter and 5 mm in height) was manufactured. After the thermochromic film was placed on top of the manufactured samples, they were placed on a hot plate at a temperature of 100 °C for an hour. The time at which the color of the thermochromic film on the samples changed from blue to red was used as a criterion of comparison for the thermal insulation behavior.

3.2.9. Statistical Analysis

Microbiological data from plate counts and SEM were transformed into logarithms of cells/mm^2. One-way and two-way analysis of variance (ANOVA) with Tukey's post hoc test were used to determine significant differences between microbiological data from surface types and bacterial (*S.* Typhimurium LT2 and *L. innocua* NADC 2841) types ($p < 0.05$). All analyses were performed by using Microsoft Office Excel (Microsoft Corp., Redmond, WA, USA) statistical software packages.

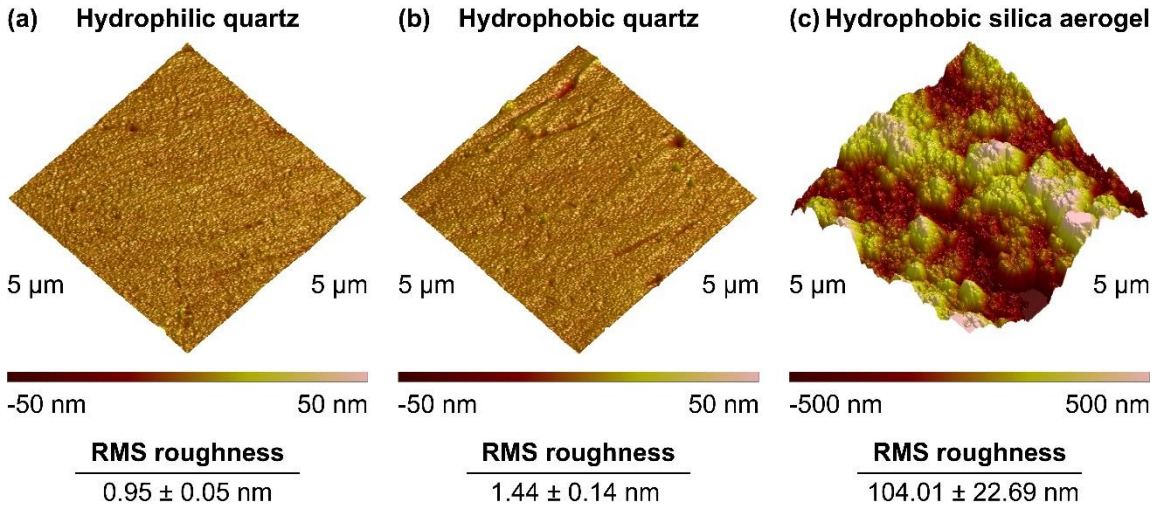

Figure 10. AFM micrographs and RMS roughness values of (a) hydrophilic quartz, (b) hydrophobic quartz, and (c) hydrophobic silica aerogel.

3.3. Results and Discussion

3.3.1. Topography and Porosity Characteristics of Silica Aerogel

Previous studies have shown that surface roughness can influence bacterial adhesion.[20,84] Hence, we characterized the surface topography of the materials used in this study to better compare their adhesion behavior. Figures 10(a)–(c) display AFM micrographs of hydrophilic nonporous quartz (SiO_2), hydrophobic nonporous quartz (SiO_2), and hydrophobic silica (SiO_2) aerogel (nanoporous) surfaces at a lower magnification. The analysis of the AFM micrographs revealed that the root-mean-square (RMS) roughness was 0.95 ± 0.05 nm, 1.44 ± 0.14 nm, and 104.01 ± 22.69 nm for hydrophilic quartz, hydrophobic quartz, and hydrophobic silica aerogel surfaces, respectively. This means that while hydrophobic silica aerogel surfaces were rougher than hydrophilic and hydrophobic quartz surfaces, the length scale of roughness for hydrophobic silica aerogel was still much smaller than diameter and length of bacteria

used in this study (i.e., 1.0–1.5 μm × 2.0–6.0 μm).[85]

BET studies on hydrophobic silica aerogel revealed that the Barrett-Joyner-Halenda (BJH) average pore diameter of hydrophobic silica aerogel was 6.58 ± 0.59 nm, the BJH pore volume was $1.10 \pm 0.10\ cm^3g^{-1}$, and the BET surface area was $761.54 \pm 3.15\ m^2g^{-1}$. These values are comparable with functionalized silica aerogel described in the literature.[86–88] Herein, it is important to note that the length scale of the bacteria is much larger than the pore diameter of the silica aerogel (i.e., 1000–1500 nm × 2000–6000 nm versus ~7 nm), thereby inhibiting the penetration of bacteria into the hydrophobic silica aerogel.

3.3.2. Characterization of Functional Groups on Silica Aerogel

To confirm the methylation reaction on quartz and silica aerogel, ATR-FTIR spectroscopy was used. Figures 11(a),(b) display ATR-FTIR spectra of pure (unreacted) TMCS, TMCS-functionalized (methylated) quartz, and TMCS-functionalized (methylated) silica aerogel surfaces. While the bare quartz and bare silica aerogel surfaces had no peak between 2800 cm^{-1} and 3000 cm^{-1}, the hydrophobic (methylated) quartz had peaks at 2850 cm^{-1}, 2920 cm^{-1}, and 2967 cm^{-1} and the hydrophobic (methylated) silica aerogel at 2900 cm^{-1}, 2962 cm^{-1}, and 2978 cm^{-1}. The presence of these peaks are attributed to symmetric and asymmetric C–H stretching from methyl groups formed upon the reaction of TMCS with silica surfaces. Unbound (free-standing) TMCS molecules had symmetric and asymmetric C–H stretching peaks at 2900 cm^{-1} and 2962 cm^{-1}. The changes in C–H stretching behavior are due to the substitution of Cl atoms by O atoms during methylation reaction and because of the transformation from the liquid state to

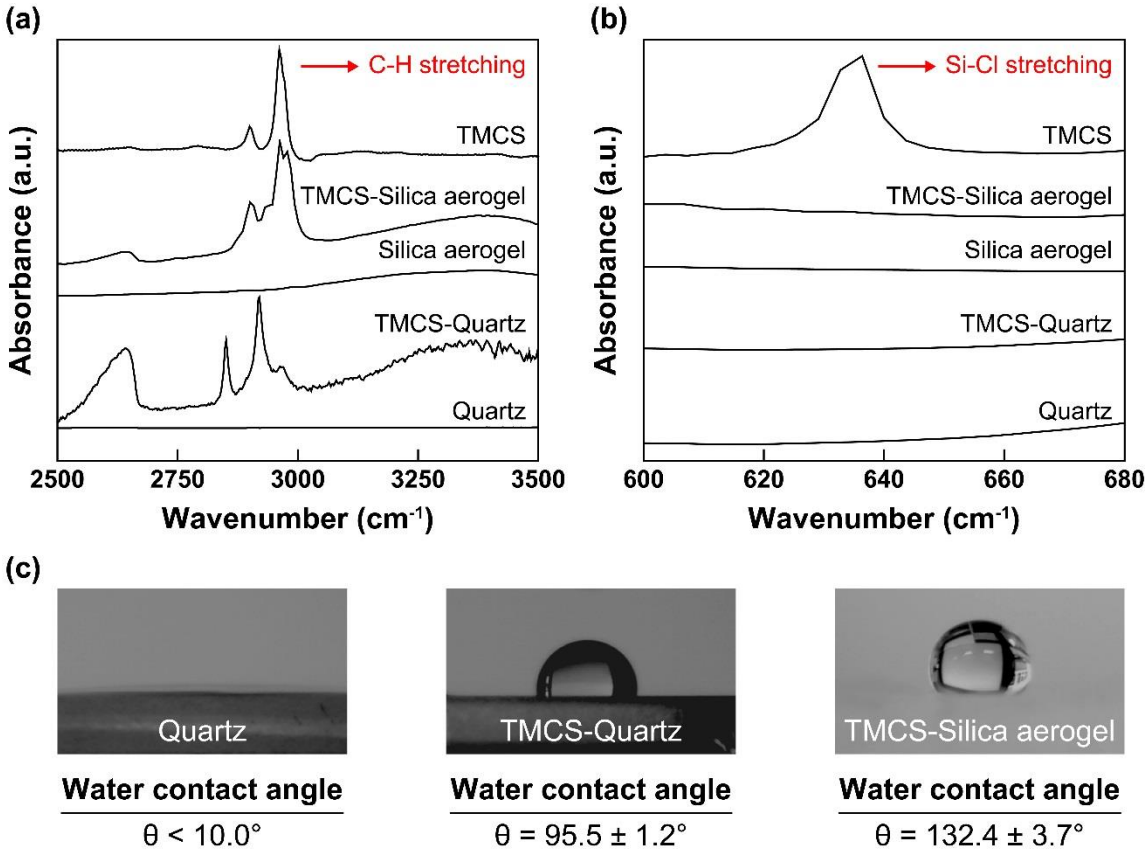

Figure 11. (a) C–H stretching region, (b) Si–Cl stretching region from ATR-FTIR spectra of TMCS, quartz (hydrophilic), silica aerogel (hydrophilic), TMCS-functionalized quartz (hydrophobic), and TMCS-functionalized silica aerogel (hydrophobic). (c) Static water contact angle measurements of quartz (hydrophilic), TMCS-functionalized quartz (hydrophobic), and TMCS-functionalized silica aerogel (hydrophobic).

crystalline state.[89] In addition, Si–Cl stretching vibration region ~620 cm^{-1} only existed for TMCS,[90] supporting the methylation reaction shown in Figure 9.

3.3.3. Wetting Characteristics of Silica Aerogel

Hydrophilic materials tend to aggregate on hydrophilic surfaces.[22,91] While bacteria can adhere on both hydrophilic and hydrophobic surfaces, bacterial attachment tends to occur significantly more on hydrophilic surfaces.[92] Therefore, it is necessary to investigate the hydrophobicity of surfaces to better explain the bacterial attachment data.

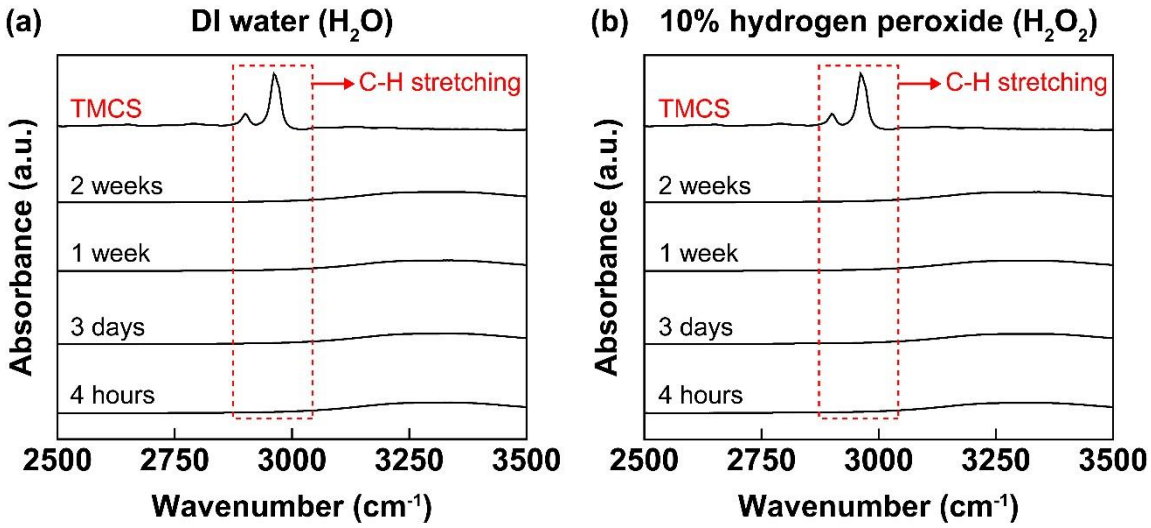

Figure 12. Characterization of chemical stability of hydrophobic silica aerogel in (a) DI water (H_2O) and (b) 10% hydrogen peroxide (H_2O_2) using ATR-FTIR spectroscopy. The absence of C–H stretching region in aqueous media suggests chemical durability of functional groups on silica aerogel surfaces.

The static water contact angle measurements (Figure 11(c)) revealed that while the neat quartz was hydrophilic ($\theta < 10.0°$), methylated quartz ($\theta = 95.5 \pm 1.2°$) and methylated silica aerogel ($\theta = 132.4 \pm 3.7°$) were hydrophobic. The difference between the contact angles of methylated quartz and silica aerogel can be explained by previous studies showing that surfaces with different roughness, textures, or crystal structures often display a variation in water contact angle values although their surface chemistry is the same.[93–95]

3.3.4. Chemical Stability of Silica Aerogel

The potential toxicity, if any, of the developed silica aerogel surfaces is directly related to their ability to release chemicals from their surfaces through detachment, degradation, or decomposition. Hence, we investigated chemical integrity and stability of hydrophobic silica aerogel in DI water (H_2O) and 10% hydrogen peroxide (H_2O_2) as a function of time using ATR-FTIR spectroscopy. As shown in Figure 12, the spectroscopic

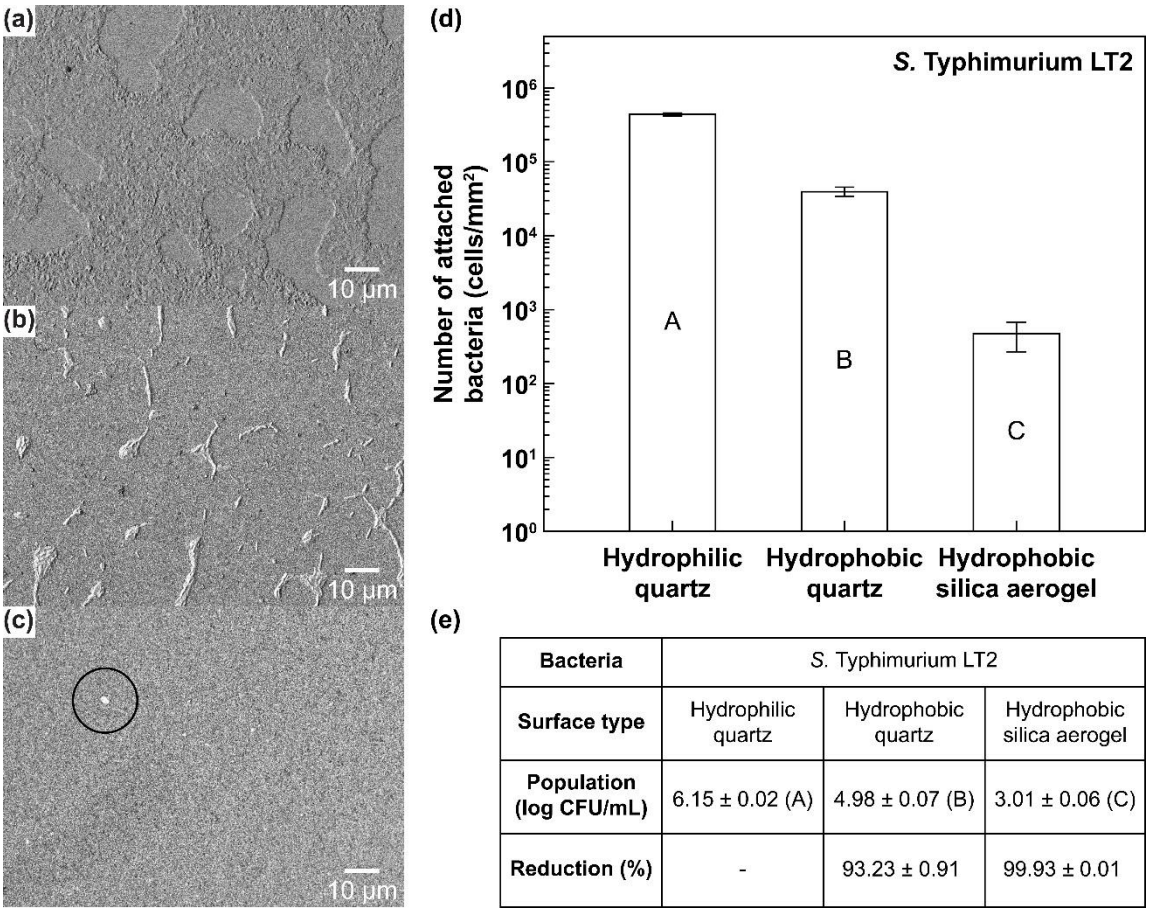

(e)

Bacteria	*S.* Typhimurium LT2		
Surface type	Hydrophilic quartz	Hydrophobic quartz	Hydrophobic silica aerogel
Population (log CFU/mL)	6.15 ± 0.02 (A)	4.98 ± 0.07 (B)	3.01 ± 0.06 (C)
Reduction (%)	-	93.23 ± 0.91	99.93 ± 0.01

Figure 13. SEM micrographs of (a) hydrophilic quartz, (b) hydrophobic quartz, and (c) hydrophobic silica aerogel (black circle indicates attached bacteria) after inoculation with *S.* Typhimurium LT2. Panel (d) relates the number of bacteria per unit area (mm^2) remaining on surfaces (a logarithmic scale is chosen for the y-axis). Bacterial adhesion was statistically different between all surfaces as determined by mean numbers of attached cells following counting ($p < 0.05$). (e) Microbiological data obtained by pour plating method. Different letters indicate statistically significant difference.

analysis revealed that solutions containing submerged silica aerogel had no free chemicals within the detection limit of 1 ppm at least for two weeks.

3.3.5. Bacterial Adhesion Behavior of Silica Aerogel

Figures 13(a)–(c) show the SEM micrographs of three different types of silica materials described above following inoculation and attachment of *S.* Typhimurium LT2.

The pristine quartz surface (hydrophilic, negative control) supported the greatest bacterial adhesion with a mean density of 5.6 ± 0.0 log cells/mm^2 (Figure 13(d)). When the quartz was methylated (hydrophobized) i.e., positive control, the bacterial adhesion decreased to a mean density of 4.6 ± 0.1 log cells/mm^2 which corresponds to $90.38 \pm 2.75\%$ of reduction. Bacterial adhesion on hydrophobic (methylated) silica aerogel surfaces led to a mean density of 2.6 ± 0.3 log cells/mm^2 which achieved a relatively high reduction of $99.91 \pm 0.05\%$. One-way ANOVA analysis showed that the difference in the adhesion of *S.* Typhimurium LT2 with respect to the sample type is statistically significant ($p < 0.05$). In addition to direct counting via scanning electron microscopy (SEM), pour plating was used to enumerate microorganisms on these samples (Figure 13(e)). Plating studies showed that compared with the negative control (pristine quartz), the positive control (methylated quartz) and silica aerogel led to a reduced number of salmonellae by 1.2 ± 0.1 log units ($93.23 \pm 0.91\%$) and by 3.1 ± 0.1 log units ($99.93 \pm 0.01\%$), respectively. According to one-way ANOVA test, these values were significantly different at $p < 0.05$ level. We note that the log reduction values were smaller in plating studies, presumably due to the lack of bacterial growth step in direct counting studies via SEM. Similar reduction trends were also observed for pathogenic *Salmonella enterica* subsp. *enterica* serovar Typhimurium str. 14028s (see Appendix A: Supplemental Information, Section A2 and Figure 36 for further details).

To determine if the above observed trends also take place for Gram-positive bacteria, we repeated direct counting via SEM and plating experiments using *L. innocua* NADC 2841. Figures 14(a)–(c) show the SEM micrographs

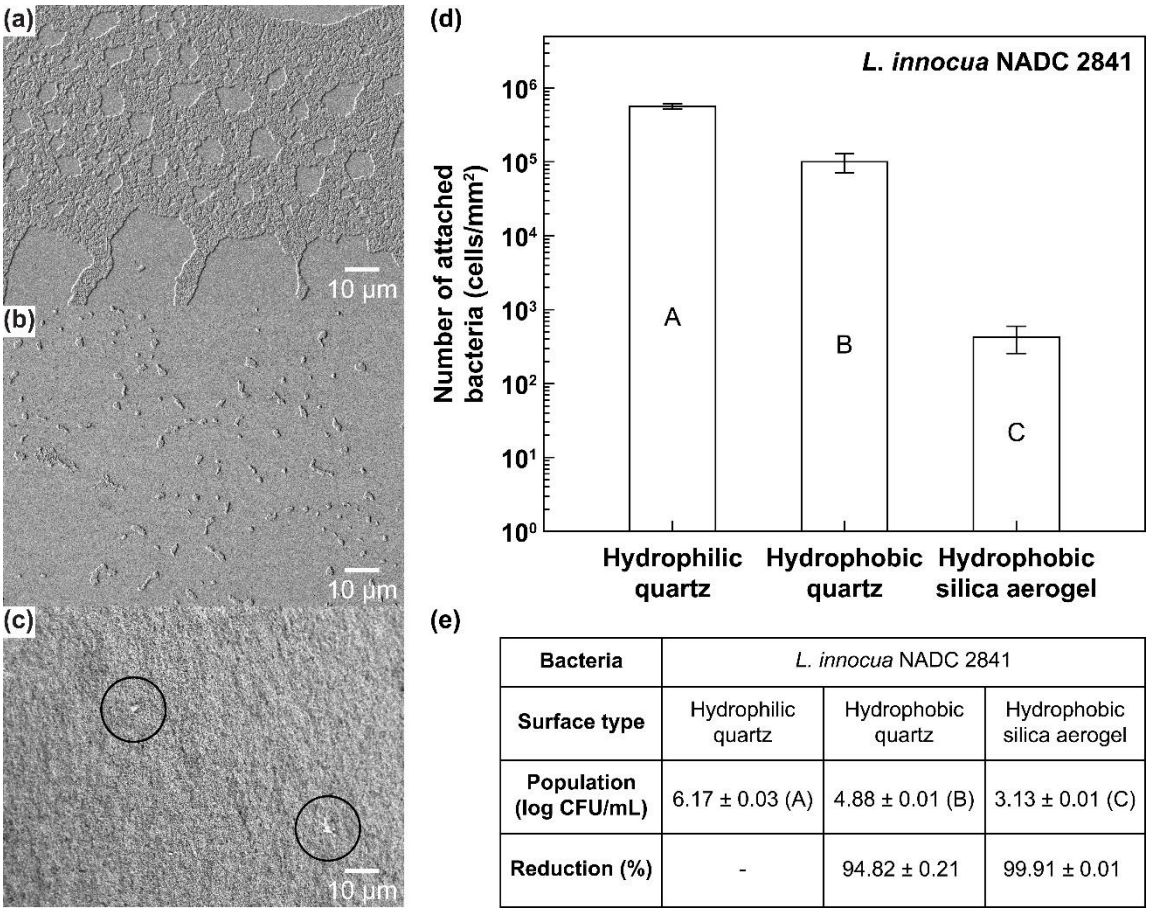

(e)

Bacteria	*L. innocua* NADC 2841		
Surface type	Hydrophilic quartz	Hydrophobic quartz	Hydrophobic silica aerogel
Population (log CFU/mL)	6.17 ± 0.03 (A)	4.88 ± 0.01 (B)	3.13 ± 0.01 (C)
Reduction (%)	-	94.82 ± 0.21	99.91 ± 0.01

Figure 14. SEM micrographs of (a) hydrophilic quartz, (b) hydrophobic quartz, and (c) hydrophobic silica aerogel (black circles indicate attached bacteria) after inoculation with *L. innocua* NADC 2841. Panel (d) relates the number of bacteria per unit area (mm^2) remaining on surfaces (a logarithmic scale is chosen for the y-axis). Bacterial adhesion was statistically different between all surfaces as determined by mean numbers of attached cells following counting ($p < 0.05$). (e) Microbiological data obtained by pour plating method. Different letters indicate statistically significant difference.

of *L. innocua* NADC 2841 attachment on three different types of silica materials described above. While hydrophilic quartz surfaces yielded a mean bacterial density of 5.8 ± 0.1 log cells/mm^2, hydrophobic quartz surfaces had a reduced number of bacteria attached with a mean density of 4.7 ± 0.0 log cells/mm^2, corresponding to 92.01 ± 1.03% reduction (Figure 14(d)). Hydrophobic silica aerogel surfaces displayed much lower

degree of bacterial attachment with a mean density of 2.5 ± 0.2 log cells/mm^2, indicating 99.94 ± 0.03% reduction in comparison to the hydrophilic quartz (negative control). In pour plating studies, using the negative control (the pristine quartz) as reference, the log reduction values were calculated to be 1.3 ± 0.0 log units (94.82 ± 0.21%) and 3.0 ± 0.0 log units (99.91 ± 0.01%) for methylated quartz (positive control) and silica aerogel, respectively (Figure 14(e)). One-way ANOVA analysis indicated that the difference in the number of *L. innocua* NADC 2841 with respect to sample type was statistically significant ($p < 0.05$) for both direct counting and traditional plating approaches. The comparison of microbiological data on three types of silica surfaces with respect to the bacterial types via two-way ANOVA indicated that for all surface types, the adhesion behavior of Gram-negative (*S.* Typhimurium LT2) and Gram-positive (*Listeria* NADC 2841) on these was not significantly different ($p > 0.05$).

Bacteria with hydrophobic cell surface tend to adhere more extensively on hydrophobic material surfaces while those with hydrophilic properties prefer hydrophilic surfaces.[96,97] Given the contact angles of water on *S.* Typhimurium and *L. innocua* NADC 2841 are between 26° and 36°, thus fairly hydrophilic, the reduction in the bacterial adhesion on the hydrophobic quartz surfaces in comparison to the hydrophilic ones is consistent with the above-mentioned phenomena.[98,99] However, the complete elimination of bacterial attachment upon changing the surface from hydrophobic quartz to hydrophobic silica aerogel cannot be explained solely by the hydrophobic effect, especially given both surfaces were functionalized with the same chemical group.

Because tail groups of TMCS are methyl groups, acid-base, hydrogen-bond, and

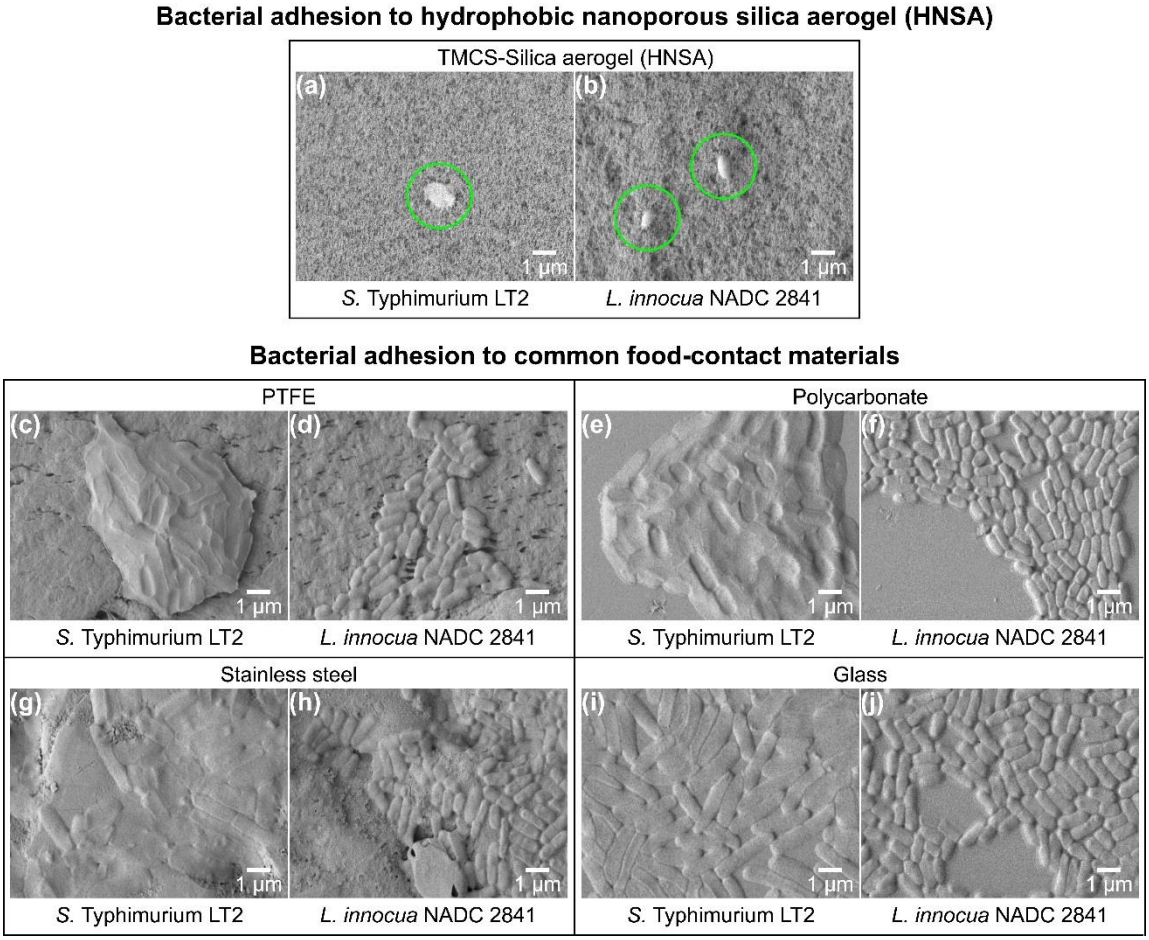

Figure 15. Comparison of bacterial (*S.* Typhimurium LT2 and *L. innocua* NADC 2841) adhesion behavior on (a), (b) hydrophobic (methylated) silica aerogel (black circles indicate attached bacteria) and (c)–(j) common food-contact materials: PTFE, polycarbonate, stainless steel, and glass.

specific ligand-receptor types of interactions between TMCS and bacteria are non-existing. Therefore, van der Waals interactions are expected to primarily govern the thermodynamics of bacterial adhesion on methylated quartz and methylated silica aerogel surfaces. The strength of van der Waals forces is directly related to the refractive index of interacting materials and dispersing medium.[36] For a given bacteria and aqueous medium, a lower refractive index of substrate will lead to a decrease in attractive van der Waals

interactions between the substrate and bacteria (see Appendix A: Supplemental Information, Section A3 for further details). Due to their nanoporous nature, silica aerogels can have much lower refractive index than nonporous silica materials (i.e., quartz).[100] Using spectroscopic ellipsometry, we found that for the methylated silica aerogel prepared, the refractive index was 1.008 ± 0.001, which is indeed much smaller than the refractive index of nonporous silica materials, 1.45–1.55. Hence, the superior ability of hydrophobic silica aerogel to inhibit bacterial attachment is attributed to the reduction of attractive van der Waals interactions due to their nanoporous nature.

Table 1. Comparison of bacterial proliferation behavior in the absence and in the presence of TMCS-Silica aerogel sample, and in the presence of 1% bleach solution against *S.* Typhimurium LT2 and *L. innocua* NADC 2841. Significant reduction was only observed for 1% bleach solution.

Bacteria	Bacterial suspension alone (control)	Bacterial suspension with TMCS-Silica aerogel	Bacterial suspension with 1% bleach solution
***S.* Typhimurium LT2**	3.7×10^8 CFU/mL[a]	3.2×10^8 CFU/mL[a]	<1 (zero) CFU/mL[a]
***L. innocua* NADC 2841**	1.1×10^9 CFU/mL[a]	1.2×10^9 CFU/mL[a]	<1 (zero) CFU/mL[a]

[a]Values of bacterial population (CFU/mL) after 4 h of exposure.

3.3.6. Comparison of Bacterial Adhesion Behavior

For a direct comparison purpose, we carried out identical dipping inoculation tests with common food-contact materials such as PTFE, polycarbonate, stainless steel, and glass as well as silica aerogel. Figure 15 displays SEM micrographs of hydrophobic (methylated) silica aerogel and common food-contact materials after inoculation

by *S.* Typhimurium LT2 and *L. innocua* NADC 2841 bacterial suspensions. Methylated silica aerogel clearly displayed superior antiadhesion performance in comparison to PTFE, polycarbonate, stainless steel, and glass. Considering that PTFE is very hydrophobic surface, improvements in inhibition of bacterial adhesion behavior for silica aerogel also support the above-mention discussion that hydrophobic effect cannot be solely responsible for the observed adhesion trends. Overall, these promising findings indicate a high inhibition efficiency of hydrophobic silica aerogel against bacterial adhesion and also show how effectively hydrophobic silica aerogel can prevent bacterial attachment compared to common food-contact materials.

3.3.7. Screening of Antimicrobial Activity

To determine if bacterial antiadhesion or antibacterial property is responsible for the log reduction trends in the bacterial attachment on silica aerogel, we carried out bacterial growth studies in the presence of silica aerogel (Table 1). In comparison to bacterial suspension without any treatment, for bacterial suspension with 1% bleach solution, a log reduction of 8–9 was observed. On the other hand, there was no change in the number of bacteria growing in the presence of silica aerogel (see Appendix A: Supplemental Information, Figure 37 for further details). Overall these findings indicate that silica aerogel displays no antibacterial activity, and hence, bacterial antiadhesion is indeed responsible for the observed inhibition trends in bacterial adhesion.

3.3.8. Measurement of Thermal Insulation Properties

The thermal insulation behavior of methylated silica aerogel and commonly used food-contact materials were compared using a thermochromic film that changes its color

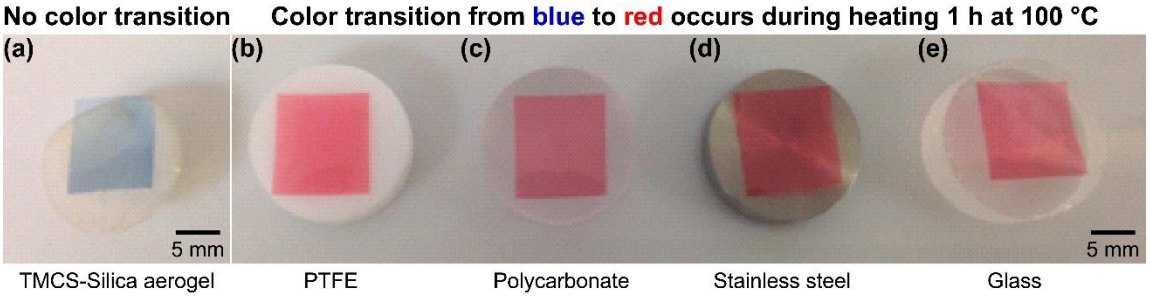

Figure 16. Comparison of thermal insulation properties of (a) hydrophobic silica aerogel (TMCS-Silica aerogel) and (b)–(e) common food-contact materials: PTFE, polycarbonate, stainless steel, and glass.

from blue to red at temperatures 40 °C or above (Figure 16). It was found that after keeping all of the surfaces on hot plate for 1 h at 100 °C, thermochromic film on all materials except hydrophobic silica aerogel changed its color blue to red. These findings indicate that methylated silica aerogel displayed superior thermal insulating performance in comparison to common food-contact surfaces. In addition, by measuring the temperatures of the silica aerogel surfaces and hot plate and the time of heating, we estimated the thermal conductivity of hydrophobic silica aerogel to be 0.052 ± 0.015 W/m·K, which is about an order of magnitude smaller than typical plastics and ceramics.[101,102]

3.4. Conclusions

In this work, we showed that the attachments of *S.* Typhimurium LT2, *L. innocua* NADC 2841, and *S.* Typhimurium 14028s on methylated (hydrophobic) silica aerogel were significantly inhibited due to its bacterial antiadhesion properties. Direct comparative studies indicated that methylated silica aerogel can prevent bacterial attachment much more effectively compared to common food-contact materials such as

polycarbonate, stainless steel, glass as well as hydrophobic PTFE. The superior ability of methylated silica aerogel to inhibit bacterial attachment is attributed to its nanoporous nature and porosity-induced reduction in the attractive van der Waals interactions between silica aerogel and bacteria. Overall, combining bacterial antiadhesion properties of hydrophobic silica aerogel with their other unique properties such as thermal insulation and ultra-light weight, can open up new avenues in the design of food-contact surfaces.

CHAPTER IV

NANOPOROUS AEROGEL AS A BACTERIA REPELLING HYGIENIC MATERIAL FOR HEALTHCARE ENVIRONMENT*

4.1. Introduction

Bacterial contamination is one of the major causes of healthcare-associated infections (HAIs). According to the statistics by the United States (US) Centers for Disease Control and Prevention (CDC), there were 721,800 HAIs due to bacteria in the US in 2011.[6] The European Centre for Disease Prevention and Control (ECDC) estimates that about 4.2 million patients acquire a HAI in the European Union (EU) each year, about 60% of which are caused by bacteria.[103,104] The recent studies on the analysis of surveillance data from the CDC and ECDC revealed that *Escherichia coli*, *Staphylococcus aureus*, *Enterococcus*, and *Pseudomonas aeruginosa* are the bacterial pathogens most commonly associated with HAIs.[5,105]

It has been well-documented that pathogenic bacteria can survive on inanimate surfaces for several months or even longer.[9] Hence, one source of pathogenic bacteria contributing to the transmission of HAIs is the healthcare environment and surfaces (e.g., bed rails, bedside tables, toilet seats, toilet rails, door handles, chairs, floor, infusion pumps, and blood pressure cuffs).[106,107] Furthermore, depending on the number, location,

*Reprinted with permission from "Nanoporous aerogel as a bacteria repelling hygienic material for healthcare environment" by Jun Kyun Oh, Nandita Kohli, Yuanzhong Zhang, Younjin Min, Arul Jayaraman, Luis Cisneros-Zevallos, Mustafa Akbulut, 2016. *Nanotechnology*, 27, 085705, Copyright 2016 by IOP Publishing Ltd.

inoculation time, and resistance types of microorganisms, it can be difficult to completely disinfect microorganisms on these surfaces using standard chemical germicides and sterilization processes.[108] For instance, upon biofilm formation, microorganisms can protect them from external physical and chemical attack through multiple mechanisms such as physical characteristics of older biofilms, genotypic variation of the bacteria, microbial production of neutralizing enzymes, and physiologic gradients within biofilms.[2,109] Attributable to these protection mechanisms, bacteria within biofilms were reported to be up to thousand times more resistant to antimicrobials than the same bacteria in suspension.[110] Considering the bacterial pathogens on hospital surfaces have been occasionally observed and the contaminated hospital surfaces lead to a myriad of potential health risks,[111,112] there is a need to develop more advanced healthcare surfaces that prevent cross-contamination and reducing transfer of microorganisms.[113] As a potential solution, previous efforts have mostly focused on the development of hygienic surfaces that are either embedded with antimicrobial agents,[26,114] grafted with antimicrobial agents,[115–117] inherently antimicrobial in nature,[118,119] or specially textured to result in bacterial repellency.[120,121] However, there are several intrinsic limitations to such strategies such as the lack of sustainable antibiotic release,[27] the toxicity to human tissues,[28] the ineffectiveness against antimicrobial-resistant bacteria,[29] the development of resistance due to continuous exposure to antimicrobial agents,[122] and the long-term bactericidal inefficiency (i.e., dead bacteria attached to surfaces still can provide attachment sites for upcoming bacteria and hinders bactericidal activity).[30]

As an alternative solution, the strategies relying on bacterial antiadhesive materials

have been utilized to produce hygienic surfaces for biotechnological and healthcare-related applications.[15,123–125] Some of these include, for example, polyethylene glycol (PEG) or zwitterionic polymer surfaces to minimize the intermolecular interactions between bacteria and surfaces,[31,32,68] stimuli-responsive surfaces with changing surface properties (i.e., wetting behavior and topography) induced by heat or shear forces,[33,34] and surface containing heparin as an antiadhesive agent prepared by layer-by-layer assembly.[35] The main limitation of these strategies is that due to their soft and hydrophilic nature, such surfaces can erode over time with physical contact or exposure to water.

As yet another alternative solution, nanotextured hygienic surfaces with superhydrophobic properties have recently gained much attention due to their ability to form air pockets that restricts bacteria on the water-side of the air-water interface.[126] In particular, surfaces with nanopillars,[127] hollow nanodiscs,[16] nanotubes,[128] hierarchical nanowrinkles,[129] and nanochannels[130] have been reported to have promising bacterial antiadhesion properties. The main concern with these strategies is that the upon prolonged exposure to water and humidity, the trapped air can be displaced, thereby decreasing their effectiveness in keeping bacterial away from the surfaces.[131]

Herein, we report the ability of hydrophobic nanoporous silica aerogel (HNSA) to inhibit the adhesion of bacteria associated with HAIs, and hence, their potential to be used as materials for healthcare environment. It is important to note that many other biomedical applications of silica aerogels such as implantable devices,[132] scaffolds,[133] and drug carrier systems[134] have recently emerged. Therefore, the knowledge of bacterial antiadhesion properties of HNSA can also be beneficial for the development of multifunctional hygienic

materials and biomedical surfaces.

4.2. Materials and Methods

4.2.1. Preparation of Substrates

Nanoporous silica (SiO_2) aerogels were synthesized via sol-gel polymerization of tetraethyl orthosilicate (TEOS; Sigma-Aldrich Co., St. Louis, MO, USA) at room temperature (23 °C). Gelation of 5 mL TEOS dissolved in 11 mL of ethanol (200 proof; Koptec, King of Prussia, PA, USA) was initiated by mixing solution with 0.37 mL of catalyst solution which was prepared by adding 1.85 g of ammonium fluoride (NH_4F; Sigma-Aldrich Co., St. Louis, MO, USA) and 22.8 mL of ammonium hydroxide (NH_4OH; Sigma-Aldrich Co., St. Louis, MO, USA) to 100 mL of water. The reaction was allowed to take place for 24 h. Once the gel had set, ethanol inside the gel was extracted by supercritical carbon dioxide (CO_2; Brazos Valley Welding Supply, Inc., Bryan, TX, USA) at the critical point (31.1 °C, 72.9 bar). After the supercritical CO_2 extraction, the obtained hydrophilic silica aerogels were submerged in 6 wt% trimethylsilyl chloride (TMCS; Sigma-Aldrich Co., St. Louis, MO, USA)/hexane (ACS grade; Avantor Performance Materials, Inc., Center Valley, PA, USA) solution for 24 h to functionalize silica aerogel as schematically illustrated in Figure 17(a). Resultant methylated silica aerogel was rinsed with hexane and dried at 60 °C until hexane evaporated completely.

Since silicon dioxide (SiO_2) was the main constituent of the developed samples, quartz (SiO_2) was selected as a control surface to ensure a chemical similarity between these. Quartz slides (Ted Pella, Inc., Redding, CA, USA) cut into 1 cm × 1 cm × 1 mm

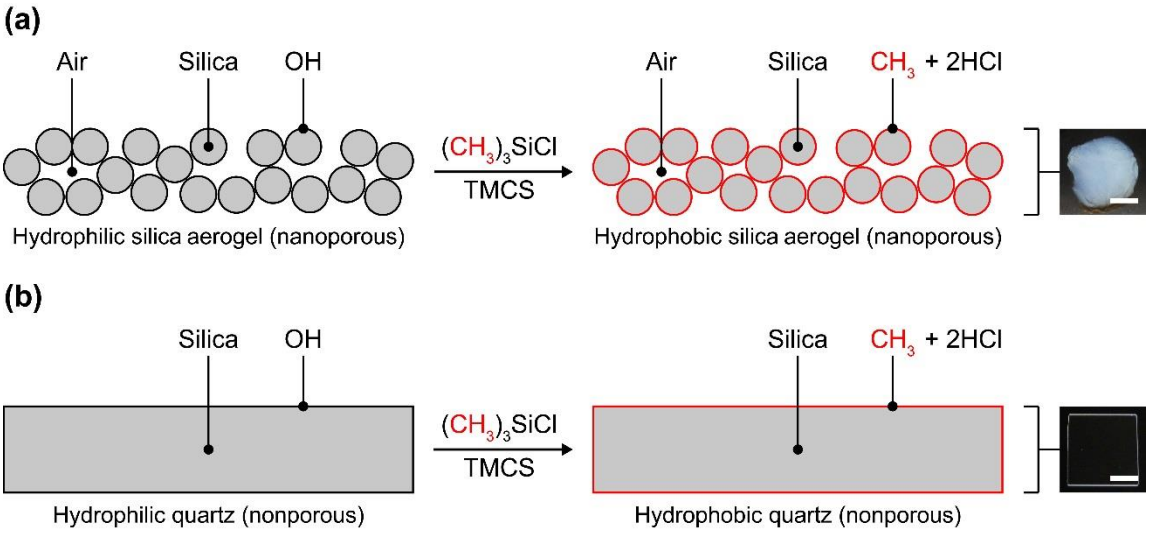

Figure 17. Schematic representation of surface modification of silica materials, (a) nanoporous silica aerogel (HNSA, scale bar: 1 cm) and (b) nonporous quartz (scale bar: 1 cm) via methylation reaction using TMCS.

were first rinsed with Milli-Q water (resistivity ≥ 18.2 MΩ·cm; EMD Millipore Corp., Billerica, MA, USA), then dried under a stream of nitrogen (N_2; Brazos Valley Welding Supply, Inc., Bryan, TX, USA). Subsequently, oxygen plasma treatment was applied at a power of 20 W, pressure of 80 mTorr, oxygen flow rate of 20 sccm, and a time of 1 min by using CS-1701 reactive-ion etcher (Nordson March, Concord, CA, USA) for cleaning purposes. We also note that oxygen plasma treatment can effectively sanitize surfaces from pre-existing bacteria.[78] Methylated quartz slides were prepared by placing quartz slides in solution of 6 wt% TMCS in hexane for 24 h, as shown in Figure 17(b). The samples were then purged under a stream of nitrogen before use.

4.2.2. SEM and AFM

Surface morphology of all samples was characterized by scanning electron microscope (SEM, JSM-7500F; JEOL, Tokyo, Japan) and atomic force microscopy (AFM,

Dimension Icon; Bruker, Santa Barbara, CA, USA). Before SEM examination, the samples were coated with 8 nm of platinum/palladium to minimize possible charging effects. The SEM micrographs were obtained at an accelerating voltage of 1 kV and emission current of 20 μA.

AFM topographic micrographs were obtained by using tapping mode in air at room temperature. Specifications of the silicon tip cantilever are nominal tip radius of 2 nm, nominal spring constant of 0.4 N/m, and nominal resonant frequency of 70 kHz. Extremely light weight HNSA samples were mounted on a glass slide by using instant glue and then placed on the stage to decrease data noise.

4.2.3. BET Measurements

Specific surface area, pore diameter, and pore volume distribution of HNSA were characterized by Brunauer-Emmett-Teller (BET) and Barrett-Joyner-Halenda (BJH) methods.[83] To achieve these values, nitrogen adsorption isotherms were measured with an ASAP2010 (Micromeritics Instrument Co., Norcross, GA, USA) at liquid nitrogen temperature of 77 K.

4.2.4. ATR-FTIR Spectroscopy and XPS

Attenuated total reflectance-Fourier transform infrared (ATR-FTIR) spectroscopy was used to characterize TMCS-functionalized quartz and TMCS-functionalized silica aerogel (i.e., HNSA) surfaces at ambient conditions. ATR-FTIR spectra were recorded with an IRPrestige-21 (Shimadzu Corp., Kyoto, Japan) system and data were analyzed using IRsolution (Shimadzu Corp., Kyoto, Japan) software version 1.40.

To confirm TMCS coverage, X-ray photoelectron spectroscopy (XPS) spectra of

TMCS-functionalized quartz and TMCS-functionalized silica aerogel (i.e., HNSA) surfaces were recorded with a PHI VersaProbe II Scanning XPS Microprobe (Physical Electronics, Chanhassen, MN, USA). XPS measurements were carried out using an Al Kα radiation source (1486.6 eV) operating at 25 W, and at a working pressure of 10^{-7} Pa.

4.2.5. Contact Angle Measurements

The surface hydrophobicity was determined by a sessile drop technique, a 5 μL water droplet was placed on different types of surfaces. The static contact angle values were measured by ImageJ (National Institutes of Health, Bethesda, MD, USA) software via low-bond axisymmetric drop shape analysis (LBADSA) plug-in.[135] The values reported are an average of six measurements.

4.2.6. Growth and Maintenance of Microorganisms

Working cultures of *Escherichia coli* O157:H7 (ATCC 700728) and *Staphylococcus aureus* were inoculated into 9 mL of tryptic soy broth (TSB; Becton, Dickinson and Co., Sparks, MD, USA) by transferring a loopful of culture from tryptic soy agar (TSA) slant. Both strains were incubated aerobically without agitation for 24 h at 37 °C. A loopful of culture was then transferred every 24 h for 2 days to fresh TSB and incubated aerobically at 37 °C. The final concentration ranging from 8.7 to 9.1 log CFU/ mL were reached by *E. coli* O157:H7 and *S. aureus* in the growth media, as determined by plate count method.

4.2.7. Inoculation of Surfaces with Bacterial Organisms

Prior to inoculation experiments, the samples (i.e., hydrophilic bare quartz, hydrophobic quartz, and HNSA) were sterilized by washing with 70% (v/v) ethanol

followed by sterile Milli-Q water rinsing. After the sterilization procedure, the samples were inoculated with bacteria by submerging them in 9 mL bacterial suspensions (8.7–9.1 log CFU/mL) for 4 h at room temperature. The treated samples were then gently removed from the bacterial suspensions to count bacteria attached to surfaces. All inoculation experiments were replicated four times.

4.2.8. Enumeration of Attached Bacteria

SEM was used to quantify the attachment of *E. coli* O157:H7 and *S. aureus* to various surfaces by direct counting. After acrolein (Sigma-Aldrich Co., St. Louis, MO, USA) inactivation, 10 nm thickness of gold coating was applied to sample surfaces to ensure electrical conductivity required by SEM technique. For quantitative analysis, at least ten different 100 μm × 100 μm scan areas (total scan area larger than 100,000 μm^2) were analyzed to count the number of attached bacteria.

4.2.9. Ellipsometry Analysis

Angle dependent ellipsometer (Nanofilm EP3-SE; Nanofilm Technology GmbH, Göttingen, Germany) was utilized to obtain the refractive index of HNSA. The measurements were carried out before and after 4 h exposure to bacterial suspensions.

4.2.10. Screening Method for Antimicrobial Activity

Bacterial suspensions of *E. coli* O157:H7 and *S. aureus* strains were grown in the presence of HNSA and in the presence of 1% (v/v) bleach solution for 4 h at room temperature. Bacterial suspensions without any treatment were used as negative control. The number of bacteria remaining in suspension was determined by pour plate method. Each condition was replicated three times.

4.2.11. Statistical Analysis

Microbiological data obtained by SEM were converted to logarithm of a cell density (log cells/mm^2). All analyses were performed by using statistical package for Microsoft Office Excel (Microsoft Corp., Redmond, WA, USA) software. The data were analyzed by one-way and two-way analysis of variance with Tukey's test to determine significant differences at a *p*-value of <0.05.

4.3. Results and Discussion

4.3.1. Topographical Characterization and Analysis of Materials

It is well-established that surface texture and roughness play an important role in bacterial adhesion on surfaces.[20,84] Hence, before proceeding with bacterial attachment experiments, we first characterized the surface topography of materials prepared for this study to better understand and compare their adhesion behavior. Figures 18(a)–(c) display SEM micrographs of hydrophilic bare quartz, hydrophobic quartz, and HNSA surfaces, showing the surface texture of each material. SEM micrographs visually highlight the differences and reveal the highly nanoporous structure of HNSA.

When the length scale of surface roughness is larger than bacteria size, bacterial colonization is enhanced because bacteria prefer surfaces/textures that increase the total contact area of bacteria-material interfaces such as valleys, depressions, pits, and edges.[47] To quantitatively compare the characteristic sizes of bacteria and surface roughness, AFM measurements on three different material surfaces were performed over a 5 μm × 5 μm area, as shown in Figures 18(d)–(f). The root-mean-square (RMS) roughness value of bare

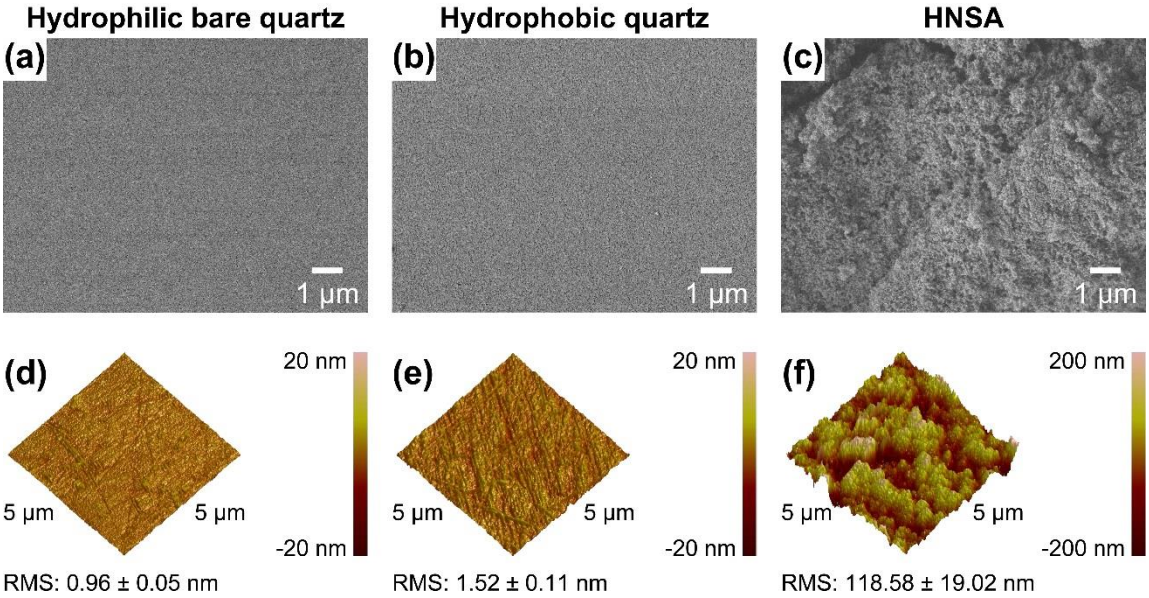

Figure 18. SEM micrographs of (a) hydrophilic bare quartz, (b) hydrophobic quartz, and (c) HNSA. (d)–(f) AFM micrographs show depth profile of each surface. RMS roughness values are shown at the bottom of AFM micrographs.

quartz surfaces were found to be 0.96 ± 0.05 nm. After surface functionalization with TMCS, RMS roughness reached 1.52 ± 0.11 nm. The small difference in RMS roughness can be attributed to the surface reaction, which introduces new Si–O bond (~148 pm) connected to Si–C bond (~318 pm) on top of bare quartz surfaces. RMS roughness of 118.58 ± 19.02 nm was obtained from HNSA surfaces. While surface roughness of HNSA surfaces was more than fifty times rougher than bare quartz and hydrophobic quartz surfaces, the scale of surface roughness was still much smaller than length and diameter of bacteria (i.e., rod-shaped *E. coli* O157:H7 is 0.5–1.0 μm wide by 1.0–4.0 μm long and spherical-shaped *S. aureus* is 0.7–1.0 μm in diameter). Thus, the physical attachment such as penetration and trapping of bacteria to HNSA surfaces can be prevented. In addition, these roughness values of HNSA meet the criterion of surface

roughness (≤1.0 μm) outlined for hygienic materials.[136]

Quantitative details of porosity characteristics of HNSA such as specific surface area (646.70 ± 5.04 m^2g^{-1}), pore diameter (19.85 ± 0.10 nm), and pore volume (3.21 ± 0.02 cm^3g^{-1}) were determined by BET and BJH methods. These values are comparable to functionalized silica-based aerogels reported previously.[87] Here, we note that pore diameter (~19 nm) of HNSA is much smaller than the bacteria dimensions ranging from 700 nm to 4000 nm as described above, thereby preventing bacterial penetration. This explanation is consistent with the reported data that pore diameter of 0.1μm was not sufficient to allow bacteria to penetrate.[137] Furthermore, HNSA showed extremely low thermal conductivity due to its high surface area and low density (see Appendix B: Supplementary Information, Section B1 and Figure 38). We calculated the thermal conductivity of HNSA to be 0.047 ± 0.015 W/m·K using time-resolved temperature measurements, which is about an order of magnitude smaller than common thermal insulation materials.[138]

4.3.2. Characterization of Functional Groups on Surfaces

Chemical modification of quartz and silica aerogel surfaces by methylation were characterized by ATR-FTIR spectroscopy, as shown in Figures 19(a),(b). ATR-FTIR spectra of pure (unreacted) TMCS, TMCS-functionalized quartz, and TMCS-functionalized silica aerogel (i.e., HNSA) surfaces showed multiple peaks that are significant, while bare quartz and bare silica aerogel surfaces had no peak between 2800 cm^{-1} and 3000 cm^{-1}. Chemically unbound TMCS molecules had symmetric and asymmetric C–H stretching peaks at 2900 cm^{-1} and 2962 cm^{-1}. On the other hand,

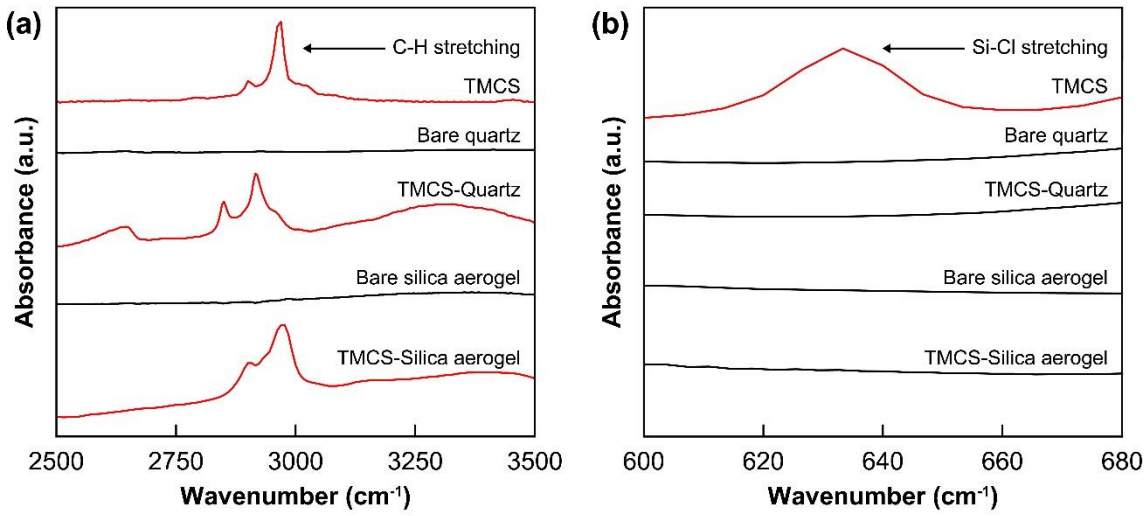

Figure 19. ATR-FTIR spectra showing (a) C–H stretching region and (b) Si–Cl stretching region of TMCS, bare quartz, TMCS-functionalized quartz, bare silica aerogel, and TMCS-functionalized silica aerogel (i.e., HNSA).

methylated quartz had peaks at 2850 cm^{-1} and 2916 cm^{-1}, and HNSA had peaks at 2900 cm^{-1} and 2970 cm^{-1}, respectively. The presence of these spectrum peaks are due to overtones and combinations of symmetric and asymmetric C–H stretching vibrations upon functionalization reactions. Furthermore, peak shifts in C–H stretching region can be explained by replacement of chlorine (Cl) atoms by oxygen (O) atoms during methylation and phase transformation of samples from the liquid state to the crystalline state.[89] In addition, Si–Cl stretching vibrations near 620 cm^{-1} only existed for TMCS, providing clear evidence of methylation.[90]

After successful functionalization of silica aerogel with TMCS, chemical stability test was conducted. HNSA samples were submerged in DI water and 10% (w/v) hydrogen peroxide (H_2O_2) for two weeks to prove chemical resistance against common environmental conditions that material may be exposed. Any chemical release, leaching,

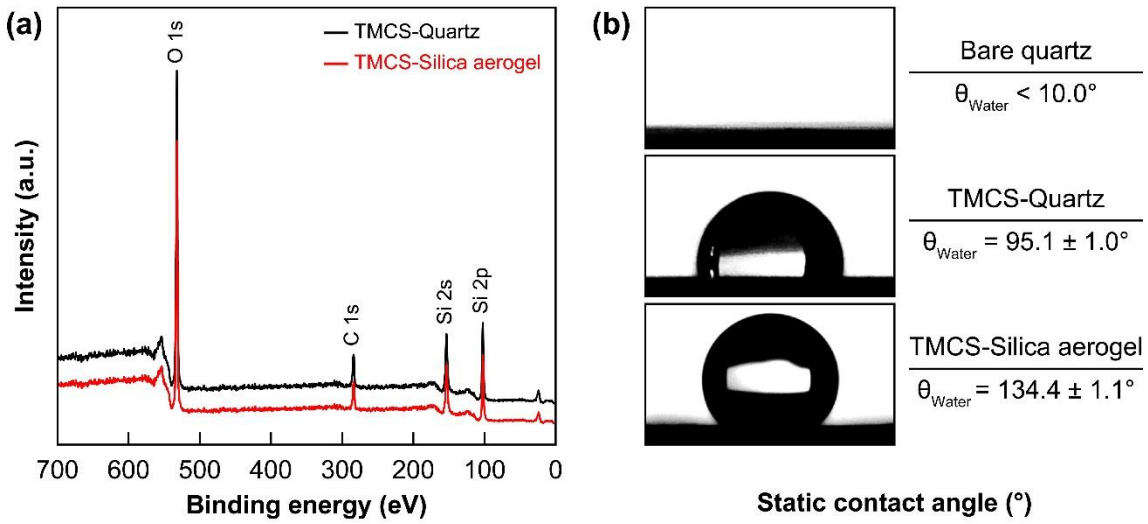

Figure 20. (a) XPS spectra of quartz and silica aerogel surfaces functionalized with TMCS. (b) The static water contact angle measurements of bare quartz, TMCS-functionalized quartz, and TMCS-functionalized silica aerogel (i.e., HNSA).

and degradation was not detected from ATR-FTIR measurements with detection limit of <1 ppm (see Appendix B: Supplemental Information, Section B2 and Figure 39).

It is known that bacterial adhesion is sensitive to the surface chemistry.[139] Therefore, it is essential to determine the degree of methylation on quartz and silica aerogel surfaces to better understand their bacterial adhesion behavior. To this end, XPS technique was used to obtain chemical information about the surface of solid materials. As shown in Figure 20(a), O 1s, C 1s, Si 2s, and Si 2p were the main peaks observed in the XPS spectra. The integration of area under these peaks was conducted to determine the relative atomic concentration of O, C, and Si atoms. The atomic percentages for C, O, and Si were ~16%, 26%, and 58%, respectively, for hydrophobic quartz. While the atomic percentages for C, O, and Si were ~15%, 25%, and 60%, respectively, for HNSA. Given that the penetration depth of XPS is about 8 nm to 10 nm and RMS roughness for HNSA

was about 118 nm, the effect of the porosity (i.e., methyl groups in the pores of HNSA) on the XPS spectra is expected to be small.[140] Therefore, these findings suggest that the degree of methylation is similar for both quartz and silica aerogel.

4.3.3. Characterization of Surface Wettability

It is well-established that surface hydrophobicity of the material has an effect on bacterial attachment. As most of the bacteria surfaces are fairly hydrophilic, it is important to study hydrophobicity of material surfaces because hydrophilic materials tend to aggregate more on hydrophilic surfaces.[141] Therefore, we have investigated surface hydrophobicity of samples to better understand bacterial attachment to material surfaces. As shown in Figure 20(b), while contact angle measured on bare quartz was hydrophilic ($\theta < 10.0°$), methylated quartz ($\theta = 95.1 \pm 1.0°$) and methylated silica aerogel ($\theta = 134.4 \pm 1.1°$) were hydrophobic. The contact angle difference in these three types of surfaces can be explained on the basis of previous studies showing that the effect of structural properties. Although materials have the same surface chemistry, physical factors such as roughness, texture, or crystal structure can result in variations in water contact angle values.[95]

4.3.4. Bacterial Adhesion Characteristics

SEM micrographs of *E. coli* O157:H7 strain attached to three different types of silica-based materials upon dip-inoculation are shown in Figures 21(a)–(c). Bacterial adhesion was greatest to hydrophilic bare quartz with a mean density of 5.79 ± 0.01 log cells/mm^2. Inoculation of hydrophobic quartz with bacteria resulted in a mean density of 5.02 ± 0.03 log cells/mm^2, which corresponds to $82.95 \pm 0.90\%$ reduction in bacterial

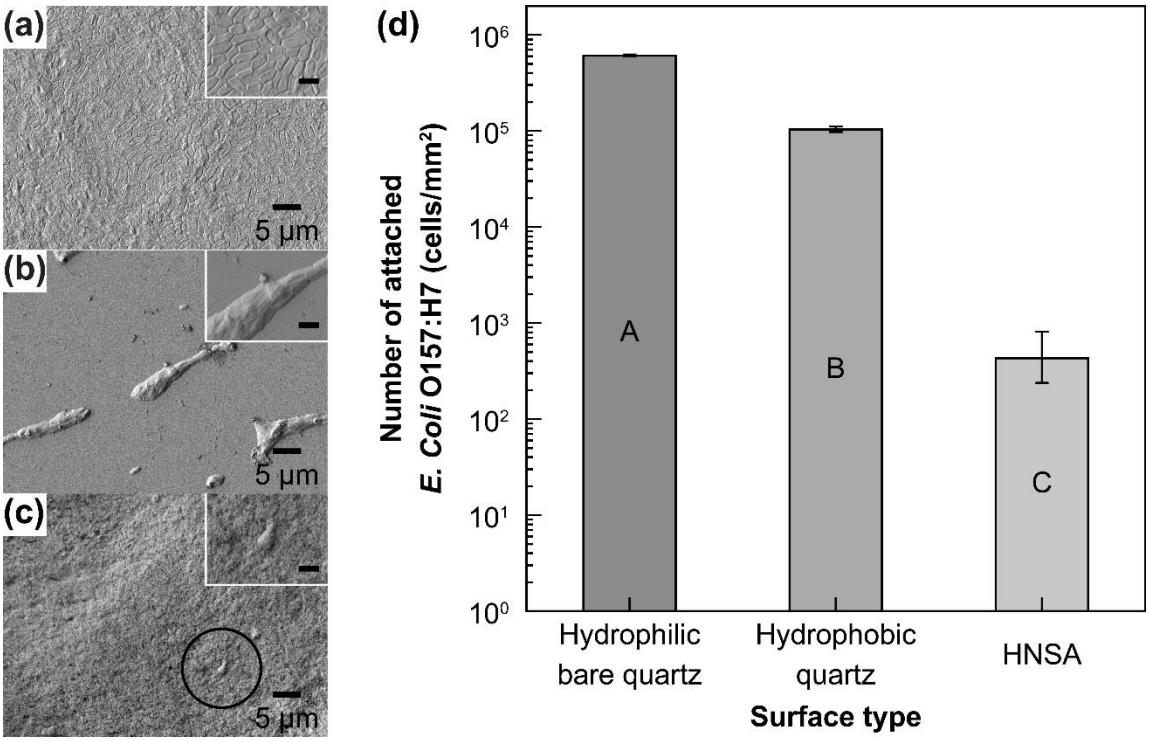

Figure 21. SEM micrographs of (a) hydrophilic bare quartz, (b) hydrophobic quartz, and (c) HNSA (black circle indicates attached bacteria) after inoculation with Gram-negative *E. coli* O157:H7. The insets show magnified images of attached bacteria (scale bar: 2 µm). (d) The average number of bacteria per unit area (mm^2) on different surfaces (*y*-axis has a logarithmic scale). Different letters (i.e., A, B, and C) indicate statistically significant difference ($p < 0.05$).

attachment in comparison to bare quartz. Bacterial adhesion on HNSA was much less, with a mean density of 2.67 ± 0.24 log cells/mm^2, indicating a reduction of 99.91 ± 0.05% in bacterial attachment in comparison to bare quartz, as shown in Figure 21(d). Similar reduction trends were also confirmed by fluorescent *E. coli* O157:H7 EDL933 strain (see Appendix B: Supplemental Information, Section B3 and Figure 40).

We also investigated the attachment of Gram-positive bacteria, *S. aureus*, to each silica-based surface using the same inoculation conditions described above (Figure 22). Mean densities of bacteria present on hydrophilic bare quartz, hydrophobic quartz, and

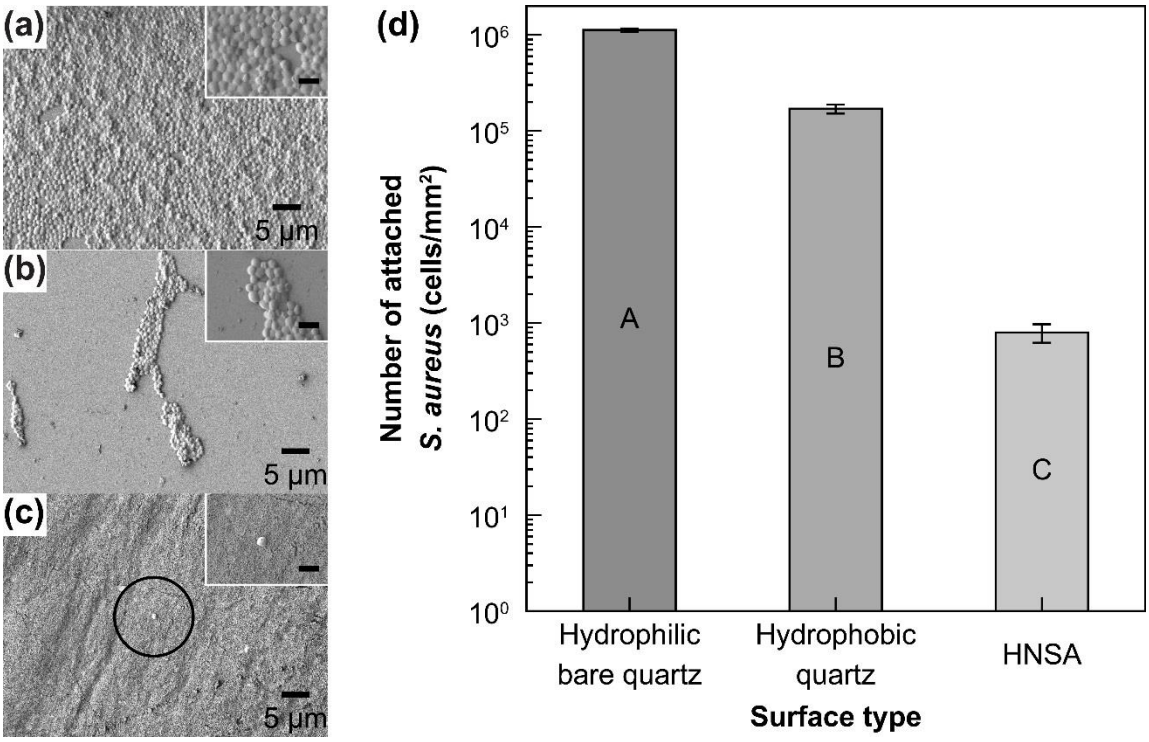

Figure 22. SEM micrographs of (a) hydrophilic bare quartz, (b) hydrophobic quartz, and (c) HNSA (black circle indicates attached bacteria) after inoculation with Gram-positive *S. aureus*. The insets show magnified images of attached bacteria (scale bar: 2 μm). (d) The average number of bacteria per unit area (mm^2) on different surfaces (*y*-axis has a logarithmic scale). Different letters (i.e., A, B, and C) indicate statistically significant difference ($p < 0.05$).

HNSA were 6.05 ± 0.02 log cells/mm^2, 5.23 ± 0.04 log cells/mm^2, and 2.89 ± 0.10 log cells/mm^2, respectively. These data indicate that bacterial adhesion was reduced by 84.90 ± 1.52% on hydrophobic quartz compare to bare quartz. The reduction reached up to 99.93 ± 0.02% on HNSA. Statistical analysis revealed that bacterial (i.e., *E. coli* O157:H7 and *S. aureus*) reduction on each surface with respect to bacterial types were not statistically significant ($p \geq 0.05$), which means they show similar reduction behavior.

Differences in bacterial adhesion behavior were observed on hydrophilic and

hydrophobic surfaces. This phenomenon can be explained in terms of the hydrophobic effect. It is known that bacteria with high surface hydrophobicity adhere more extensively on hydrophobic surfaces while bacteria with low surface hydrophobicity prefer hydrophilic surfaces.[96] Hence, considering that *E. coli* O157:H7 and *S. aureus* are hydrophilic with water contact angles of 15–32°,[99] our observed trends are in accordance with prior studies.

However, the reduction in bacterial adhesion to HNSA compared to hydrophobic quartz cannot be entirely explained by the hydrophobic effect. We attributed the superior bacterial antiadhesion characteristics of HNSA to two phenomena: (i) the formation of air pockets upon contacting with aqueous suspensions and (ii) the reduction of van der Waals interactions between bacteria and HNSA due to the porosity. First, considering the highly hydrophobic nature of HNSA, the trapping of air pockets inside surface roughness is likely to occur. Such gas pockets have previously been reported to prevent bacteria to reach the crevices and valleys of surfaces.[142] This phenomenon reduces the effective contact area between bacteria and solid surfaces, thereby leading to the reduced probability of adhesion. Second, since both hydrophobic quartz and HNSA were functionalized with methyl groups, van der Waals interactions are expected to make a significant contribution to the bacterial adhesion on these surfaces. As a first approximation, van der Waals interactions are additive (body forces), and can, hence, be calculated by integrating the pairwise potentials from individual dipoles that are distributed over the volume of bacteria and HNSA.[143,144] Hence, one can expect that the attractive van der Waals interactions between bacteria and HNSA will significantly weaken due to the presence of pores in HNSA.

However, this is only true when pores are filled with air (or empty), not filled with water. To check this point, using spectroscopic ellipsometry, the refractive index of HNSA was measured under dry conditions and after submerging in bacterial suspensions for 4 h and found to be 1.008 ± 0.001 and 1.013 ± 0.001, respectively. These values are much lower than the refractive index of nonporous silica materials (i.e., 1.45–1.55), indicating that almost all pores are filled with air.

Table 2. Screening of antimicrobial activity of HNSA against *E. coli* O157:H7 and *S. aureus*. Different letters (i.e., A and B) indicate statistically significant difference ($p < 0.05$).

Bacteria	Negative control[a]	with HNSA[b]	with 1% bleach solution[c]
***E. coli* O157:H7**	1.2×10^9 CFU/mL (A)	1.3×10^9 CFU/mL (A)	<1 (zero) CFU/mL (B)
S. aureus	4.3×10^8 CFU/mL (A)	3.8×10^8 CFU/mL (A)	<1 (zero) CFU/mL (B)

[a]Bacteria cultured under standard growth conditions. [b]Bacteria cultured in the presence of HNSA. [c]Bacteria cultured in the presence of 1% bleach solution.

4.3.5. Screening of Antimicrobial Activity

To confirm that our observation is due to the antiadhesion properties of material not antimicrobial activity, additional screening tests were performed. Studies of *E. coli* O157:H7 and *S. aureus* growth were carried out in the presence of HNSA and 1% bleach solution by pour plate method (Table 2). Comparison of bacterial colony-forming unit (CFU) revealed that 8–9 log reduction was observed for samples containing 1% bleach solution. On the other hand, bacterial growth behavior was similar in the absence (negative control) and in the presence of HNSA. Overall, antimicrobial activity

was not detected in samples tested with HNSA, showing bacterial antiadhesion properties of HNSA is indeed responsible for the observed inhibitory effects.

4.4. Conclusions

Nanoporous silica aerogels were synthesized by using a sol-gel method and modified into a hydrophobic surface via a silane-based methylation reaction. The success of surface modification and hydrophobization was confirmed using ATR-FTIR spectroscopy, XPS, and contact angle measurements. Hydrophobically-modified nanoporous silica aerogel (HNSA) showed excellent antiadhesion properties against common Gram-negative and Gram-positive bacterial pathogens (i.e., *E. coli* and *S.aureus*) that cause nosocomial infections. The superior antiadhesive behavior was attributed primarily to the formation of air pockets preventing bacteria to reach to crevices and valleys of surfaces, and secondarily to the decreased strength of attractive van der Waals interactions between bacteria and HNSA due to the reduced body-forces arising from the existence of pores throughout HNSA. Overall, the observed bacterial antiadhesion properties of HNSA, combined with its other intriguing properties such as extremely light weight, superior acoustic absorption, and biocompatibility can offer new opportunities in designing novel multifunctional hygienic materials for healthcare environment.

CHAPTER V

BACTERIALLY ANTIADHESIVE, OPTICALLY TRANSPARENT SURFACES INSPIRED FROM RICE LEAVES*

5.1. Introduction

Bacterial fouling is responsible not only for the functional deterioration of numerous surfaces and devices but also for the transmission of infection and disease through such surfaces and devices.[2] Bacterial adhesion to a surface, which is the first step in bacterial fouling, is governed by the interplay among the physicochemical, interfacial, and geometrical characteristics of the surface and bacteria.[145] Hence, various surface-modification approaches have been applied and considered to manipulate the interactions between bacteria and surfaces and to prevent bacterial attachment to surfaces.[24,30,127] To this end, in particular, surfaces based on nature-inspired approaches have shown promising potential in the reduction and inhibition of bacterial adhesion.[33,125] In the light of increasing global concerns about antimicrobial resistance (AMR),[29] such surfaces are increasingly needed to provide alternative or complementary solutions to antimicrobial surfaces.

One of the key challenges for nature-inspired bacterial antiadhesive surfaces is the integration of transparency and the bacterial antiadhesion within a single surface. This is

*Reprinted with permission from "Bacterially antiadhesive, optically transparent surfaces inspired from rice leaves" by Jun Kyun Oh, Xiaoxu Lu, Younjin Min, Luis Cisneros-Zevallos, Mustafa Akbulut, 2015. *ACS Applied Materials & Interfaces*, 7, 19274–19281, Copyright 2015 by American Chemical Society.

primarily because surface texture and roughness including the ones inspired from biological materials often lead to light scattering as predicted by analytic scattering models and rigorous electromagnetic theories.[146,147] The transparency is generally inversely correlated with the scattering of light.[148] With the increasing number of emerging biomedical applications and optical devices requiring high levels of transparency, as well as operations in bacterial media,[12,13] the need for overcoming this challenge has intensified.

Plant tissues display a unique and rich variety of optical properties governed by their ultrastructure.[149] When light travels across different tissue layers, its characteristics are modified. Depending on the photosynthetic or photomorphogenic needs, a tissue layer can be responsible for light propagation, light trapping, light gradients, focusing and lens effects, and wavelength-specific surface reflection.[150] For instance, to achieve the efficient use of light energy, upper layers of most leaves (i.e., cuticle and epidermis) are often designed to allow an efficient passage of light.[151] On the other hand, the mesophyll, which is packed with chloroplasts, is responsible for the scattering and absorption of light.[152] One can hypothesize that it is possible to use the guiding principles behind plant tissues to design new optical materials through bioinspiration.

Herein, we report a rice leaf-inspired approach to produce novel surfaces with optical transparency and repellency against bacterial suspensions. The rice leaf was especially selected for bioinspiration due to its unique hollow nanodisc texture, which reduces "the total roughness volume" compared to solid pillar-type bioinspirations. The biomimetic "rice leaf-like surfaces" (RLLS) showed strong water and bacterial suspension repellency with static contact angles of 155.7 ± 1.2° and 150.6 ± 1.0°, respectively. In

addition, RLLS displayed excellent bacterial antiadhesion properties with an adhesion inhibition efficiency of >99.9% for both pathogenic Gram-negative *Escherichia coli* O157:H7 and Gram-positive *Staphylococcus aureus* in comparison to pristine quartz surfaces (negative control). In this study, these two microorganisms were selected for two reasons: first, pathogenic bacterial strains tend to adhere to surfaces more strongly than nonpathogenic ones;[153] and second, according to the US Centers for Disease Control and Prevention (CDC), the most common pathogens that cause hospital-acquired infections are *E. coli*, *S. aureus*, and *Pseudomonas aeruginosa*. Furthermore, RLLS demonstrated optical-grade transparency (i.e., ≥92% transmission) due to the relatively small roughness volume achieved through hollow nanodisc morphology.

5.2. Materials and Methods

5.2.1. Leaf Materials from Rice Plant

Fully developed rice leaf (*Oryza sativa* L. ssp. *japonica* cv. Calmati-202) was obtained from the Division of Agriculture and Natural Resources at University of California, Davis, CA, USA. The received rice leaves were kept in a water bath before use. Fresh leaves were cut into 5 mm × 5 mm flat areas and immediately used afterward to prevent drying.

5.2.2. Bioinspired Surface Preparation

Quartz (SiO_2) slides (Ted Pella, Inc., Redding, CA, USA) cut into 1 cm × 1 cm × 1 mm were first rinsed with water purified by a Milli-Q Advantage system A10 (EMD Millipore Corp., Billerica, MA, USA), yielding Milli-Q water with resistivity of 18.2

MΩ·cm, and left to dry at room temperature (23 °C). Subsequently, oxygen plasma treatment by CS-1701 reactive-ion etcher (RIE; Nordson MARCH, Concord, CA, USA) was applied to remove organic adsorbates on the surfaces: these slides were used as hydrophilic quartz controls. “Rice leaf-like surfaces” (RLLS) were fabricated by self-masking reactive-ion etching (SM-RIE) of quartz surfaces for which the operational parameters were critical in manipulating surface morphology. The following conditions gave rise to RLLS: flow rates of tetrafluoromethane (CF_4) at 22.5 sccm and oxygen (O_2) at 2.5 sccm, pressure of 80 mTorr, radio frequency (RF) power of 200 W, and etching time of 20 min.

To enable superhydrophobicity, the etched quartz surfaces with rice leaf-like surface texture were functionalized with trimethylsilyl chloride (TMCS; Sigma-Aldrich Co., St. Louis, MO, USA) by placing these in 6% TMCS in hexane (Avantor Performance Materials, Inc., Center Valley, PA, USA). The silanation reaction was allowed to take place for 24 h. Afterward, surfaces were rinsed with hexane and dried under a stream of nitrogen gas (N_2; Brazos Valley Welding Supply, Inc., Bryan, TX, USA) before use. The same functionalization procedure was also used for the smooth (unetched) quartz surfaces to create hydrophobic quartz controls.

5.2.3. Physical and Chemical Characterization of Surfaces

Surface morphology of the samples was characterized using scanning electron microscope (SEM, JSM-7500F; JEOL, Tokyo, Japan). In SEM experiments, the surfaces were coated with 8 nm of platinum/palladium (Pt/Pd) to reduce charging effects.

The surface roughness was quantified by atomic force microscopy (AFM,

Dimension Icon; Bruker, Santa Barbara, CA, USA). Amplitude and height images were obtained in the tapping mode. The silicon tip cantilever with nominal spring constant of 0.4 N/m, nominal tip radius of 2 nm, and the nominal resonant frequency of 70 kHz were used.

The TMCS functionalized silica-based materials (i.e., quartz and RLLS) were characterized using attenuated total reflectance-Fourier transform infrared (ATR-FTIR) spectroscopy. ATR-FTIR spectra were recorded on an IRPrestige-21 (Shimadzu Corp., Kyoto, Japan) system and analyzed using IRsolution (Shimadzu Corp., Kyoto, Japan) software version 1.40.

X-ray photoelectron spectroscopy (XPS) measurements of TMCS coverage on silica surfaces were characterized using PHI VersaProbe II Scanning XPS Microprobe (Physical Electronics, Chanhassen, MN, USA). The measurements were carried out using an Al Kα radiation source (1486.6 eV) operating at 25 W and under high-vacuum conditions at a pressure of 10^{-7} Pa.

To determine the wetting characteristics of surfaces, static and dynamic contact angles of water and bacterial suspension were measured.[154] The contact angles were analyzed by contact angle plug-in for ImageJ (National Institutes of Health (NIH), Bethesda, MD, USA) software. The contact angle values reported on each surface were obtained by averaging six measurements at room temperature (23 °C).

5.2.4. Growth and Maintenance of Microorganisms

Escherichia coli O157:H7 and *Staphylococcus aureus* were obtained from the Food Microbiology Laboratory Culture Collection in the Department of Animal Science

at Texas A&M University, College Station, TX, USA. Working cultures of *E. coli* O157:H7 and *S. aureus* were grown in tryptic soy broth (TSB; Becton, Dickinson and Co., Sparks, MD, USA) with 24 h incubation aerobically at 37 °C. A loopful of bacterial culture in TSB was transferred twice to fresh TSB every 24 h and reincubated at 37 °C, resulting in bacterial suspensions to a final concentration of 8.7–9.1 log CFU/mL.

5.2.5. Bacterial Adhesion Assay Under Static Conditions

Rice leaves cut into 5 mm × 5 mm were immersed in 9.0 mL of bacterial suspensions (8.7–9.1 log CFU/mL) and incubated for 4 h at room temperature (23 °C). The treated rice leaves were then gently removed from the bacterial suspensions to count attached bacteria on surfaces. When removing the samples, we made sure that samples were drawn in a single vertical motion from the bacterial suspension and held vertically for 3 min to allow remaining droplets to slide away so that drying effects were not superimposed on the results of adhesion. All inoculation experiments were replicated four times. The same experimental procedure was used for pristine quartz, hydrophobic quartz, and RLLS.

SEM was employed to quantify the attachment of *E. coli* O157:H7 and *S. aureus* on various surfaces. After acrolein (Sigma-Aldrich Co., St. Louis, MO, USA) inactivation, 10 nm of gold (Au) coating was applied to sample surfaces to ensure electrical conductivity required by SEM technique. For quantitative analysis, 100 μm × 100 μm of SEM images from at least nine different areas were analyzed to count the number of attached bacteria. Experiments were repeated three times for each sample.

5.2.6. Bacterial Adhesion Assay Under Dynamic Conditions

Flow experiments were carried out using a custom flow chamber with 1 cm × 1 cm window made out of the material of interest. Bacterial adhesion behavior on RLLS window was compared with pristine quartz window (uncoated) and hydrophobic quartz window (methylated) by replacing the chamber window in each experiment. For all surfaces, the flow rate of bacterial suspension inside the chamber was controlled to be 2.5 μL/s.

Images of flowing bacteria were visualized using differential interference contrast (DIC) microscopy (Stallion Digital Imaging Workstation; Carl Zeiss, Jena, Germany) at a frame rate of 0.5 fps. Movies created by stacking images obtained at various time points were analyzed manually with ImageJ software to count attached bacteria on surfaces.

5.2.7. Screening of Antimicrobial Activity

To determine if antimicrobial activity or bacterial antiadhesion is responsible for the observed trends, *E. coli* O157:H7 and *S. aureus* strains were grown in the presence of TMCS-functionalized RLLS and in the presence of 1% (v/v) bleach solution for 4 h at room temperature (23 °C). Bacteria in the absence of any treatment were used as negative controls. To count the number of bacteria remaining, pour plate method was used by taking 1.0 mL of bacterial suspension from each dilution to make serial dilutions. The results are reported as colony-forming units per milliliter (CFU/mL) and replicated three times.

5.2.8. Optical Transparency

Transparency of material was studied by measuring transmittance via UV-vis-NIR spectrophotometry (U-4100; Hitachi, Tokyo, Japan). Transmission spectra were recorded

at a wavelength range of 400–800 nm.

5.2.9. Pressure and Chemical Stability Tests

Autoclaving is one of the most effective and common methods for sterilization. To confirm mechanical stability of RLLS upon autoclaving, RLLS was placed in an autoclave (Amsco Lab 250; Steris Corp., Mentor, OH, USA) chamber at 121 °C for 20 min under 20 psi pressure conditions.

Chemical stability of RLLS immersed in 10% hydrogen peroxide (H_2O_2, 30% solution; Avantor Performance Materials, Inc., Center Valley, PA, USA) solution was monitored as a function of time. To confirm if any of surface groups are detaching from RLLS with time, aliquots from the solution containing immersed RLLS were collected and analyzed using ATR-FTIR spectroscopy at 4 h, 3 days, 1 week, 2 weeks, and 3 weeks.

5.2.10. Statistical Analysis

Statistical analysis was performed by using the statistical package for Microsoft Office Excel (Microsoft Corp., Redmond, WA, USA) software. Microbiological data from microscope images were log-transformed prior to statistical analysis. One-way and two-way analysis of variance (ANOVA) with Tukey's post hoc test was used to determine statistical significance of differences between microbiological data from surface types and types of bacteria at a *p*-value of <0.05.

5.3. Results and Discussion

5.3.1. Interfacial and Bacterial Adhesion Characteristics of Rice Leaf

Plant surfaces, highly sophisticated structures, are responsible for multiple

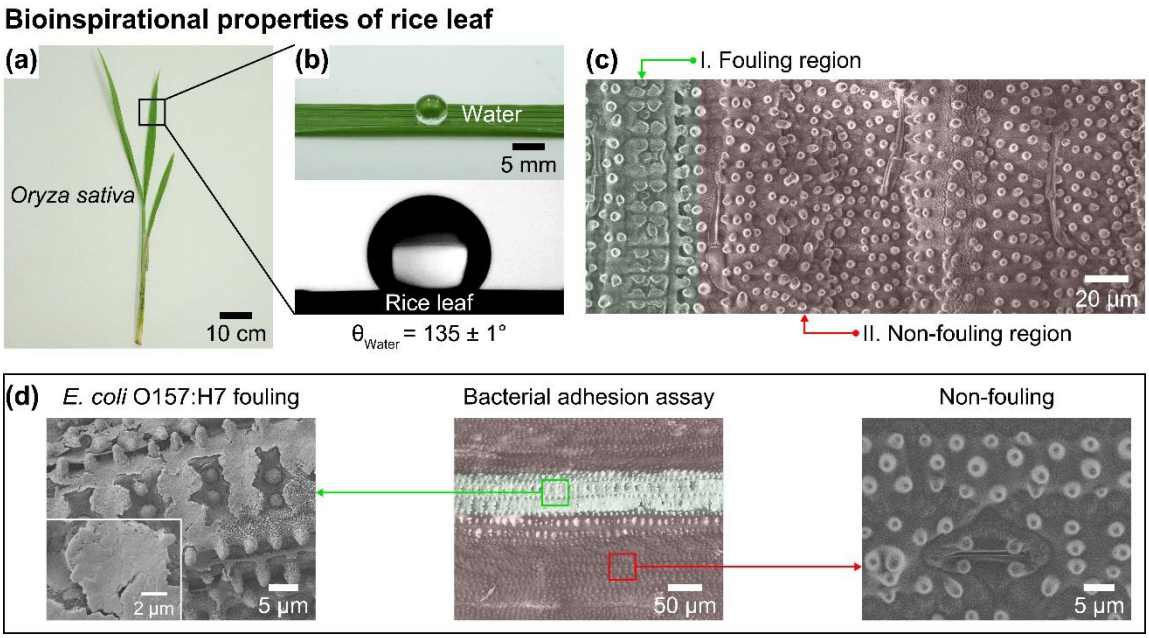

Figure 23. (a) Photograph of *Oryza sativa* rice leaf, (b) wetting characteristics of water on rice leaf, (c) SEM micrograph showing the texture (ultrastructure) of rice leaf, and (d) bacterial adhesion behavior on rice leaf.

functions such as the reduction of water loss, the control of surface wetting, the recognition of pathogens and insects, the inhibition of contaminant adhesion, the maintenance of physiological integrity, and the reduction of surface temperature. These functions are strongly dependent on the surface chemistry and structure.[155] As such, our initial focus was on the interfacial characteristics of rice leaves (*Oryza sativa*), which resulted in a water contact angle of 135.1 ± 1.4° on them under static conditions, indicating their highly hydrophobic nature (Figures 23(a),(b)). The morphology responsible for such a wetting behavior involved multiple length scales: (i) submillimeter-scale groove array with an average width of 155.4 ± 14.2 μm and depth of 19.6 ± 1.7 μm, (ii) highly ordered, microscale, and clover-shaped features located on the apex of grooves with a radius of 6.3 ± 0.5 μm, and (iii) hollow microdiscs located at the bottom and sides of grooves with an

outer diameter of 3.4 ± 0.5 μm, inner diameter of 1.5 ± 0.4 μm, and height of 3.4 ± 0.6 μm (Figure 23(c) and see Appendix C: Supplemental Information, Figure 41). Previous studies on rice leaves reported that the microdiscs and microclovers are responsible for their superhydrophobicity while the groove arrays provide an energy barrier to travel in orthogonal directions and contribute to the anisotropic sliding phenomenon.[156]

It is known that surface roughness and texture can greatly influence bacterial adhesion.[20] Hence, after characterizing the surface structure of rice leaves, we focused on their bacterial adhesion behavior. As shown in Figure 23(d), there were two distinct behaviors: while there was significant bacterial (*E. coli* O157:H7) adhesion on the regions where microclovers are located, i.e., the apex of grooves, there was no detectable bacterial adhesion on the regions where microdiscs are located, i.e., the bottom and sides of grooves. This trend can be attributed to the morphological characteristics of bacterial antiadhesion regions: micropillar-type structures including microdiscs are known to often cause the transition from the Wenzel state to the Cassie-Baxter state, where the formation of air pockets can prevent bacterial attachment.[43] In addition, due to their hollow nature, the total volume of air pockets on hollow microdiscs can be enhanced in comparison to the Cassie-Baxter state of solid microdiscs and micropillars, thereby further inhibiting bacterial access to the surface. In addition to the surface structure, there may be additional factors responsible for the observed trend such as surface chemistry of microdiscs (see Appendix C: Supplemental Information for further discussion).

5.3.2. Fabrication of RLLS

Bioinspired surfaces are typically fabricated via bottom-up approaches such as

layer-by-layer assembly and nanoparticle deposition, direct replicating method using polymers (e.g., polydimethylsiloxane, poly(vinyl alcohol), and polyurethane), and top-down approaches such as soft lithography.[157] The main limitation of bottom-up approaches is the challenges associated with their scale-up and mass production.[158] Direct replicating method allows only the exact replication of surface texture. When a modification in the texture size or dimension of the fabricated surface is needed, this approach becomes unfeasible. Furthermore, direct replication often relies on soft, low adhesion energy polymers to enable their peeling off from the original pattern.[159] However, such soft polymers tend to suffer from the lack of mechanical and scratch resistance.[160] Top-down photolithography, the most common method to fabricate nature-inspired surfaces, requires multiple steps, i.e., exposure, development, deposition, and lift-off.[161]

Here, we describe a self-masking reactive-ion etching (SM-RIE) approach that overcomes the above-mentioned limitations (Figure 24(a)). The principles driving the formation of hollow nanodiscs were that (i) due to the preferential vertical transport of ions, RIE gives rise to anisotropic etch profiles;[162] (ii) due to its crystal structure, the etching rates show variations in different crystal planes of quartz;[163] and (iii) RIE using CF_4 often leads to the polymerization of fluorocarbons (C_xF_y),[164] which can form nano/microdroplets on quartz and act as masks for directing etching.[165,166] SM-RIE allowed a strong control over topographical and structural characteristics of the surfaces by adjusting etching time, CF_4/O_2 flow rates, pressure, and radio frequency (RF) power (see Appendix C: Supplemental Information, Figure 42). At relatively low CF_4/O_2 flow rates and low RF power, it was possible to produce hollow nanodiscs that mimicked rice

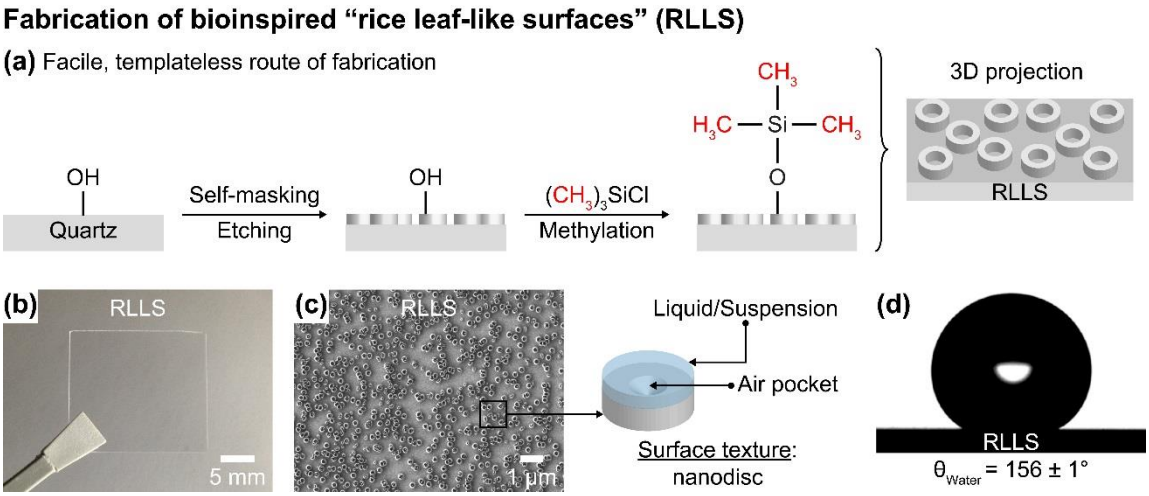

Figure 24. (a) Fabrication process of bioinspired "rice leaf-like surfaces" (RLLS), (b) photograph of RLLS, (c) SEM micrograph of RLLS surface, and (d) wetting characteristics of water on RLLS. Statistical analysis of SEM and AFM micrographs revealed that inner diameter of nanodiscs was 163.0 ± 10.5 nm, outer diameter was 198.2 ± 9.3 nm, height was 436.7 ± 12.6 nm, average spacing between nanodiscs was 214.6 ± 153.4 nm, and ratio of the total rim area to total projection area was ~0.06.

leaf in a single-step process (Figures 24(b),(c)).

5.3.3. Wetting Characteristics of RLLS

Hydrophilic materials tend to aggregate on hydrophilic surfaces.[22] While bacteria can adhere on both hydrophobic and hydrophilic surfaces, bacterial attachment tends to occur significantly more on hydrophilic surfaces due to their hydrophilic nature.[23] Therefore, it is necessary to investigate the wetting characteristics of the developed surfaces to gain insight into their bacterial adhesion behaviors. The static water contact angle measurements revealed that, while the pristine quartz was hydrophilic ($\theta < 10.0°$), methylated quartz ($\theta = 95.9 \pm 1.1°$) and RLLS ($\theta = 155.7 \pm 1.2°$) were hydrophobic and superhydrophobic, respectively (Figure 24(d)). The super-repellency of surfaces was also valid for concentrated *E. coli* O157:H7 suspension (9.1 ± 0.1 log CFU/mL) with a static

contact angle of $\theta = 150.6 \pm 1.0°$ (see Appendix C: Supplemental Information, Figure 43), which is quite useful for various purposes such as stain release, lubricity, and water repelling.[167,168] Advancing and receding contact angle measurements revealed that water and bacteria suspension had contact angle hysteresis of ~2.5° and ~2.1°, respectively. Such low hysteresis indicates that RLLS surface is uniform and fairly homogeneous and that interaction between surface and liquid (or suspension) is weak.[169]

Slight differences in surface tensions of water ($\sigma = 72.1$ mN/m) and bacterial suspensions ($\sigma = 66.3–69.7$ mN/m) are likely to be responsible for ~5.0° difference in static contact angle and dynamic contact angle measurements.[170] Approximately 85.0° increase in the contact angle changing from pristine quartz to methylated quartz is attributed to the surface chemistry effect, due to intrinsically low surface energy of the methyl group.[171] On the other hand, a difference of ~60.0° in the contact angle of methylated quartz and RLLS is ascribed to the surface roughness and topography.[95]

5.3.4. Investigation of Bacterial Adhesion on RLLS Under Static Conditions

Hydrodynamics can significantly influence the transport of bacteria from bulk liquid to surfaces.[172,173] Hence, bacterial adhesion to the developed surface was investigated under both static and dynamic conditions. Upon inoculating surfaces with bacterial suspension—i.e., *E. coli*O157:H7 or *S. aureus* at a concentration of 8.7–9.1 log CFU/mL under static conditions for 4 h—pristine quartz, hydrophobic quartz, and RLLS surfaces displayed significantly different bacterial adhesion behavior (Figures 25(a)–(c)). To be specific, for *E. coli* O157:H7, the pristine quartz surface supported the greatest bacterial adhesion with a mean density of 5.8 ± 0.0 log cells/mm^2. When the quartz was

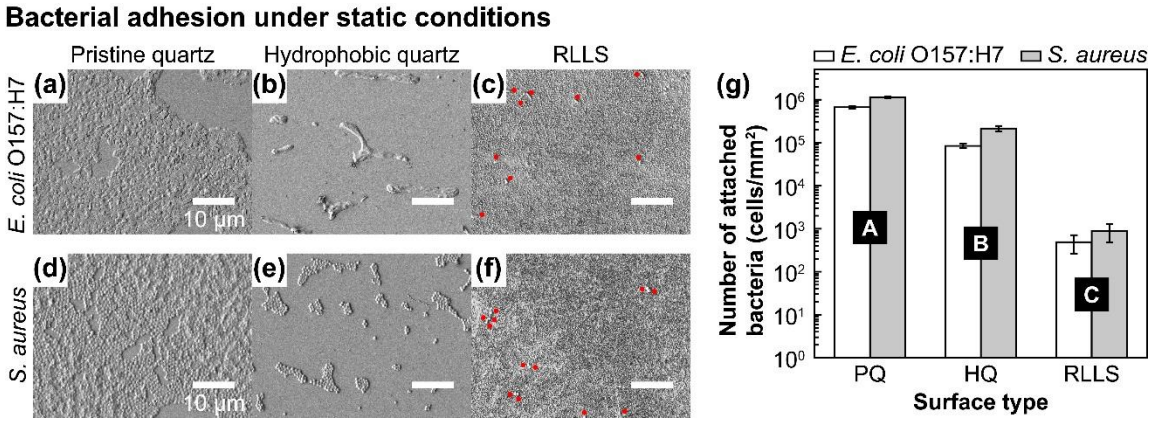

Figure 25. SEM micrographs of bacterial attachment on pristine quartz (PQ), hydrophobic quartz (HQ), and RLLS surfaces for (a)–(c) *E. coli* O157:H7 and (d)–(f) *S. aureus* (bacteria on RLLS surfaces were highlighted with red). (g) The bacterial attachment density as a function of surface type. Different letters (i.e., A, B, and C) indicate statistically significant differences ($p < 0.05$).

methylated, the bacterial adhesion significantly decreased to a mean density of 4.9 ± 0.1 log cells/mm^2. Ultimately, significantly less bacterial adhesion was detected on RLLS surfaces, counts were 2.7 ± 0.2 log cells/mm^2, corresponding to >99.9% reduction in bacterial adhesion in comparison to pristine quartz surfaces. As shown in Figures 25(d)–(f), similar trends were also observed for *S. aureus*: the number of adherent bacteria decreased from 6.1 ± 0.0 to 2.9 ± 0.2 log cells/mm^2 upon changing the surface from pristine quartz to RLLS. A closer look at Figures 25(c),(f) revealed that the attachment of bacteria was correlated with the existence of unpatterned regions (see Figure 24(c)) on RLLS. This result further highlights the importance of hollow nanodisc texture in preventing bacterial attachment (see Appendix C: Supplemental Information, Figure 44 for further comparison). Figure 25(g) summarizes these adhesion behaviors of *E. coli* O157:H7 and *S. aureus* with respect to surface type.

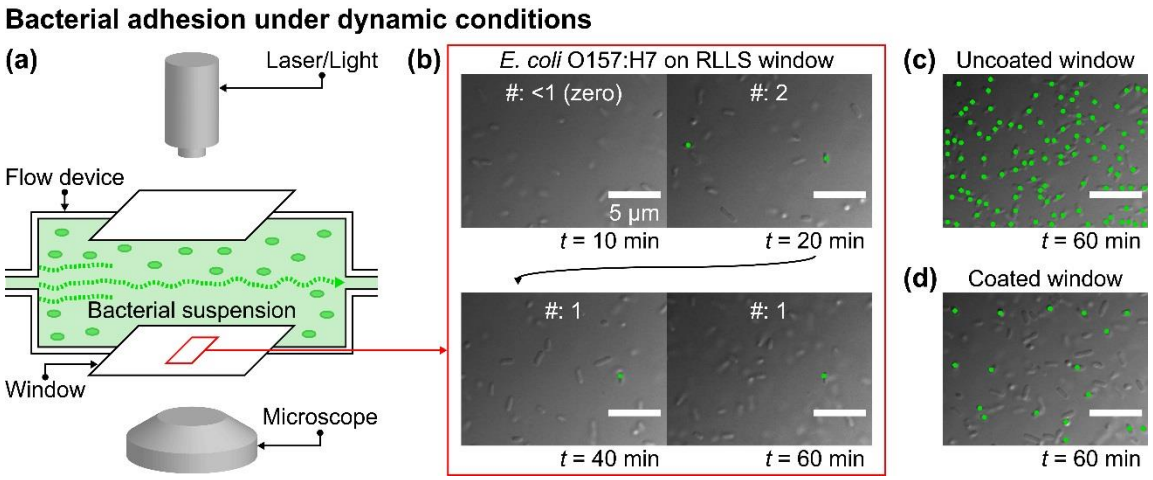

Figure 26. (a) Schematic illustration of the experimental setup used in studying bacterial adhesion under dynamic conditions. (b) Time-resolved micrographs of bacterial attachment on RLLS window obtained via differential interference contrast (DIC) microscopy. The fully adhered bacteria are highlighted with green. Comparison of bacterial attachment on RLLS with (c) uncoated window and (d) coated window (methylated) at a dynamic bacterial exposure time of 60 min.

5.3.5. Investigation of Bacterial Adhesion on RLLS Under Dynamic Conditions

Prior studies have shown that the presence of a flow-field can facilitate or hinder the bacterial adhesion on a surface depending on the shear rates. In general, low shear rates result in an increased adhesion whereas high shear rates lead to a decreased adhesion.[174–176] Therefore, there is a need to ensure that the developed surfaces are also effective in reducing bacterial attachment under the flow conditions that promote bacterial adhesion. To this end, real-time bacterial adhesion behavior on RLLS was monitored using a customized flow chamber that imitates a typical fluidic channel of biosensor at low flow (shear) rates. The developed surface demonstrated excellent bacterial (Gram-negative *E. coli* O157:H7) antiadhesion properties during dynamic flow conditions (Figures 26(a),(b)). Similar reduction trends were also observed against Gram-positive *S. aureus*. The number

of adhering bacteria on RLLS was mostly constant during the continuous operation of 60 min, indicating the bacterial antiadhesion characteristics of these surfaces. On the other hand, the number of adhering bacteria increased linearly with increasing flow time for pristine and methylated quartz window surfaces (Figures 26(c),(d) and see Appendix C: Supplemental Information, Table 3). The previous studies reported that the initial stages of bacterial adhesion tend to follow a linear adhesion kinetics with respect to time,[139,177–179] which is consistent with the trends observed in pristine and methylated quartz surfaces. The loss of sensitivity in biosensors due to the accumulation of bacteria on flow chamber windows is a major problem in diagnostic assays.[180] The superior bacterial antiadhesion properties of RLLS window can help maintain sensor sensitivity by minimizing distortions in the light or laser path (i.e., interference, absorption, and reflection), flow direction, and flow velocity occurring through bacterial adhesion.

RLLS was chemically functionalized with a monolayer of TMCS in this study. If TMCS leaches away from the surfaces, it may lead to bacterial killing through an (unexpected) antibiotic effect. Hence, to determine whether the observed trends are indeed due to antiadhesion properties rather than an antimicrobial effect, a bacterial proliferation assay was performed. The data showed that the growth of bacterial cultures did not change in the presence of RLLS: bacterial concentrations reached ~8–9 log CFU/mL for both standard culture media (negative control) and standard culture media containing RLLS surface (see Appendix C: Supplemental Information, Figure 45).

5.3.6. Possible Mechanisms of Bacterial Antiadhesion

The desirable antiadhesion characteristics can be attributed to two factors: (i) a

large volume of air pockets (gaps) and (ii) a small ratio of the total rim area to the total projection area. First, the contact angle data indicated the superhydrophobic nature of RLLS. Superhydrophobic surfaces are associated with the transition from the Wenzel state to the Cassie-Baxter state and the formation of air pockets.[43] The presence of air pockets constitutes a physical barrier for bacteria to reach the material surfaces. Second, the structural characterization of hollow nanodiscs indicated that the areal ratio of solid/liquid interface to gas/liquid interface is small (i.e., ~0.06) due to their hollow nature. This information, coupled with the fact that the rim width (i.e., ~9 nm) of nanodiscs is much smaller than the length scales of bacteria (i.e., ~500−4000 nm), suggests a decreased probability for a bacterium to find a solid surface on which to attach itself (see Appendix C: Supplemental Information, Figure 46).

5.3.7. Optical Transparency of RLLS

Although the developed materials have very promising bacterial antiadhesion and superhydrophobic properties, they cannot be used as the components of bio-optical devices unless these satisfy the optical-grade transparency, i.e., ≥92.0% within the visible light spectrum from 400 to 700 nm. It is a well-known challenge that typical surface topography and roughness modification strategies used for producing superhydrophobic surfaces lead to the loss of transparency to the levels below 90%, sometimes even down to 60%.[181] By inspiring from the outermost layers of rice leaves, we were able to produce surfaces with hollow nanodisc morphology, yielding optically transparent surfaces (Figures 27(a),(b)). The comparison of transparency via UV-vis-NIR spectrophotometry indicated that pristine quartz (blue square) and RLLS (red circle) had a similar

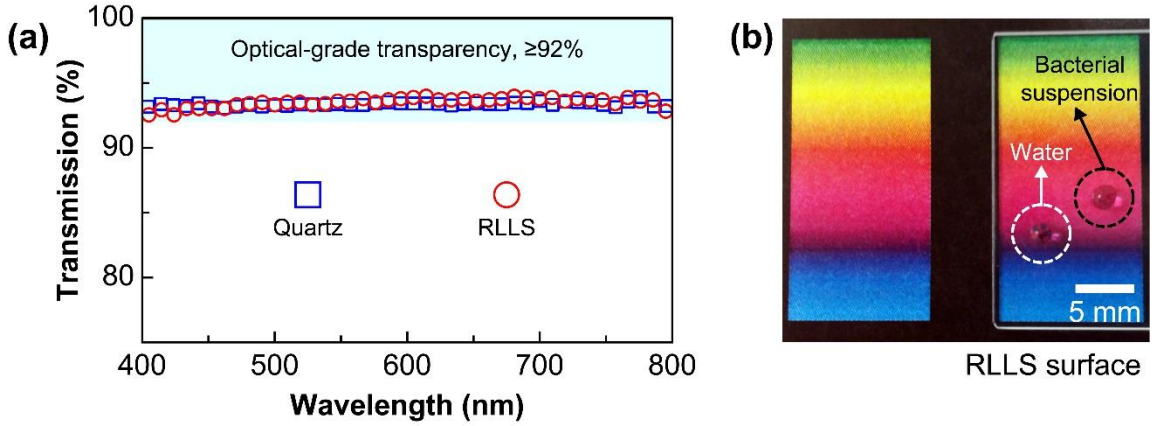

Figure 27. (a) Transmission spectra of pristine quartz (blue square) and RLLS (red circle) obtained by UV-vis-NIR spectrophotometry. (b) Wetting behavior of water and bacterial suspension on transparent RLLS surface.

transmission level of 92% in the visible light spectrum. This is ascribed to the fact that root-mean-square (RMS) roughness of RLLS surfaces (~35 nm) and pristine quartz (~2 nm) was much smaller than the wavelength of visible light.[182]

5.3.8. Mechanical and Chemical Stability

For optically transparent materials, mechanical integrity and robustness of surface texture are important issues to consider because the optical transparency should not deteriorate under operational conditions. As such, RLLS was tested under standard sterilization conditions, which is a 20 min sterilization process at 121 °C and 20 psi by autoclave. These conditions are much harsher than typical operation pressure (i.e., <15 psi) of biosensors and microfluidic devices.[183] It was found that, after autoclaving, no surface deformation occurred, surface superhydrophobicity remained the same, and bacterial antiadhesion properties and optical-grade transparency were also preserved, indicating robust durability of RLLS (see Appendix C: Supplemental Information, Figure 47).

In addition, devices and surfaces coming in contact with bacteria are generally sterilized with chemical sanitizers such as hydrogen peroxide (H_2O_2). Therefore, it is necessary to ensure the chemical stability of the developed bioinspired surfaces in such solutions. To this end, we investigated the chemical stability of functional groups of RLLS in 10% hydrogen peroxide solution over 3 weeks and observed no significant detachment of chemical groups and no change in wetting characteristics of the surface (see Appendix C: Supplemental Information, Figure 48).

5.4. Conclusions

This study presents a single-step approach involving a templateless, self-masking reactive-ion etching for producing rice leaf-inspired surfaces that prevent microorganisms from attaching to them. In particular, bacterial repellency is demonstrated with respect to pathogenic Gram-negative *E. coli* O157:H7 and Gram-positive *S. aureus* under both static and dynamic conditions. The desirable bacterial antiadhesion characteristics of RLLS are ascribed to two factors associated with hollow nanodisc texture: (i) a large volume of air pockets (gaps) and (ii) a small areal ratio of solid/liquid interface to gas/liquid interface. One distinguishing feature of the developed rice leaf-inspired surfaces is that they also display optical-level transparency in the visible spectrum (i.e., ≥92% transmission). The combination of bacterial antiadhesion and optical transparency can be achieved presumably because of a reduced total roughness volume of hollow nanodiscs compared to solid (nonhollow) textures utilized in typical bacterial antiadhesive surfaces. Overall, a synergistic combination of bacterial antiadhesion properties and optical-grade

transparency can open up new avenues in the design of antibiofouling surfaces and be beneficial for a broad set of applications and devices including biosensors, endoscopes, microfluidic, bio-optical, lab-on-a-chip, and touchscreen devices.

CHAPTER VI

SURFACE MODIFICATION OF FOOD PROCESSING AND HANDLING GLOVES FOR ENHANCED FOOD SAFETY AND HYGIENE*

6.1. Introduction

Foodborne illnesses are a global concern as they lead to morbidity and mortality with increasing rates throughout the world.[48,49] Bacterial pathogens such as *Salmonella* spp., *Escherichia coli*, *Campylobacter* spp., *Staphylococcus aureus*, *Listeria monocytogenes*, and *Bacillus cereus* are some of the major causes of foodborne illnesses.[184,185] According to the US Centers for Disease Control and Prevention report 2013, bacterial pathogens account for 70.7% of all foodborne illnesses for meat and poultry, 43.8% for dairy and eggs, 42.0% for grains and beans, 24.1% for fish and shellfish, and 22.3% for produce.[186] Bacterial pathogens can come into contact with food and food products at any stage of "food-preparation", i.e., harvesting, slaughtering, processing, [187]handling, and storage.[188,189] While there are various procedures for effective disinfecting of food-contact surfaces and reducing other bacterial contaminants,[187,190–195] such disinfection could be rescinded due to possible mishandled after cleaning and sanitizing. Hence, it is a common practice to use gloves to handle food and food products after sanitation processes.[196] From a food safety perspective, gloves serve for two purposes:

*Reprinted with permission from "Surface modification of food processing and handling gloves for enhanced food safety and hygiene" by Jun Kyun Oh, William Rapisand, Ming Zhang, Yagmur Yegin, Younjin Min, Alejandro Castillo, Luis Cisneros-Zevallos, Mustafa Akbulut, 2016. *Journal of Food Engineering*, 187, 82–91, Copyright 2016 by Elsevier Ltd.

(i) to reduce the possibility of cross-contamination from food to food and (ii) to eliminate the possibility of transmission of pathogenic bacteria from human hands to food.

While the use of gloves improves food safety and hygiene, and is desired for food processing and handling,[197] gloves are not completely problem-free. For instance, when glove surfaces come into contact with bacterial pathogens, bacterial adhesion occurs and the bacteria can subsequently form biofilm on these surfaces.[51] If formed, bacterial biofilms are particularly difficult to eliminate using hygienic practices such as physical washing (e.g., brushing, scrubbing, and sonication) and chemical treatments (e.g., alcohol-based disinfectant, chlorine-based sanitizer, and hydrogen peroxide-based solution), because bacteria are embedded in their own extracellular polymeric substances (EPSs), which guard bacteria against external physical forces and chemical agents attack.[198] Along these lines,[199] have reported the occurrence of bacterial retention on glove surfaces and the possibility of glove-facilitated bacterial transport. Kotwal et al.[200] found that transfer of *Salmonella* from porcine skins to thick latex, thin latex, and nitrile gloves can take place with the transfer rate of 40%, 27%, and 19%, respectively. Brar and Danyluk[201] reported that *Salmonella* can transfer from disposable latex gloves to tomatoes with a transfer coefficient of 32% and 29% under wet and dry conditions, respectively, and from tomatoes to gloves with a transfer coefficient of 37% and 39% under wet and dry conditions, respectively. Overall, it is fair to claim that wearing gloves does not fully ensure the prevention of cross-contamination and transmission of pathogenic bacteria during food processing and handling.

To avoid the scenarios of cross-contamination and transmission of pathogenic

bacteria through glove surfaces, research efforts have been undertaken, in particular, towards antimicrobial modifications of glove surfaces.[202] Surface functionalization with antimicrobial agents have been shown to be capable of preventing the spread of pathogenic bacteria. For example, antimicrobial agent (i.e., polyhexanide) generating glove surfaces,[203] glove surfaces impregnated with antiseptic dye (i.e., chlorhexidine),[204] and active release of disinfectant (i.e., chlorine dioxide) from the glove surfaces upon stimulation with moisture or light[205] have recently been reported. However, while gloves bearing antimicrobial agents reduce the bacterial growth and improve food safety, there are several issues that still need to be overcome such as the ineffectiveness against antimicrobial-resistant bacteria,[29] the development of antimicrobial resistance (AMR) due to continuous exposure to antimicrobial agents,[122] and the long-term antimicrobial inefficiency.[30]

An alternative approach in reducing cross-contamination and transmission of pathogenic bacteria is the development of bacteria-repellent and antiadhesive surfaces. These surfaces reduce the bacterial adhesion to the surface of interest or repel bacteria from the surface of interest.[14,206] In other words, the goal is to minimize the number of bacteria reaching/attaching to the surface rather than disinfect bacteria reaching/attaching to the surface. Some examples of above-mentioned approaches for food safety applications can be enumerated, such as bacteria-repellent polyethylene glycol (PEG)-coated surfaces,[68] zwitterionic surfaces,[70] functional biomimetic surfaces,[71] nanoporous methylated surfaces,[15] stimuli-responsive surfaces capable of surface deformation induced by shear forces,[33] and multilayer films containing heparin as an antiadhesive agent.[35]

While there are a number of studies reporting applications of these modifications on common food-contact surfaces such as stainless steel,[207] quartz glass,[16] paper,[208] polycarbonate,[209] polytetrafluoroethylene (PTFE),[125] and polyurethane,[210] the incorporation of gloves with bacterial antiadhesion properties have not been achieved yet.

Herein, we report the preparation of gloves with bacterial antiadhesion properties for food processing and handling applications using a scalable and facile dip-coating method. The coating has been applied on the three different types of gloves (i.e., latex, nitrile, and polyethylene) and achieved through the deposition and polymerization of "fluorinated silica nanoparticles" (FSNs) on glove surfaces. To evaluate the bacterial antiadhesion properties of the developed gloves, Gram-negative *S.* Typhimurium LT2 and Gram-positive *S. aureus* were utilized through an inoculation assay. The mechanical durability and chemical stability of FSN-coated gloves were investigated using scanning electron microscopy (SEM), nanotribometry, and attenuated total reflectance-Fourier transform infrared (ATR-FTIR) spectroscopy.

6.2. Materials and Methods

6.2.1. Preparation of Glove Surfaces

Three different types of disposable gloves, i.e., latex (Polymed; Sempermed USA, Inc., Clearwater, FL, USA), nitrile (Upperhand; Maytex Co., Hayward, CA, USA), and polyethylene (Poly-D; Ansell, Richmond, Australia) commonly used glove materials for food processing and handling were prepared for the comparative studies. Gloves were first rinsed with Milli-Q water (resistivity $\geq$ 18.2 MΩ·cm) produced by a Milli-Q water

purification system (Milli-Q Advantage A10; EMD Millipore Corp., Billerica, MA, USA), and left to dry at room temperature (23 °C).

6.2.2. Preparation of FSNs

100 mg of silica (SiO_2; Sigma-Aldrich Co., St. Louis, MO, USA) nanoparticles with average diameter of ~200 nm was suspended in 15 mL of hexane (Avantor Performance Materials, Inc., Center Valley, PA, USA), and then 5 mM of trichloro (1H,1H,2H,2H-perfluorooctyl)silane (FDTS; Sigma-Aldrich Co., St. Louis, MO, USA) was added to obtain "fluorinated silica nanoparticles" (FSNs). FSNs were homogeneously suspended under sonication for 20 min using a probe ultrasonicator (SJIA-2000W; Ningbo Haishu Sklon Electronics Instruments Co., Ltd., Ningbo, Zhejiang, China). The FSN suspension was then left for 1 h to allow the silane to fully react with silica nanoparticles.

6.2.3. Dip-Coating of Glove Surfaces

FSNs were deposited on glove surfaces by dip-coating method (Figure 28). Latex, nitrile, and polyethylene gloves were first cut into 1 cm × 1 cm pieces. Gloves were then dipped into the FSN suspension. The method involved dipping gloves for 30 s and then allowing gloves to dry for 30 s five times over a 5-min period. FSN-coated gloves were then left to dry at room temperature for 24 h.

6.2.4. Surface Characterization

Surface morphology of glove surfaces were examined by scanning electron microscope (SEM, JSM-7500F; JEOL, Tokyo, Japan). Before SEM examination, the samples were coated with 8 nm of platinum/palladium (Pt/Pd) to minimize possible charging effects. The SEM was operated at an accelerating voltage of 1 kV and emission

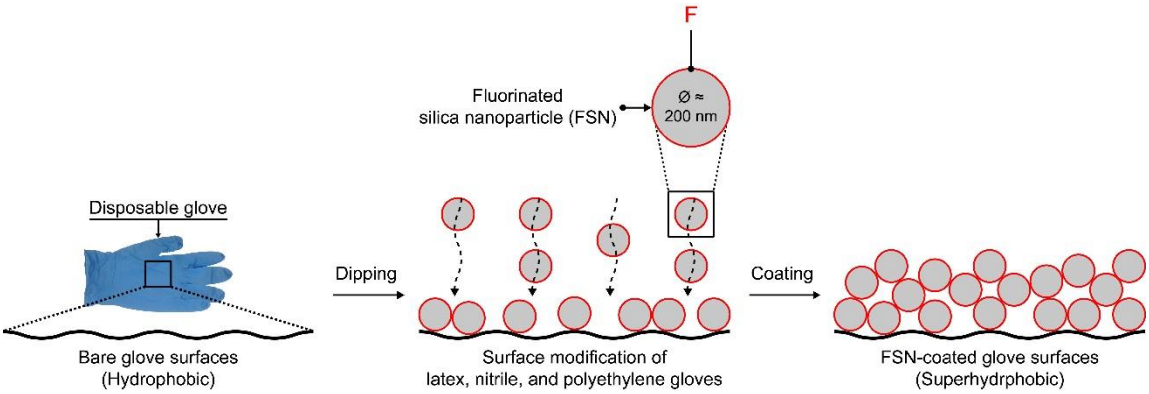

Figure 28. Schematic illustration of surface modification of disposable gloves with "fluorinated silica nanoparticles" (FSNs) to achieve bacteria-repellent and antiadhesion properties.

current of 20 μA.

Topographic characteristics of glove surfaces were investigated by Dektak 3 stylus profilometer (Veeco Instruments, Inc., Plainview, NY, USA) with a scan length of 100 μm to obtain surface roughness values. The samples were mounted on a glass slide by using a double-sided tape and then placed onto the stage to decrease data noise.

The chemical interactions between glove surfaces and FDTS-functionalized silica nanoparticles were characterized by attenuated total reflectance-Fourier transform infrared (ATR-FTIR) spectroscopy technique. ATR-FTIR spectra were measured using IRPrestige-21 (Shimadzu Corp., Kyoto, Japan) system and analyzed using IRsolution version 1.40 software (Shimadzu Corp., Kyoto, Japan).

In order to determine the wetting characteristics of glove surfaces, the static water contact angles were measured for the three different types of glove surfaces using the sessile drop technique. Reported contact angles on each surface were obtained by averaging five measurements at room temperature with the same droplet volume (5 μL).

Contact angles were analyzed using ImageJ software (National Institutes of Health (NIH), Bethesda, MD, USA) via low-bond axisymmetric drop shape analysis (LBADSA) plug-in.[135]

6.2.5. Growth and Maintenance of Microorganisms

Working cultures of *Salmonella enterica* subsp. *enterica* serovar Typhimurium str. LT2 (ATCC 700720) and *Staphylococcus aureus* (Food Microbiology Laboratory, Department of Animal Science, Texas A&M University, College Station, TX, USA) were obtained by scraping a portion of a culture on a tryptic soy agar (TSA; Becton, Dickinson and Co., Sparks, MD, USA) slant, and transferring to 9 mL of tryptic soy broth (TSB; Becton, Dickinson and Co., Sparks, MD, USA). These bacterial cultures were incubated aerobically without agitation at 37 °C for 24 h. After 24 h, a loopful of culture was transferred to fresh TSB, and reincubated at 37 °C for 24 h twice consecutively. The final concentrations reached by *S.* Typhimurium LT2 and *S. aureus* in the growth medium ranged from 8.6 to 9.0 log CFU/mL.

6.2.6. Surface Inoculation

For inoculation, bare and FSN-coated gloves were submerged in 9 mL of a bacterial suspension (8.6–9.0 1og CFU/mL) at room temperature for 1 h and 24 h. The samples were gently removed from the bacterial suspension in a single vertical motion. After, the samples were rinsed in sterile Milli-Q water (10 mL) to dislodge loosely attached cells, and then transferred to sterile Petri dish for further bacterial adhesion assay. Bacteria that were not removed by Milli-Q water rinse were assumed to be attached. All experiments were carried out in an appropriate biological safety cabinet under sterile

conditions. Inoculation experiments were replicated four times.

6.2.7. Bacterial Adhesion Assay

Bacterial attachment on glove surfaces with and without surface modification was assessed by plate count using the pour plating method and by direct enumeration on glove surfaces using SEM. For plate counts, gloves that were dip-inoculated for 1 h were vortex-mixed in 0.1% (w/v) peptone water for 10 min to detach bacteria from the glove surfaces. After, serial dilutions of peptone water containing detached bacteria were made and plated on TSA plate. Bacterial densities were determined after 24 h of aerobic incubation at 37 °C and represented the density of bacteria that were attached onto the glove surfaces. All experiments were replicated four times.

The direct enumeration of attached bacteria on glove surfaces using SEM was conducted on gloves that were dipped in the inoculum for 1 h and 24 h. Prior to SEM imaging, bacteria were inactivated by acrolein (Sigma-Aldrich Co., St. Louis, MO, USA) and a thin layer (10 nm) of Pt/Pd film was deposited on the sample surfaces to ensure the electrical conductivity required by SEM technique. For statistical reliability, at least ten different areas of 100 μm × 100 μm (i.e., entire scan area larger than 100,000 μm^2) from the three different samples of the same type of glove surface were observed. As a direct counting approach, SEM micrographs were analyzed using ImageJ to quantify the attachment of *S.* Typhimurium LT2 and *S. aureus* to glove surfaces.

6.2.8. Mechanical Robustness and Chemical Stability of Glove Coating

Shear strength of glove coating was investigated using a nanotribometer (NTR; Anton Paar TriTec SA, Peseux, Switzerland). Produce-attached tip was used in the

measurements. To prepare produce-attached tip, a spinach leaf cut into 3 mm × 3 mm piece was attached to the tip by using an instant glue. All tests were conducted using a cantilever spring with normal and tangential stiffness of 55.9 N/m and 36.8 N/m, respectively, at normal load of 10 mN, which provides a pressure of ~5000 N/m^2. These experimental conditions were chosen based on a previous report suggesting grip force for common produce, e.g., strawberry (~1300 N/m^2), carrot (~4300 N/m^2), and apple (~5000 N/m^2).[211] Before and after shearing experiments, the presence of wear and surface damage were investigated by SEM examination as well as measuring surface roughness of FSN-coated gloves using a profilometer.

Chemical stability of FSN-coated gloves was determined in deionized (DI) water as a function of time by monitoring if there is any chemical leaching from FSN-coated glove surfaces. This was achieved through analyzing aliquots collected from the samples (i.e., FSN-coated glove pieces submerged in DI water) using ATR-FTIR spectroscopy, with detection limit of <1 ppm. While average time of wearing disposable glove is usually less than 4 h, the measurements were conducted at submersion time of 24 h, which present a sufficient condition.

6.2.9. Statistical Analysis

The microbiological data were log-transformed prior to the statistical analysis. One-way and two-way analysis of variance (ANOVA) with Tukey's post hoc test was used to determine whether there were significant differences in the microbiological data between types of glove surfaces and types of bacteria, at a significance level of 0.05. All statistical analyses were performed using Analysis ToolPak-Excel (Microsoft Corp.,

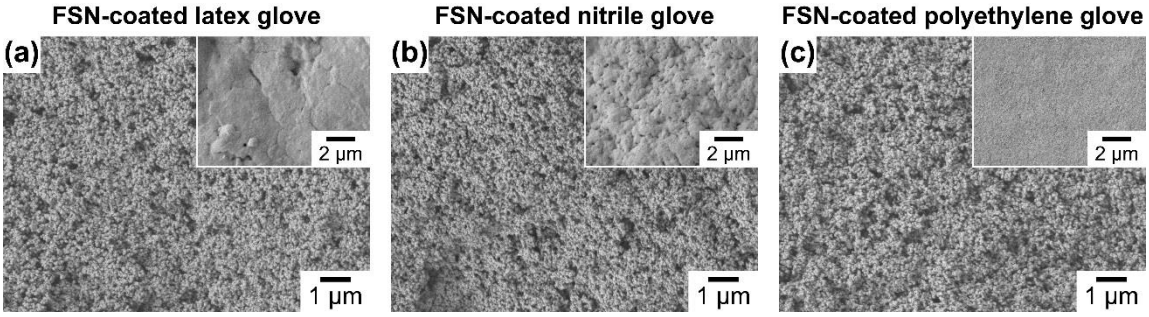

Figure 29. SEM micrographs of FSN-coated (a) latex, (b) nitrile, and (c) polyethylene glove surfaces. Insets: SEM micrographs of bare latex, nitrile, and polyethylene glove surfaces, respectively.

Redmond, WA, USA) via statistical packages.

6.3. Results and Discussion

6.3.1. Characterization of FSN-Coated Glove Surfaces

Previous studies have shown that nanoscale and microscale surface roughness can influence bacterial adhesion.[20,84] When the length scale of surface roughness is larger than bacterial size, bacterial colonization can be enhanced because bacteria prefer to attach to concave surfaces (e.g., valleys, pits, edges, and depressions) due to increase in bacteria-surface total contact area.[47] Hence, we characterized the surface topography of glove surfaces used in this study to better understand their bacterial adhesion behavior. SEM micrographs visually reveal nanostructures covering FSN-coated latex, nitrile, and polyethylene glove surfaces without interstices, as shown in Figures 29(a)–(c). To quantitatively compare the dimensional characteristics of bacterial size and surface roughness of gloves, the profilometer measurements were performed. The surface metrology measurements of FSN-coated latex, nitrile, and polyethylene gloves showed

that the root-mean-square (RMS) roughness were 419 ± 34 nm, 406 ± 28 nm, and 395 ± 40 nm, respectively. This means that surface roughness length scales of FSN-coated gloves were smaller than bacterial size (e.g., rod-shaped *S.* Typhimurium LT2 is 700–1500 nm wide by 2000–5000 nm long and spherical-shaped *S. aureus* is 600–1000 nm in diameter), thereby inhibiting the physical attachment such as penetration and trapping of bacteria into FSN-coated glove surfaces. Moreover, surface roughness of FSN-coated gloves meets the specific surface roughness value (≤800 nm) for proper hygienic design criteria for food-contact surfaces.[11]

For the chemical modification of glove surfaces, fluorinated silane compound is selected due to its high affinity to silica.[212] Also, trifluoromethyl ($–CF_3$) functional groups are preferred over other nonpolar functional groups, because surface energy (γ) decreases as hydrogen (H) atoms are replaced with fluorine (F) atoms in the following orders: $–CH_2 > –CH_3 > –CF_2 > –CF_2H > –CF_3$.[213] While bacteria can adhere on both hydrophilic and hydrophobic surfaces, it is known that bacterial attachment tends to occur significantly more on hydrophilic surfaces.[46] Hence, we used trifluoromethyl functional groups to coat glove surfaces in order to reduce the intermolecular interactions between bacteria and surfaces. The presence of trifluoromethyl groups on glove surfaces was confirmed by ATR-FTIR spectroscopy analysis for all three different types of gloves (Figure 30(a)). To be specific, there was a peak at ~1050 cm^{-1}, corresponding to C–F stretching,[214] for each glove surface upon dip-coating.

Surface topography and chemical properties can act synergistically and influence the ability of water dispersing bacteria to come in contact with surfaces in a non-linear

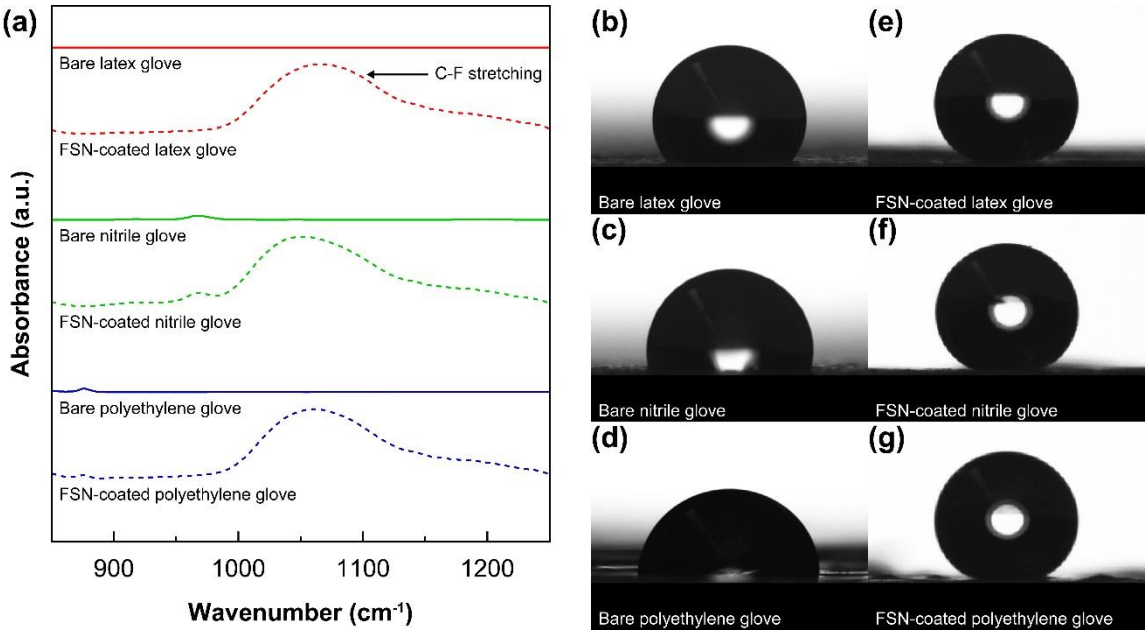

Figure 30. (a) C–F stretching region from ATR-FTIR spectra of bare and FSN-coated gloves. (b)–(g) The static water contact angle measurements of bare and FSN-coated gloves.

fashion by creating air-pockets.[215] As such, we also studied the wetting characteristics of gloves surfaces with water. Figures 30(b)–(g) compare the contact angle of water droplets on bare and FSN-coated glove surfaces. The static water contact angle measurements revealed that bare latex ($\theta = 126.7 \pm 1.4°$), nitrile ($\theta = 97.2 \pm 0.4°$), and polyethylene ($\theta = 90.9 \pm 0.5°$) gloves were hydrophobic. On the other hand, their FSN-coated versions were superhydrophobic with a contact angle of $\theta = 162.5 \pm 0.7°$ (latex), $\theta = 162.7 \pm 1.1°$ (nitrile), and $\theta = 163.9 \pm 0.6°$ (polyethylene). Superhydrophobic surfaces are well-known as having self-cleaning properties (often termed the "lotus effect"), which is beneficial for reducing bacterial adhesion.[126,216]

6.3.2. Bacterial Attachment to Glove Surfaces: Plating Counting Method

After preparing and fully characterizing interfacial properties of the modified

glove surfaces, we compared the bacterial adhesion behavior on such surfaces with that on bare glove surfaces. Figure 31(a) shows the plate count results of the three different types of gloves, following inoculation and attachment of Gram-negative *S.* Typhimurium LT2. The mean populations of bacteria attached on bare latex, nitrile, and polyethylene glove surfaces were 5.3 ± 0.1 log CFU/mL, 5.3 ± 0.1 log CFU/mL, and 5.1 ± 0.1 log CFU/mL, respectively, indicating that these surfaces supported bacterial attachment. When latex, nitrile, and polyethylene gloves were modified with FSNs to achieve a superhydrophobic character, bacterial attachment decreased, as indicated by the mean bacterial populations of 3.4 ± 0.2 log CFU/mL, 3.4 ± 0.1 log CFU/mL, and 3.3 ± 0.1 log CFU/mL, respectively, corresponding to >98.2% in bacterial attachment. One-way ANOVA analysis showed the difference in the adhesion of *S.* Typhimurium LT2 with respect to the presence or absence of coating was statistically significant ($p < 0.05$).

The above observed trends also took place for Gram-positive bacteria, as observed in the plating experiments using *S. aureus*. Figure 31(b) graph shows the plate count results of *S. aureus* attachment on the three different types of gloves. Bare latex, nitrile, and polyethylene glove surfaces yielded mean densities of 5.5 ± 0.1 log CFU/mL, 5.4 ± 0.1 log CFU/mL, and 5.3 ± 0.1 log CFU/mL, respectively. In contrast, superhydrophobic FSN-coated latex, nitrile, and polyethylene gloves had a reduced the number of bacteria, with mean densities of 3.5 ± 0.2 log CFU/mL, 3.5 ± 0.2 log CFU/mL, and 3.2 ± 0.2 log CFU/mL, respectively, which corresponds to >98.5% reduction. According to one-way ANOVA analysis, the difference in the number of *S. aureus* with respect to the presence or absence of coating was statistically significant ($p < 0.05$).

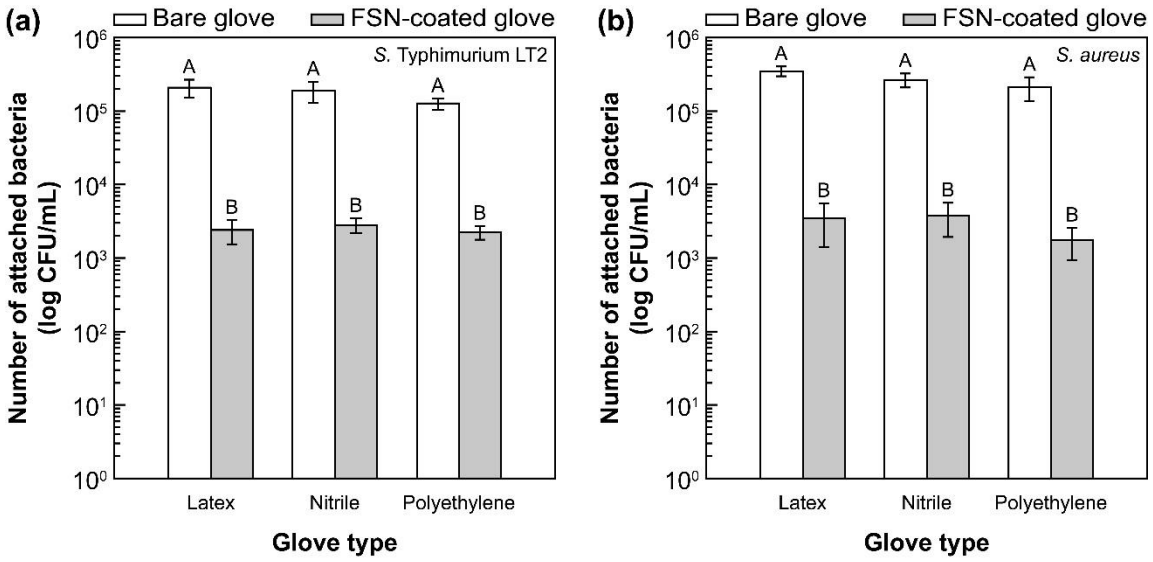

Figure 31. The comparison of bacterial attachment to bare and FSN-coated gloves for (a) *S.* Typhimurium LT2 and (b) *S. aureus* upon 1 h exposure to bacteria. The data were obtained by the pour plating method. The different letters (i.e., A and B) indicate a statistically significant difference ($p < 0.05$) between bare and FSN-coated gloves.

Overall, plating studies showed that the number of *S.* Typhimurium LT2 and *S. aureus* with the use of FSN coating on gloves decreased by 1–2 log units in comparison to bare gloves and by 5.3–5.6 log units in comparison to the inoculation concentration. The comparison of microbiological data on the three different types of glove surfaces with respect to types of bacteria via two-way ANOVA analysis indicated that the adhesion behavior of *S.* Typhimurium LT2 and *S. aureus* to glove surfaces were not statistically significant ($p \geq 0.05$), indicating a similar reduction behavior for all types of gloves upon FSN coating.

6.3.3. Bacterial Attachment to Glove Surfaces: SEM Method

In addition to the pour plating method, SEM was also used to enumerate bacteria on glove surfaces to gain insight into the distribution and localization of bacteria on these

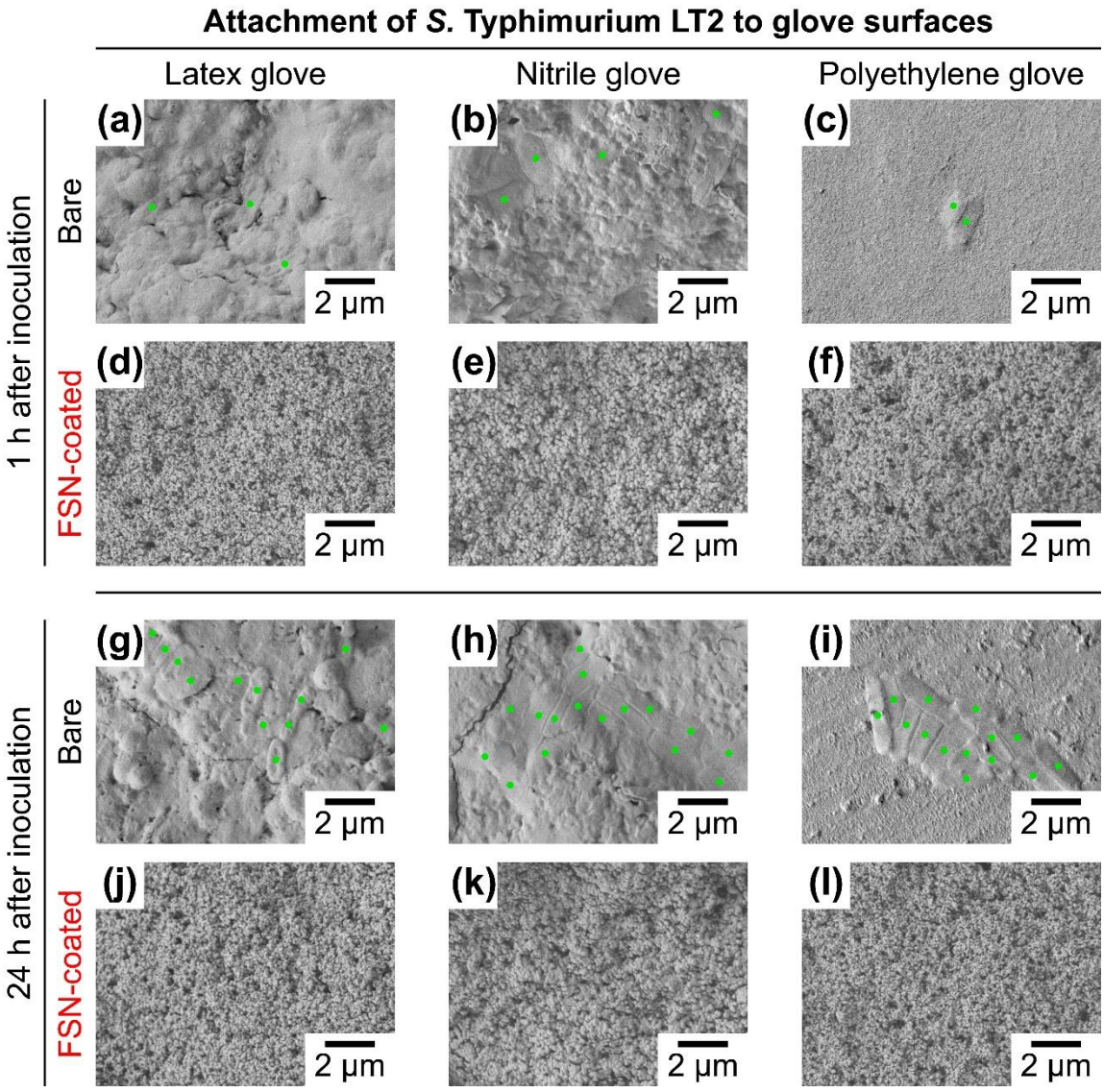

Figure 32. SEM micrographs of attached *S.* Typhimurium LT2 to bare and FSN-coated gloves after (a)–(f) 1 h and (g)–(l) 24 h exposure to bacteria. Bacteria on glove surfaces were highlighted with green.

surfaces. Figure 32 shows the SEM micrographs of *S.* Typhimurium LT2 attached on the three different types of glove surfaces upon 1 h and 24 h inoculation. After 1 h exposure to bacteria, bacterial attachment to bare latex, nitrile, and polyethylene gloves resulted in mean densities of 4.1 ± 0.2 log cells/mm^2, 4.0 ± 0.2 log cells/mm^2, and 4.0 ± 0.1 log

cells/mm^2, respectively (Figures 32(a)–(c)). Inoculation of FSN-coated latex, nitrile, and polyethylene gloves resulted in mean densities of 2.3 ± 0.1 log cells/mm^2, 2.2 ± 0.0 log cells/mm^2, and 2.3 ± 0.2 log cells/mm^2, respectively. (Figures 32(d)–(f)), which corresponds to >97.7% reduction in bacterial attachment in comparison to bare gloves. After 24 h exposure to bacteria, bacterial attachment to bare latex, nitrile, and polyethylene gloves resulted in mean densities of 4.9 ± 0.1 log cells/mm^2, 5.1 ± 0.1 log cells/mm^2, and 5.0 ± 0.0 log cells/mm^2, respectively (Figures 32(g)–(i)). Inoculation of FSN-coated latex, nitrile, and polyethylene gloves resulted in mean densities of 2.7 ± 0.2 log cells/mm^2, 2.6 ± 0.2 log cells/mm^2, and 2.6 ± 0.2 log cells/mm^2, respectively. (Figures 32(j)–(l)), which corresponds to >99.3% reduction in bacterial attachment in comparison to bare gloves. In essence, bacterial attachment to superhydrophobic FSN-coated gloves was much less than bare gloves, with reduced the number of *S.* Typhimurium LT2 by 1–2 log units.

We also enumerated the attachment of *S. aureus* to each glove surface using the same inoculation conditions. Figure 33 shows the SEM micrographs of latex, nitrile, and polyethylene glove surfaces after 1 h and 24 h inoculation with *S. aureus*. After 1 h exposure to bacteria, a mean density of bacteria present on bare latex, nitrile, and polyethylene gloves was 4.3 ± 0.3 log cells/mm^2, 4.2 ± 0.2 log cells/mm^2, and 4.3 ± 0.1 log cells/mm^2, respectively (Figures 33(a)–(c)). Inoculation of FSN-coated gloves resulted in mean densities of 2.4 ± 0.0 log cells/mm^2, 2.5 ± 0.2 log cells/mm^2, and 2.5 ± 0.2 log cells/mm^2, respectively (Figures 33(d)–(f)), which corresponds to reduction in bacterial attachment by >98.1% upon 1 h inoculation. After 24 h exposure to bacteria, a mean

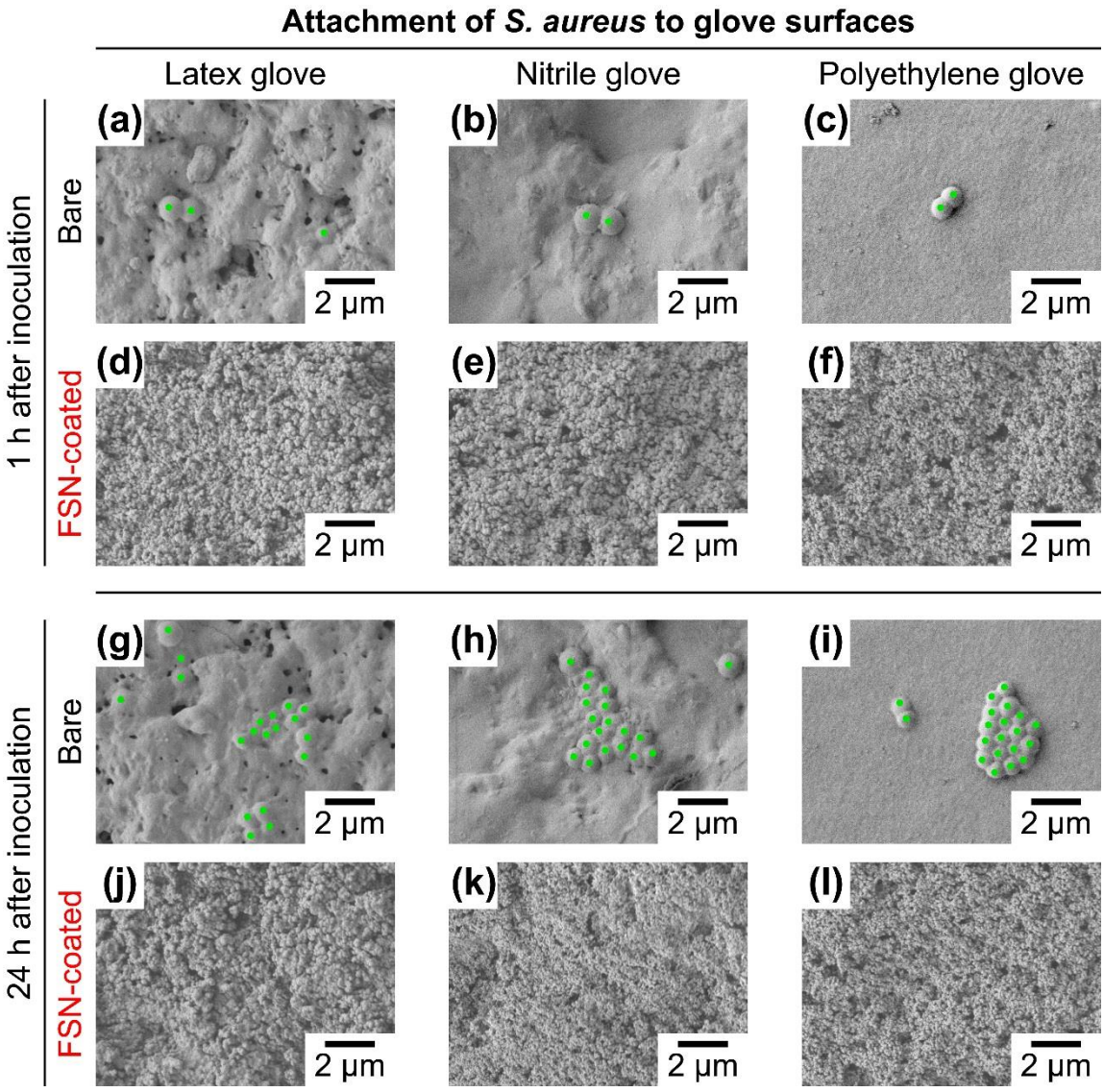

Figure 33. SEM micrographs of attached *S. aureus* to bare and FSN-coated gloves after (a)–(f) 1 h and (g)–(l) 24 h exposure to bacteria. Bacteria on glove surfaces were highlighted with green.

density of bacteria present on bare latex, nitrile, and polyethylene gloves was 4.9 ± 0.2 log cells/mm^2, 4.9 ± 0.3 log cells/mm^2, and 5.1 ± 0.1 log cells/mm^2, respectively (Figures 33(g)–(i)). Inoculation of FSN-coated latex, nitrile, and polyethylene gloves resulted in mean densities of 2.7 ± 0.3 log cells/mm^2, 2.9 ± 0.2 log cells/mm^2, and 2.9 ± 0.2 log

cells/mm^2, respectively (Figures 33(j)–(l)). These data indicate that bacterial attachment was reduced by >99.1% on FSN-coated gloves compared to bare gloves upon 24 h inoculation.

Both plate count and SEM results demonstrated that superhydrophobic FSN-coated gloves effectively inhibit bacterial attachment in comparison to bare gloves. Even with 24 h exposure to bacterial suspensions, *S.* Typhimurium LT2 and *S. aureus* were less likely to reside on FSN-coated glove surfaces. This phenomenon can be explained in terms of the wetting transition from the Wenzel state to the Cassie-Baxter state due to FSN coating on the surfaces.[43] The transition into the Cassie-Baxter state implies that air-pockets form when water comes into contact with glove surfaces, thereby decreasing effective (real) contact area between glove surfaces and water containing bacterial pathogens.[217] Our results can also be explained in terms of hydrophobic effect.[22,218] Prior studies showed that the contact angle of water on *S*. Typhimurium LT2 and *S. aureus* layer collected on a filter ranged from 15° to 27°.[99,219] When these bacteria with highly hydrophilic cell surfaces come into contact with nonpolar surfaces, unfavorable intermolecular interactions arise, inhibiting bacterial attachment.

6.3.4. Mechanical Robustness and Chemical Stability of FSN-Coated Gloves

Maintaining superhydrophobic properties of FSN-coated gloves are important to ensure bacterial antiadhesion performance of the coating during usage. In this context, we evaluated shear strength of FSN coating on gloves to determine mechanical durability of FSN-coated gloves (Figure 34(a)). All shearing experiments were carried out under the normal load of 10 mN for 10 cycles using a produce-attached tip. As shown in Figures

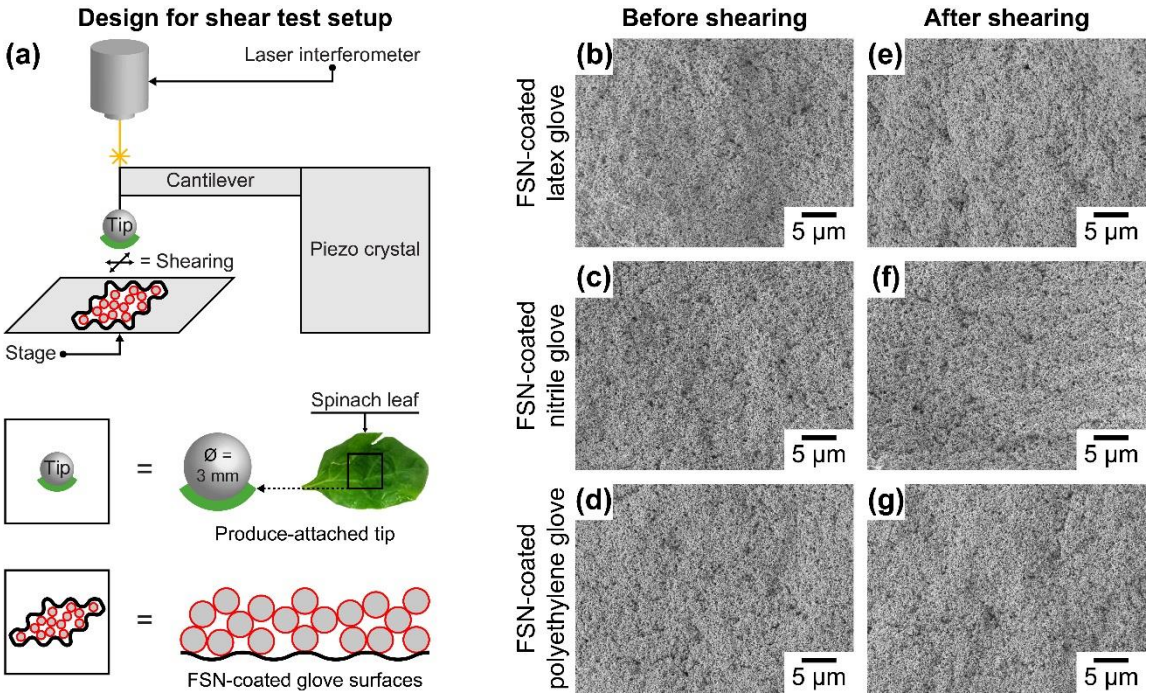

Figure 34. (a) Schematic drawing of shear test setup to evaluate mechanical durability between produce-attached tip and FSN-coated glove surfaces. SEM micrographs of before (b)–(d) and after (e)–(g) shear test, showing shear resistance of FSN-coated gloves.

34(b)–(g), FSN-coated glove surfaces showed similar surface morphology before and after shearing with a produce-attached tip, indicating practical mechanical durability. Furthermore, difference in surface roughness values before and after shearing were measured using a profilometer. Before shearing, RMS roughness of FSN-coated latex, nitrile, and polyethylene glove surfaces were 419 ± 34 nm, 406 ± 28 nm, and 395 ± 40 nm, respectively. Similar results were obtained after shearing as well: 426 ± 42 nm, 405 ± 47 nm, and 403 ± 43 nm, respectively, which indicates mechanical durability of FSN-coated gloves.

The potential toxicity, if any, of the developed gloves are directly related to the ability to leach chemicals from their FDTS-functionalized silica nanoparticle surfaces

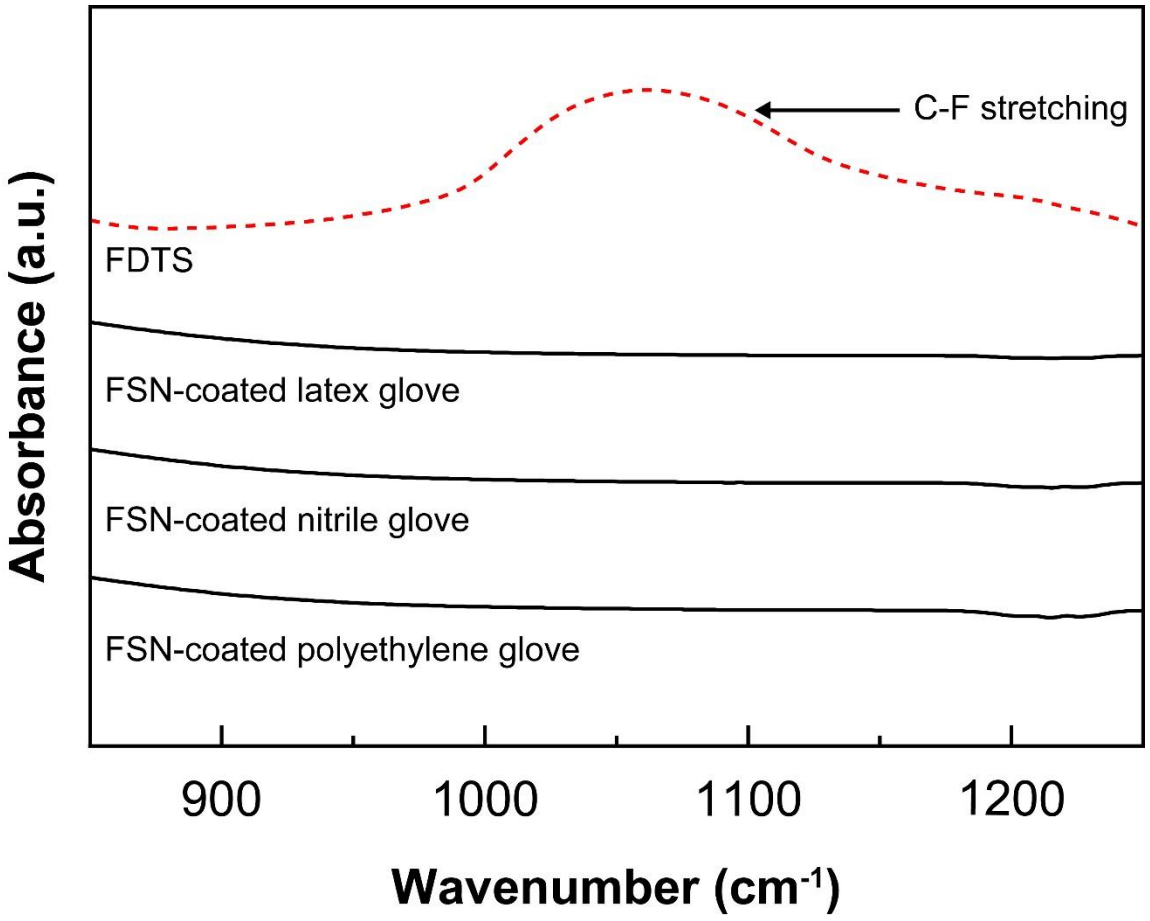

Figure 35. ATR-FTIR spectra of aliquots collected from the samples (i.e., FSN-coated glove pieces submerged in DI water). The absence of C–F stretching region suggest chemical stability of functional groups on glove surfaces.

through detachment, degradation, or decomposition of fluoro groups. Hence, we investigated chemical stability of FSN-coated gloves in DI water as a function of time using ATR-FTIR spectroscopy. Unbound FDTS molecules had symmetric and asymmetric C–F stretching peak near 1050 cm^{-1}. The spectroscopic analysis revealed that FSN-coated gloves submerged in DI water has no chemical leaching and present the absences of free chemicals within the detection limit of 1 ppm at least in a 24-h period (Figure 35).

6.4. Conclusions

Cross-contamination and transmission of pathogenic bacteria during food processing and handling has become an issue throughout the world. Gloves are the most commonly used protective equipment or barriers against bacterial contamination. However, recent studies have pointed out that the use of gloves, while improving food safety to some extent, may be insufficient to completely prevent the spread of pathogenic bacteria. Herein, we report surface modification of latex, nitrile, and polyethylene gloves with "fluorinated silica nanoparticles" (FSNs) to further limit bacteria adhesion. This in turn should further reduce the risk of potential cross-contamination and transmission of pathogenic bacteria associated with glove surfaces, which already reduces the bacterial contamination to some extent. The bacterial antiadhesion properties of FSN-coated gloves was confirmed against Gram-negative *S.* Typhimurium LT2 and Gram-positive *S. aureus*, with significantly greater (1–2 log units) bacterial populations on bare gloves than on modified gloves, via plate counting and direct SEM visualization after dip-inoculation. The ability of FSN-coated gloves to inhibit bacterial attachment is attributed to their nanotextured morphology and low surface energy, the synergistic combination of which leads to superhydrophobic surfaces. Superhydrophobicity translates into a reduced effective (real) contact between glove surfaces and water containing bacterial pathogens, decreasing the probability of bacteria to reach glove surfaces. Overall, the promising bacterial antiadhesion properties of FSN-coated gloves as well as a scalable and facile nature of the dip-coating method can offer a simple solution for enhancing microbiological food safety and hygiene of disposable gloves used in the food industry.

CHAPTER VII

SUMMARY

In Chapter I, a brief review is presented on the importance of bacterial antiadhesive materials and the factors that influence bacterial attachment. Studies of bacterial adhesion behavior are important because of their relevance to human health and diseases. This dissertation provides insights into the effect of the surface properties on bacterial adhesion. Also, based on these fundamental studies, materials that can prevent bacterial attachment effectively without generating any antimicrobial activity were presented. Sol-gel method, reactive-ion etching (RIE) method, and dip-coating method were used to fabricate bacteria repelling hygienic materials. Food safety related bacteria (i.e., *Salmonella* and *Listeria*) and healthcare-associated infections (HAIs) related bacteria (i.e., *E. coli* and *S. aureus*) were selected for the studies.

In Chapter II, the effect of the surface physical and chemical properties on bacterial adhesion are presented. By modifying surface nano/microroughness of hydrophobic surfaces, we are able to vary water contact angle from ~90° to ~160° or higher. Comparing 18 different surfaces of roughness within this regime show bacterial adhesion trends. Water contact angle higher than 150° is so-called superhydrophobic surfaces. We found interesting bacterial adhesion behavior in superhyrophobic regime, which significantly reduced bacterial attachment to surfaces. Moreover, for a better understanding of the chemical properties influencing interactions between bacteria and surfaces, we have prepared different well-defined surface chemistry surfaces by self-assembled monolayers

(SAMs) of alkanethiols and investigate the kinetics of bacterial adhesion process in terms of the effect of the surface chemistry. It was clear that bacteria are more likely to adhere to hydrophilic surfaces.

In Chapter III and Chapter IV, hydrophobically-modified silica aerogels were synthesized via sol-gel method. The bacterial antiadhesion properties of hydrophobically-modified silica aerogels, with other distinctive characteristics including superior thermal insulation and ultra-light weight, make these aerogels attractive candidates for novel food-contact surfaces to improve food safety. Moreover, findings from the study also showed that hydrophobic nanoporous silica aerogel (HNSA) has potential as an antiadhesive hygienic material that can inhibit exogenous bacterial contamination related to HAIs. The results suggest that the use of HNSA as surfaces that come into contact with bacterial pathogens in the healthcare environment can improve bacterial hygiene, and therefore, may reduce the rate of HAIs.

In Chapter V, RIE method has been applied and developed rice leaf-inspired surfaces. The biomimetic "rice leaf-like surfaces" (RLLS) involved unique hollow nanodisc morphology and showed strong bacterial suspension repellency with inhibition efficiency of > 99.9%. Furthermore, different from most other bioinspired antibiofouling surfaces, we were able to maintain optical-grade transparency (i.e., ≥92% transmission) by minimizing roughness volume through hollow nanodisc morphology. We anticipate that the combination of bacterial antiadhesion efficiency, optical-grade transparency, and convenient single-step method of preparation makes RLLS a very attractive candidate surface for biosensors, endoscopes, microfluidic and bio-optical instruments, lab-on-a-

chip, and touchscreen devices.

In Chapter VI, surface modification of gloves made of materials such as latex, nitrile, and polyethylene are presented. We report a surface modification by dip-coating method involving "fluorinated silica nanoparticles" (FSNs) to improve the protective ability against bacterial contamination of disposable glove surfaces. The bacterial populations on FSN-coated latex, nitrile and polyethylene gloves was reduced by 1–2 log units in comparison to bare gloves, which already reduce the bacterial attachment to some extent.

Based on the conclusions of this work, it is believed that the future work should focus on fabricating materials with improved bacterial antiadhesion properties for long-term (i.e., several months or even longer) period. Secondly, determining the effect of the surface charge on bacterial adhesion by combining QCM-D, SEM, and DIC microscopy techniques should perform to further reduce the bacterial adhesion. Thirdly, determining the effect of the microscale surface roughness on bacterial adhesion by combining SEM, AFM, and confocal microscopy techniques should perform to prevent bacterial attachment more effectively. Finally, fabricating superomniphobic (i.e., repels both water and oil) surfaces with ultra-low surface energy is required, which can be utilized as a promising antibiofouling surfaces in the near future.

REFERENCES

(1) Humphrey, T. *Nat. Rev. Microbiol.* **2004**, *2*, 504–509.

(2) Hall-Stoodley, L.; Costerton, J.; Stoodley, P. *Nat. Rev. Microbiol.* **2004**, *2*, 95–108.

(3) Brooks, J. D.; Flint, S. H. *Int. J. Food Sci. Technol.* **2008**, *43*, 2163–2176.

(4) Truelstrup Hansen, L.; Vogel, B. F. *Int. J. Food Microbiol.* **2011**, *146*, 88–93.

(5) Sievert, D. M.; Ricks, P.; Edwards, J. R.; Schneider, A.; Patel, J.; Srinivasan, A.; Kallen, A.; Limbago, B.; Fridkin, S. *Infect. Control Hosp. Epidemiol.* **2013**, *34*, 1–14.

(6) Magill, S. S.; Edwards, J. R.; Bamberg, W.; Beldavs, Z. G.; Dumyati, G.; Kainer, M. A.; Lynfield, R.; Maloney, M.; McAllister-Hollod, L.; Nadle, J.; Ray, S. M.; Thompson, D. L.; Wilson, L. E.; Fridkin, S. K. *N. Engl. J. Med.* **2014**, *370*, 1198–1208.

(7) Mangram, A. J.; Horan, T. C.; Pearson, M. L.; Silver, L. C.; Jarvis, W. R. *Infect. Control Hosp. Epidemiol.* **1999**, *20*, 247–280.

(8) Scott, E.; Bloomfield, S. F. *J. Appl. Bacteriol.* **1990**, *68*, 271–278.

(9) Kramer, A.; Schwebke, I.; Kampf, G. *BMC Infect. Dis.* **2006**, *6*, 130.

(10) Harris, S. J.; Cormican, M.; Cummins, E. *Hum. Ecol. Risk Assess. An Int. J.* **2012**, *18*, 767–809.

(11) Flint, S. H.; Brooks, J. D.; Bremer, P. J. *J. Food Eng.* **2000**, *43*, 235–242.

(12) Massad-Ivanir, N.; Shtenberg, G.; Zeidman, T.; Segal, E. *Adv. Funct. Mater.* **2010**, *20*, 2269–2277.

(13) McConney, M. E.; Anderson, K. D.; Brott, L. L.; Naik, R. R.; Tsukruk, V. V. *Adv. Funct. Mater.* **2009**, *19*, 2527–2544.

(14) Oh, J. K.; Kohli, N.; Zhang, Y.; Min, Y.; Jayaraman, A.; Cisneros-Zevallos, L.; Akbulut, M. *Nanotechnology* **2016**, *27*, 085705.

(15) Oh, J. K.; Perez, K.; Kohli, N.; Kara, V.; Li, J.; Min, Y.; Castillo, A.; Taylor, M.; Jayaraman, A.; Cisneros-Zevallos, L.; Akbulut, M. *Food Control* **2015**, *52*, 132–141.

(16) Oh, J. K.; Lu, X.; Min, Y.; Cisneros-Zevallos, L.; Akbulut, M. *ACS Appl. Mater. Interfaces* **2015**, *7*, 19274–19281.

(17) Oh, J. K.; Rapisand, W.; Zhang, M.; Yegin, Y.; Min, Y.; Castillo, A.; Cisneros-Zevallos, L.; Akbulut, M. *J. Food Eng.* **2016**, *187*, 82–91.

(18) An, Y. H.; Friedman, R. J. *J. Biomed. Mater. Res.* **1998**, *43*, 338–348.

(19) Donlan, R. M. *Emerg. Infect. Dis.* **2002**, *8*, 881–890.

(20) Truong, V. K.; Lapovok, R.; Estrin, Y. S.; Rundell, S.; Wang, J. Y.; Fluke, C. J.; Crawford, R. J.; Ivanova, E. P. *Biomaterials* **2010**, *31*, 3674–3683.

(21) Taylor, R. L.; Verran, J.; Lees, G. C.; Ward, A. J. *J. Mater. Sci. Mater. Med.* **1998**, *9*, 17–22.

(22) Chandler, D. *Nature* **2005**, *437*, 640–647.

(23) Zhang, X.; Shi, F.; Niu, J.; Jiang, Y.; Wang, Z. *J. Mater. Chem.* **2008**, *18*, 621–633.

(24) Banerjee, I.; Pangule, R. C.; Kane, R. S. *Adv. Mater.* **2011**, *23*, 690–718.

(25) Ferreira, L.; Zumbuehl, A. *J. Mater. Chem.* **2009**, *19*, 7796–7806.

(26) Flannagan, R. S.; Cosío, G.; Grinstein, S. *Nat. Rev. Microbiol.* **2009**, *7*, 355–366.

(27) Hetrick, E. M.; Schoenfisch, M. H. *Chem. Soc. Rev.* **2006**, *35*, 780–789.

(28) Marambio-Jones, C.; Hoek, E. M. V. *J. Nanoparticle Res.* **2010**, *12*, 1531–1551.

(29) Rasko, D. A.; Sperandio, V. *Nat. Rev. Drug Discov.* **2010**, *9*, 117–128.

(30) Puckett, S. D.; Taylor, E.; Raimondo, T.; Webster, T. J. *Biomaterials* **2010**, *31*, 706–713.

(31) Li, G.; Cheng, G.; Xue, H.; Chen, S.; Zhang, F.; Jiang, S. *Biomaterials* **2008**, *29*, 4592–4597.

(32) Roosjen, A.; van der Mei, H. C.; Busscher, H. J.; Norde, W. *Langmuir* **2004**, *20*, 10949–10955.

(33) Shivapooja, P.; Wang, Q.; Orihuela, B.; Rittschof, D.; López, G. P.; Zhao, X. *Adv. Mater.* **2013**, *25*, 1430–1434.

(34) Cunliffe, D.; de las Heras Alarcón, C.; Peters, V.; Smith, J. R.; Alexander, C. *Langmuir* **2003**, *19*, 2888–2899.

(35) Fu, J.; Ji, J.; Yuan, W.; Shen, J. *Biomaterials* **2005**, *26*, 6684–6692.

(36) Israelachvili, J. N. *Intermolecular and surface forces*; 3rd ed.; Academic Press, **2011**.

(37) Hansen, M. C.; Udsen, C.; Palmer, R. J.; Molin, S.; White, D. C. *Microbiology* **2001**, *147*, 1383–1391.

(38) Friedlander, R. S.; Vlamakis, H.; Kim, P.; Khan, M.; Kolter, R.; Aizenberg, J. *Proc. Natl. Acad. Sci.* **2013**, *110*, 5624–5629.

(39) Decuzzi, P.; Ferrari, M. *Biomaterials* **2010**, *31*, 173–179.

(40) Li, X.-M.; Reinhoudt, D.; Crego-Calama, M. *Chem. Soc. Rev.* **2007**, *36*, 1350–1368.

(41) Singh, A. V.; Vyas, V.; Patil, R.; Sharma, V.; Scopelliti, P. E.; Bongiorno, G.; Podestà, A.; Lenardi, C.; Gade, W. N.; Milani, P. *PLoS One* **2011**, *6*, e25029.

(42) Lee, C.; Kim, C.-J. *Phys. Rev. Lett.* **2011**, *106*, 014502.

(43) Chen, L.; Yang, G.; Wang, S. *Small* **2012**, *8*, 962–965.

(44) Dettre, R. H.; Johnson Jr., R. E. *Adv. Chem. Ser.* **1964**, *43*, 136–144.

(45) Yoshimitsu, Z.; Nakajima, A.; Watanabe, T.; Hashimoto, K. *Langmuir* **2002**, *18*, 5818–5822.

(46) Boks, N. P.; Norde, W.; van der Mei, H. C.; Busscher, H. J. *Microbiology* **2008**, *154*, 3122–3133.

(47) Wu, Y.; Zitelli, J. P.; TenHuisen, K. S.; Yu, X.; Libera, M. R. *Biomaterials* **2011**, *32*, 951–960.

(48) Akhtar, S.; Sarker, M. R.; Hossain, A. *Crit. Rev. Microbiol.* **2014**, *40*, 348–359.

(49) Shi, X.; Zhu, X. *Trends Food Sci. Technol.* **2009**, *20*, 407–413.

(50) Stepanovic, S.; Cirkovic, I.; Ranin, L.; Svabic-Vlahovic, M. *Lett. Appl. Microbiol.* **2004**, *38*, 428–432.

(51) Chmielewski, R. A. N.; Frank, J. F. *Compr. Rev. Food Sci. Food Saf.* **2003**, *2*, 22–32.

(52) Rossi, E. M.; Scapin, D.; Tondo, E. C. *J. Infect. Dev. Ctries.* **2013**, *7*, 229–234.

(53) Schlisselberg, D. B.; Yaron, S. *Food Microbiol.* **2013**, *35*, 65–72.

(54) Abban, S.; Jakobsen, M.; Jespersen, L. *Food Microbiol.* **2012**, *31*, 139–147.

(55) Takahashi, H.; Kuramoto, S.; Miya, S.; Kimura, B. *Food Control* **2011**, *22*, 633–637.

(56) Chia, T. W. R.; Goulter, R. M.; McMeekin, T.; Dykes, G. A.; Fegan, N. *Food Microbiol.* **2009**, *26*, 853–859.

(57) Giaouris, E. D.; Nychas, G.-J. E. *Food Microbiol.* **2006**, *23*, 747–752.

(58) Beresford, M. R.; Andrew, P. W.; Shama, G. *J. Appl. Microbiol.* **2001**, *90*, 1000–1005.

(59) Denes, A. R.; Somers, E. B.; Wong, A. C. L.; Denes, F. *J. Appl. Polym. Sci.* **2001**, *81*, 3425–3438.

(60) Sinde, E.; Carballo, J. *Food Microbiol.* **2000**, *17*, 439–447.

(61) Wilks, S. A.; Michels, H.; Keevil, C. W. *Int. J. Food Microbiol.* **2005**, *105*, 445–454.

(62) Kusumaningrum, H. *Int. J. Food Microbiol.* **2003**, *85*, 227–236.

(63) Moore, C. M.; Sheldon, B. W.; Jaykus, L.-A. *J. Food Prot.* **2003**, *66*, 2231–2236.

(64) Perez, K. L.; Lucia, L. M.; Cisneros-Zevallos, L.; Castillo, A.; Taylor, T. M. *Int. J. Food Microbiol.* **2012**, *156*, 76–82.

(65) Hoelzer, K.; Pouillot, R.; Gallagher, D.; Silverman, M. B.; Kause, J.; Dennis, S. *Int. J. Food Microbiol.* **2012**, *157*, 267–277.

(66) Verran, J.; Packer, A.; Kelly, P. J.; Whitehead, K. a. *J. Adhes. Sci. Technol.* **2010**, *24*, 2271–2285.

(67) Mérian, T.; Goddard, J. M. *J. Agric. Food Chem.* **2012**, *60*, 2943–2957.

(68) Zhang, M.; Yang, F.; Pasupuleti, S.; Oh, J. K.; Kohli, N.; Lee, I.-S.; Perez, K.; Verkhoturov, S. V.; Schweikert, E. A.; Jayaraman, A.; Cisneros-Zevallos, L.; Akbulut, M. *Int. J. Food Microbiol.* **2014**, *185*, 73–81.

(69) Kingshott, P.; Wei, J.; Bagge-Ravn, D.; Gadegaard, N.; Gram, L. *Langmuir* **2003**, *19*, 6912–6921.

(70) Cheng, G.; Zhang, Z.; Chen, S.; Bryers, J. D.; Jiang, S. *Biomaterials* **2007**, *28*, 4192–4199.

(71) Bixler, G. D.; Bhushan, B. *Nanoscale* **2014**, *6*, 76–96.

(72) Krishnan, S.; Ayothi, R.; Hexemer, A.; Finlay, J. A.; Sohn, K. E.; Perry, R.; Ober, C. K.; Kramer, E. J.; Callow, M. E.; Callow, J. A.; Fischer, D. A. *Langmuir* **2006**, *22*, 5075–5086.

(73) Beltrán-Osuna, Á. A.; Cao, B.; Cheng, G.; Jana, S. C.; Espe, M. P.; Lama, B. *Langmuir* **2012**, *28*, 9700–9706.

(74) Privett, B. J.; Youn, J.; Hong, S. A.; Lee, J.; Han, J.; Shin, J. H.; Schoenfisch, M. H. *Langmuir* **2011**, *27*, 9597–9601.

(75) Hu, C.; Liu, S.; Li, B.; Yang, H.; Fan, C.; Cui, W. *Adv. Healthc. Mater.* **2013**, *2*, 1314–1321.

(76) Gurav, J. L.; Jung, I.-K.; Park, H.-H.; Kang, E. S.; Nadargi, D. Y. *J. Nanomater.* **2010**, *2010*, 1–11.

(77) Schmidt, M.; Schwertfeger, F. *J. Non-Cryst. Solids* **1998**, *225*, 364–368.

(78) Zhang, M.; Oh, J. K.; Cisneros-Zevallos, L.; Akbulut, M. *J. Food Eng.* **2013**, *119*, 425–432.

(79) Niemira, B. A. *Annu. Rev. Food Sci. Technol.* **2012**, *3*, 125–142.

(80) Tamon, H.; Kitamura, T.; Okazaki, M. *J. Colloid Interface Sci.* **1998**, *197*, 353–359.

(81) Kwok, D. Y.; Gietzelt, T.; Grundke, K.; Jacobasch, H.-J.; Neumann, A. W.

Langmuir **1997**, *13*, 2880–2894.

(82) Stauffer, C. E. *J. Phys. Chem.* **1965**, *69*, 1933–1938.

(83) Barrett, E. P.; Joyner, L. G.; Halenda, P. P. *J. Am. Chem. Soc.* **1951**, *73*, 373–380.

(84) Cañas, N.; Kamperman, M.; Völker, B.; Kroner, E.; McMeeking, R. M.; Arzt, E. *Acta Biomater.* **2012**, *8*, 282–288.

(85) Wang, J.; Chen, C. *Biotechnol. Adv.* **2009**, *27*, 195–226.

(86) Hrubesh, L. W. *J. Non-Cryst. Solids* **1998**, *225*, 335–342.

(87) Hüsing, N.; Schubert, U. *Angew. Chemie Int. Ed.* **1998**, *37*, 22–45.

(88) Pool, R. *Science* **1990**, *247*, 807–807.

(89) Porter, M. D.; Bright, T. B.; Allara, D. L.; Chidsey, C. E. D. *J. Am. Chem. Soc.* **1987**, *109*, 3559–3568.

(90) Du, Y.; Du, X.; George, S. M. *J. Phys. Chem. C* **2007**, *111*, 219–226.

(91) Grant, L. M.; Tiberg, F.; Ducker, W. a. *J. Phys. Chem. B* **1998**, *102*, 4288–4294.

(92) Lima, P. M.; São José, J. F. B.; Andrade, N. J.; Pires, A. C. S.; Ferreira, S. O. *Food Control* **2013**, *30*, 157–161.

(93) Anselme, K.; Davidson, P.; Popa, A. M.; Giazzon, M.; Liley, M.; Ploux, L. *Acta Biomater.* **2010**, *6*, 3824–3846.

(94) Drelich, J.; Miller, J. D. *J. Colloid Interface Sci.* **1994**, *164*, 252–259.

(95) Wenzel, R. N. *J. Phys. Colloid Chem.* **1949**, *53*, 1466–1467.

(96) Satou, N.; Satou, J.; Shintani, H.; Okuda, K. *J. Gen. Microbiol.* **1988**, *134*, 1299–1305.

(97) Hogt, a H.; Dankert, J.; De Vries, J. A.; Feijen, J. *Microbiology* **1983**, *129*, 2959–

2968.

(98) Woodling, S. E.; Moraru, C. I. *J. Food Sci.* **2005**, *70*, M345–M351.

(99) Dickson, J. S.; Koohmaraie, M. *Appl. Environ. Microbiol.* **1989**, *55*, 832–836.

(100) Yang, H.-S.; Choi, S.-Y.; Hyun, S.-H.; Park, C.-G. *Thin Solid Films* **1999**, *348*, 69–73.

(101) Singh, S. P.; Burgess, G.; Singh, J. *Packag. Technol. Sci.* **2008**, *21*, 25–35.

(102) Venkateswara Rao, A.; Pajonk, G. M.; Haranath, D. *Mater. Sci. Technol.* **2001**, *17*, 343–348.

(103) European Centre for Disease Prevention and Control. *Annual Epidemiological Report 2014*; **2015**.

(104) Huttner, A.; Harbarth, S.; Carlet, J.; Cosgrove, S.; Goossens, H.; Holmes, A.; Jarlier, V.; Voss, A.; Pittet, D. *Antimicrob. Resist. Infect. Control* **2013**, *2*, 31.

(105) Zarb, P.; Coignard, B.; Griskeviciene, J.; Muller, A.; Vankerckhoven, V.; Weist, K.; Goossens, M. M.; Vaerenberg, S.; Hopkins, S.; Catry, B.; Monnet, D. L.; Goossens, H.; Suetens, C. *Eurosurveillance* **2012**, *17*, 1–16.

(106) Calfee, D. P. *Annu. Rev. Med.* **2012**, *63*, 359–371.

(107) Boyce, J. M. *J. Hosp. Infect.* **2007**, *65*, 50–54.

(108) Rutala, W. A.; Weber, D. J. *Am. J. Infect. Control* **2013**, *41*, S2–S5.

(109) Fux, C. A.; Costerton, J. W.; Stewart, P. S.; Stoodley, P. *Trends Microbiol.* **2005**, *13*, 34–40.

(110) Vickery, K.; Pajkos, A.; Cossart, Y. *Am. J. Infect. Control* **2004**, *32*, 170–176.

(111) Weber, D. J.; Anderson, D.; Rutala, W. a. *Curr. Opin. Infect. Dis.* **2013**, *26*, 338–

344.

(112) Otter, J. A.; Yezli, S.; French, G. L. *Infect. Control Hosp. Epidemiol.* **2011**, *32*, 687–699.

(113) Page, K.; Wilson, M.; Parkin, I. P. *J. Mater. Chem.* **2009**, *19*, 3819–3831.

(114) Shukla, A.; Fleming, K. E.; Chuang, H. F.; Chau, T. M.; Loose, C. R.; Stephanopoulos, G. N.; Hammond, P. T. *Biomaterials* **2010**, *31*, 2348–2357.

(115) Costa, F.; Carvalho, I. F.; Montelaro, R. C.; Gomes, P.; Martins, M. C. L. *Acta Biomater.* **2011**, *7*, 1431–1440.

(116) Onaizi, S. A.; Leong, S. S. J. *Biotechnol. Adv.* **2011**, *29*, 67–74.

(117) Gottenbos, B. *J. Antimicrob. Chemother.* **2001**, *48*, 7–13.

(118) Grass, G.; Rensing, C.; Solioz, M. *Appl. Environ. Microbiol.* **2011**, *77*, 1541–1547.

(119) Roe, D.; Karandikar, B.; Bonn-Savage, N.; Gibbins, B.; Roullet, J.-B. *J. Antimicrob. Chemother.* **2008**, *61*, 869–876.

(120) Nowlin, K.; Boseman, A.; Covell, A.; LaJeunesse, D. *J. R. Soc. Interface* **2014**, *12*, 20140999.

(121) Ivanova, E. P.; Hasan, J.; Webb, H. K.; Gervinskas, G.; Juodkazis, S.; Truong, V. K.; Wu, A. H. F.; Lamb, R. N.; Baulin, V. A.; Watson, G. S.; Watson, J. A.; Mainwaring, D. E.; Crawford, R. J. *Nat. Commun.* **2013**, *4*, 2838.

(122) Levy, S. B.; Marshall, B. *Nat. Med.* **2004**, *10*, S122–S129.

(123) MacCallum, N.; Howell, C.; Kim, P.; Sun, D.; Friedlander, R.; Ranisau, J.; Ahanotu, O.; Lin, J. J.; Vena, A.; Hatton, B.; Wong, T.-S.; Aizenberg, J. *ACS Biomater. Sci. Eng.* **2015**, *1*, 43–51.

(124) Freschauf, L. R.; McLane, J.; Sharma, H.; Khine, M. *PLoS One* **2012**, *7*, e40987.

(125) Epstein, A. K.; Wong, T.-S.; Belisle, R. a; Boggs, E. M.; Aizenberg, J. *Proc. Natl. Acad. Sci.* **2012**, *109*, 13182–13187.

(126) Zhang, X.; Wang, L.; Levänen, E. *RSC Adv.* **2013**, *3*, 12003–12020.

(127) Xu, L.-C.; Siedlecki, C. A. *Acta Biomater.* **2012**, *8*, 72–81.

(128) Ercan, B.; Taylor, E.; Alpaslan, E.; Webster, T. J. *Nanotechnology* **2011**, *22*, 295102.

(129) Efimenko, K.; Finlay, J.; Callow, M. E.; Callow, J. A.; Genzer, J. *ACS Appl. Mater. Interfaces* **2009**, *1*, 1031–1040.

(130) Perera-Costa, D.; Bruque, J. M.; González-Martín, M. L.; Gómez-García, A. C.; Vadillo-Rodríguez, V. *Langmuir* **2014**, *30*, 4633–4641.

(131) Zhang, J.; Sheng, X.; Jiang, L. *Langmuir* **2009**, *25*, 1371–1376.

(132) Sabri, F.; Sebelik, M. E.; Meacham, R.; Boughter, J. D.; Challis, M. J.; Leventis, N. *PLoS One* **2013**, *8*, e66348.

(133) Jung, S. M.; Jung, H. Y.; Dresselhaus, M. S.; Jung, Y. J.; Kong, J. *Sci. Rep.* **2012**, *2*, 849.

(134) Quintanar-Guerrero, D.; Ganem-Quintanar, A.; Nava-Arzaluz, M. G.; Piñón-Segundo, E. *Expert Opin. Drug Deliv.* **2009**, *6*, 485–498.

(135) Stalder, A. F.; Melchior, T.; Müller, M.; Sage, D.; Blu, T.; Unser, M. *Colloids Surfaces A Physicochem. Eng. Asp.* **2010**, *364*, 72–81.

(136) Kinnari, T. J.; Esteban, J.; Zamora, N.; Fernandez, R.; López-Santos, C.; Yubero, F.; Mariscal, D.; Puertolas, J. A.; Gomez-Barrena, E. *Clin. Microbiol. Infect.* **2010**, *16*, 1036–1041.

(137) Wang, Y.; Hammes, F.; Boon, N.; Egli, T. *Environ. Sci. Technol.* **2007**, *41*, 7080–7086.

(138) Pierre, A. C.; Pajonk, G. M. *Chem. Rev.* **2002**, *102*, 4243–4266.

(139) Pranzetti, A.; Salaün, S.; Mieszkin, S.; Callow, M. E.; Callow, J. A.; Preece, J. A.; Mendes, P. M. *Adv. Funct. Mater.* **2012**, *22*, 3672–3681.

(140) Fadley, C. S.; Baird, R. J.; Siekhaus, W.; Novakov, T.; Bergström, S. Å. L. *J. Electron Spectros. Relat. Phenomena* **1974**, *4*, 93–137.

(141) Ong, Y.-L.; Razatos, A.; Georgiou, G.; Sharma, M. M. *Langmuir* **1999**, *15*, 2719–2725.

(142) Truong, V. K.; Webb, H. K.; Fadeeva, E.; Chichkov, B. N.; Wu, A. H. F.; Lamb, R.; Wang, J. Y.; Crawford, R. J.; Ivanova, E. P. *Biofouling* **2012**, *28*, 539–550.

(143) Larsen, R. J.; Zukoski, C. F. *J. Chem. Phys.* **2012**, *136*, 054901.

(144) DelRio, F. W.; de Boer, M. P.; Knapp, J. a; David Reedy, E.; Clews, P. J.; Dunn, M. L. *Nat. Mater.* **2005**, *4*, 629–634.

(145) Campoccia, D.; Montanaro, L.; Arciola, C. R. *Biomaterials* **2013**, *34*, 8533–8554.

(146) Xu, L.; Karunakaran, R. G.; Guo, J.; Yang, S. *ACS Appl. Mater. Interfaces* **2012**, *4*, 1118–1125.

(147) Deng, X.; Mammen, L.; Butt, H.-J.; Vollmer, D. *Science* **2012**, *335*, 67–70.

(148) Rahmawan, Y.; Xu, L.; Yang, S. *J. Mater. Chem. A* **2013**, *1*, 2955–2969.

(149) Vogelmann, T. C. *Annu. Rev. Plant Physiol. Plant Mol. Biol.* **1993**, *44*, 231–251.

(150) Mandoli, D. F.; Briggs, W. R. *Proc. Natl. Acad. Sci.* **1982**, *79*, 2902–2906.

(151) Fukshansky, L.; Fukshansky-Kazarinova, N.; Remisowsky, A. M. v. *Appl. Opt.*

1991, *30*, 3145–3153.

(152) Vogelmann, T. C.; Bornman, J. F.; Yates, D. J. *Physiol. Plant.* **1996**, *98*, 43–56.

(153) Smyth, C. J.; Jonsson, P.; Olsson, E.; Soderlind, O.; Rosengren, J.; Hjertén, S.; Wadström, T. *Infect. Immun.* **1978**, *22*, 462–472.

(154) Kwok, D. Y.; Neumann, A. W. *Adv. Colloid Interface Sci.* **1999**, *81*, 167–249.

(155) Koch, K.; Bhushan, B.; Barthlott, W. *Soft Matter* **2008**, *4*, 1943–1963.

(156) Wu, D.; Wang, J.-N.; Wu, S.-Z.; Chen, Q.-D.; Zhao, S.; Zhang, H.; Sun, H.-B.; Jiang, L. *Adv. Funct. Mater.* **2011**, *21*, 2927–2932.

(157) Min, W.-L.; Jiang, B.; Jiang, P. *Adv. Mater.* **2008**, *20*, 3914–3918.

(158) Lu, W.; Lieber, C. M. *Nat. Mater.* **2007**, *6*, 841–850.

(159) Feng, L.; Zhang, Y.; Xi, J.; Zhu, Y.; Wang, N.; Xia, F.; Jiang, L. *Langmuir* **2008**, *24*, 4114–4119.

(160) Hensel, R.; Finn, A.; Helbig, R.; Braun, H.-G.; Neinhuis, C.; Fischer, W.-J.; Werner, C. *Adv. Mater.* **2014**, *26*, 2029–2033.

(161) Pokroy, B.; Epstein, A. K.; Persson-Gulda, M. C. M.; Aizenberg, J. *Adv. Mater.* **2009**, *21*, 463–469.

(162) Jansen, H.; Gardeniers, H.; Boer, M. De; Elwenspoek, M.; Fluitman, J. *J. Micromech. Microeng.* **1996**, *6*, 14–28.

(163) Hedlund, C.; Lindberg, U.; Bucht, U.; Soderkvist, J. *J. Micromech. Microeng.* **1993**, *3*, 65–73.

(164) Stoffels, W. W. *J. Vac. Sci. Technol. A Vacuum, Surfaces, Film.* **1998**, *16*, 87–95.

(165) Lohmüller, T.; Helgert, M.; Sundermann, M.; Brunner, R.; Spatz, J. P. *Nano Lett.*

2008, *8*, 1429–1433.

(166) Hsu, C.-H.; Lo, H.-C.; Chen, C.-F.; Wu, C. T.; Hwang, J.-S.; Das, D.; Tsai, J.; Chen, L.-C.; Chen, K.-H. *Nano Lett.* **2004**, *4*, 471–475.

(167) Blossey, R. *Nat. Mater.* **2003**, *2*, 301–306.

(168) Quirynen, M.; Bollen, C. M. *J. Clin. Periodontol.* **1995**, *22*, 1–14.

(169) Gao, L.; McCarthy, T. J. *Langmuir* **2006**, *22*, 6234–6237.

(170) Absolom, D. R.; Lamberti, F. V.; Policova, Z.; Zingg, W.; van Oss, C. J.; Neumann, A. W. *Appl. Environ. Microbiol.* **1983**, *46*, 90–97.

(171) Ma, M.; Hill, R. M. *Curr. Opin. Colloid Interface Sci.* **2006**, *11*, 193–202.

(172) Lecuyer, S.; Rusconi, R.; Shen, Y.; Forsyth, A.; Vlamakis, H.; Kolter, R.; Stone, H. A. *Biophys. J.* **2011**, *100*, 341–350.

(173) Rijnaarts, H. H.; Norde, W.; Bouwer, E. J.; Lyklema, J.; Zehnder, A. J. *Appl. Environ. Microbiol.* **1993**, *59*, 3255–3265.

(174) Mannoor, M. S.; Zhang, S.; Link, A. J.; McAlpine, M. C. *Proc. Natl. Acad. Sci.* **2010**, *107*, 19207–19212.

(175) Emerson, R. J.; Camesano, T. A. *Appl. Environ. Microbiol.* **2004**, *70*, 6012–6022.

(176) Thomas, W. E.; Trintchina, E.; Forero, M.; Vogel, V.; Sokurenko, E. V. *Cell* **2002**, *109*, 913–923.

(177) Lüdecke, C.; Jandt, K. D.; Siegismund, D.; Kujau, M. J.; Zang, E.; Rettenmayr, M.; Bossert, J.; Roth, M. *PLoS One* **2014**, *9*, e84837.

(178) Mohamed, N.; Rainier, T. R.; Ross, J. M. *Biotechnol. Bioeng.* **2000**, *68*, 628–636.

(179) Busscher, H. J.; Uyen, M. H.; van Pelt, A. W.; Weerkamp, A. H.; Arends, J. *Appl.*

Environ. Microbiol. **1986**, *51*, 910–914.

(180) Bhatia, S. N.; Ingber, D. E. *Nat. Biotechnol.* **2014**, *32*, 760–772.

(181) Wong, T.-S.; Kang, S. H.; Tang, S. K. Y.; Smythe, E. J.; Hatton, B. D.; Grinthal, A.; Aizenberg, J. *Nature* **2011**, *477*, 443–447.

(182) Nakajima, A.; Fujishima, A.; Hashimoto, K.; Watanabe, T. *Adv. Mater.* **1999**, *11*, 1365–1368.

(183) Laser, D. J.; Santiago, J. G. *J. Micromech. Microeng.* **2004**, *14*, R35–R64.

(184) Kirk, M. D.; Pires, S. M.; Black, R. E.; Caipo, M.; Crump, J. A.; Devleesschauwer, B.; Döpfer, D.; Fazil, A.; Fischer-Walker, C. L.; Hald, T.; Hall, A. J.; Keddy, K. H.; Lake, R. J.; Lanata, C. F.; Torgerson, P. R.; Havelaar, A. H.; Angulo, F. J. *PLOS Med.* **2015**, *12*, e1001921.

(185) Tauxe, R. V.; Doyle, M. P.; Kuchenmüller, T.; Schlundt, J.; Stein, C. E. *Int. J. Food Microbiol.* **2010**, *139*, S16–S28.

(186) Painter, J. A.; Hoekstra, R. M.; Ayers, T.; Tauxe, R. V.; Braden, C. R.; Angulo, F. J.; Griffin, P. M. *Emerg. Infect. Dis.* **2013**, *19*, 407–415.

(187) Chang, A. S.; Schneider, K. R. *J. Food Sci.* **2012**, *77*, M65–M69.

(188) DeVita, M. D.; Wadhera, R. K.; Theis, M. L.; Ingham, S. C. *J. Foodserv.* **2007**, *18*, 76–79.

(189) Todd, E. C. D.; Greig, J. D.; Bartleson, C. A.; Michaels, B. S. *J. Food Prot.* **2007**, *70*, 2199–2217.

(190) Azlin-Hasim, S.; Cruz-Romero, M. C.; Ghoshal, T.; Morris, M. A.; Cummins, E.; Kerry, J. P. *Innov. Food Sci. Emerg. Technol.* **2015**, *27*, 136–143.

(191) Surowsky, B.; Schlüter, O.; Knorr, D. *Food Eng. Rev.* **2015**, *7*, 82–108.

(192) Zhang, M.; Oh, J. K.; Huang, S.-Y.; Lin, Y.-R.; Liu, Y.; Mannan, M. S.; Cisneros-Zevallos, L.; Akbulut, M. *J. Food Eng.* **2015**, *161*, 8–15.

(193) Lavoine, N.; Givord, C.; Tabary, N.; Desloges, I.; Martel, B.; Bras, J. *Innov. Food Sci. Emerg. Technol.* **2014**, *26*, 330–340.

(194) Sung, S.-Y.; Sin, L. T.; Tee, T.-T.; Bee, S.-T.; Rahmat, A. R. *Innov. Food Sci. Emerg. Technol.* **2014**, *26*, 406–414.

(195) Nguyen, H. D. N.; Yuk, H.-G. *Food Control* **2013**, *29*, 236–240.

(196) Todd, E. C. D.; Michaels, B. S.; Greig, J. D.; Smith, D.; Bartleson, C. A. *J. Food Prot.* **2010**, *73*, 1762–1773.

(197) Green, L. R.; Radke, V.; Mason, R.; Bushnell, L.; Reimann, D. W.; Mack, J. C.; Motsinger, M. D.; Stigger, T.; Selman, C. a. *J. Food Prot.* **2007**, *70*, 661–666.

(198) Corcoran, M.; Morris, D.; De Lappe, N.; O'Connor, J.; Lalor, P.; Dockery, P.; Cormican, M. *Appl. Environ. Microbiol.* **2014**, *80*, 1507–1514.

(199) Kaneko, K.; Hayashidani, H.; Takahashi, K.; Shiraki, Y.; Limawongpranee, S.; Ogawa, M. *J. Food Prot.* **1999**, *62*, 800–804.

(200) Kotwal, G.; Lee, C.-C.; Kang, W.; Cannon, J. In *2014 IAFP Annual Meeting*; 2014.

(201) Brar, P. K.; Danyluk, M. D. *J. Food Prot.* **2013**, *76*, 1342–1349.

(202) Bastarrachea, L. J.; Denis-Rohr, A.; Goddard, J. M. *Annu. Rev. Food Sci. Technol.* **2015**, *6*, 97–118.

(203) Leitgeb, J.; Schuster, R.; Eng, A.-H.; Yee, B.-N.; Teh, Y.-P.; Dosch, V.; Assadian, O. *Antimicrob. Resist. Infect. Control* **2013**, *2*, 27.

(204) Reitzel, R. A.; Dvorak, T. L.; Hachem, R. Y.; Fang, X.; Jiang, Y.; Raad, I. *Am. J. Infect. Control* **2009**, *37*, 294–300.

(205) Barza, M. *Clin. Infect. Dis.* **2004**, *38*, 857–863.

(206) Fadeeva, E.; Truong, V. K.; Stiesch, M.; Chichkov, B. N.; Crawford, R. J.; Wang, J.; Ivanova, E. P. *Langmuir* **2011**, *27*, 3012–3019.

(207) Yang, W. J.; Cai, T.; Neoh, K.-G.; Kang, E.-T.; Dickinson, G. H.; Teo, S. L.-M.; Rittschof, D. *Langmuir* **2011**, *27*, 7065–7076.

(208) Jin, C.; Jiang, Y.; Niu, T.; Huang, J. *J. Mater. Chem.* **2012**, *22*, 12562–12567.

(209) Ding, X.; Yang, C.; Lim, T. P.; Hsu, L. Y.; Engler, A. C.; Hedrick, J. L.; Yang, Y. Y. *Biomaterials* **2012**, *33*, 6593–6603.

(210) Park, K. D.; Kim, Y. S.; Han, D. K.; Kim, Y. H.; Lee, E. H. B.; Suh, H.; Choi, K. S. *Biomaterials* **1998**, *19*, 851–859.

(211) Pettersson, A.; Ohlsson, T.; Davis, S.; Gray, J. O.; Dodd, T. J. *Innov. Food Sci. Emerg. Technol.* **2011**, *12*, 344–351.

(212) Vansant, E. F.; Voort, P. Van Der; Vrancken, K. C. In *Studies in Surface Science and Catalysis*; **1995**; Vol. 93, pp. 3–30.

(213) Hare, E. F.; Shafrin, E. G.; Zisman, W. A. *J. Phys. Chem.* **1954**, *58*, 236–239.

(214) Zeitler, V. A.; Brown, C. A. *J. Phys. Chem.* **1957**, *61*, 1174–1177.

(215) Lorenzetti, M.; Dogša, I.; Stošicki, T.; Stopar, D.; Kalin, M.; Kobe, S.; Novak, S. *ACS Appl. Mater. Interfaces* **2015**, *7*, 1644–1651.

(216) Fürstner, R.; Barthlott, W.; Neinhuis, C.; Walzel, P. *Langmuir* **2005**, *21*, 956–961.

(217) Crick, C. R.; Ismail, S.; Pratten, J.; Parkin, I. P. *Thin Solid Films* **2011**, *519*, 3722–

3727.

(218) Neu, T. R. *Microbiol. Rev.* **1996**, *60*, 151–166.

(219) van Loosdrecht, M. C.; Lyklema, J.; Norde, W.; Schraa, G.; Zehnder, A. J. *Appl. Environ. Microbiol.* **1987**, *53*, 1893–1897.

(220) Roosjen, A.; Busscher, H. J.; Norde, W.; van der Mei, H. C. *Microbiology* **2006**, *152*, 2673–2682.

(221) Liu, P. Y.; Chin, L. K.; Ser, W.; Ayi, T. C.; Yap, P. H.; Bourouina, T.; Leprince-Wang, Y. *Procedia Eng.* **2014**, *87*, 356–359.

(222) Sanchis, A.; Brown, A. P.; Sancho, M.; Martínez, G.; Sebastián, J. L.; Muñoz, S.; Miranda, J. M. *Bioelectromagnetics* **2007**, *28*, 393–401.

(223) Hiemenz, Paul C. Rajagopalan, R. *Principles of colloid and surface chemistry*; 3rd ed.; CRC Press, **1997**.

(224) Born, M.; Wolf, E. *Principles of optics: Electromagnetic theory of propagation, interference and diffraction of light*; 7th ed.; Cambridge University Press, **1999**.

(225) Boling, N.; Glass, A.; Owyoung, A. *IEEE J. Quantum Electron.* **1978**, *14*, 601–608.

(226) Kim, J.-M.; Lee, Y. B.; Chae, S. K.; Ahn, D. J. *Adv. Funct. Mater.* **2006**, *16*, 2103–2109.

(227) Uchiyama, T.; Okuyama, K. *Phytochemistry* **1990**, *29*, 91–92.

APPENDIX A

SUPPLEMENTAL INFORMATION FOR CHAPTER III

A1. Preparation of Thermochromic Films

The first step of preparing such a film was to dissolve 10, 12-pentacosadiynoic acid (PCDA; TCI America, Portland, OR, USA) in chloroform ($CHCl_3$; Sigma-Aldrich Co., St. Louis, MO, USA) to prepare polydiacetylene (PDA) vesicles. After removing organic solvent (chloroform) by N_2 gas purging, DI water was added to make the final concentration 1 mM. Then, PDA was embedded in a polyvinyl alcohol (PVA, M_w=89,000–98,000 g/mol; Sigma-Aldrich Co., St. Louis, MO, USA) film by mixing PDA solution to 10 wt% PVA solution. Sequentially, the mixed solution was poured into a mold and left to dry at room temperature (23 °C) for 3 days before peeling off from the mold.

A2. Preparation, Inoculation, and Enumeration of S. Typhimurium 14028s

Salmonella enterica subsp. *enterica* serovar Typhimurium (ATCC 14028; American Type Culture Collection, Manassas, VA, USA) were obtained from the Department of Chemical Engineering Laboratory Culture Collection at Texas A&M University (College Station, TX, USA). In order to utilize fluorescent microscope for visualization of the microorganisms on the various surfaces, *S*. Typhimurium 14028s was transformed with a green fluorescent protein (GFP) expressing plasmid pCM18.[37] Working cultures of *S*. Typhimurium 14028s were obtained by transferring an isolate from a Luria-Bertani (LB) + 0.2% (w/v) glucose agar plate to 9.0 mL of TSB containing 30 µg/mL erythromycin to maintain pCM18 in culture. The cultures were incubated

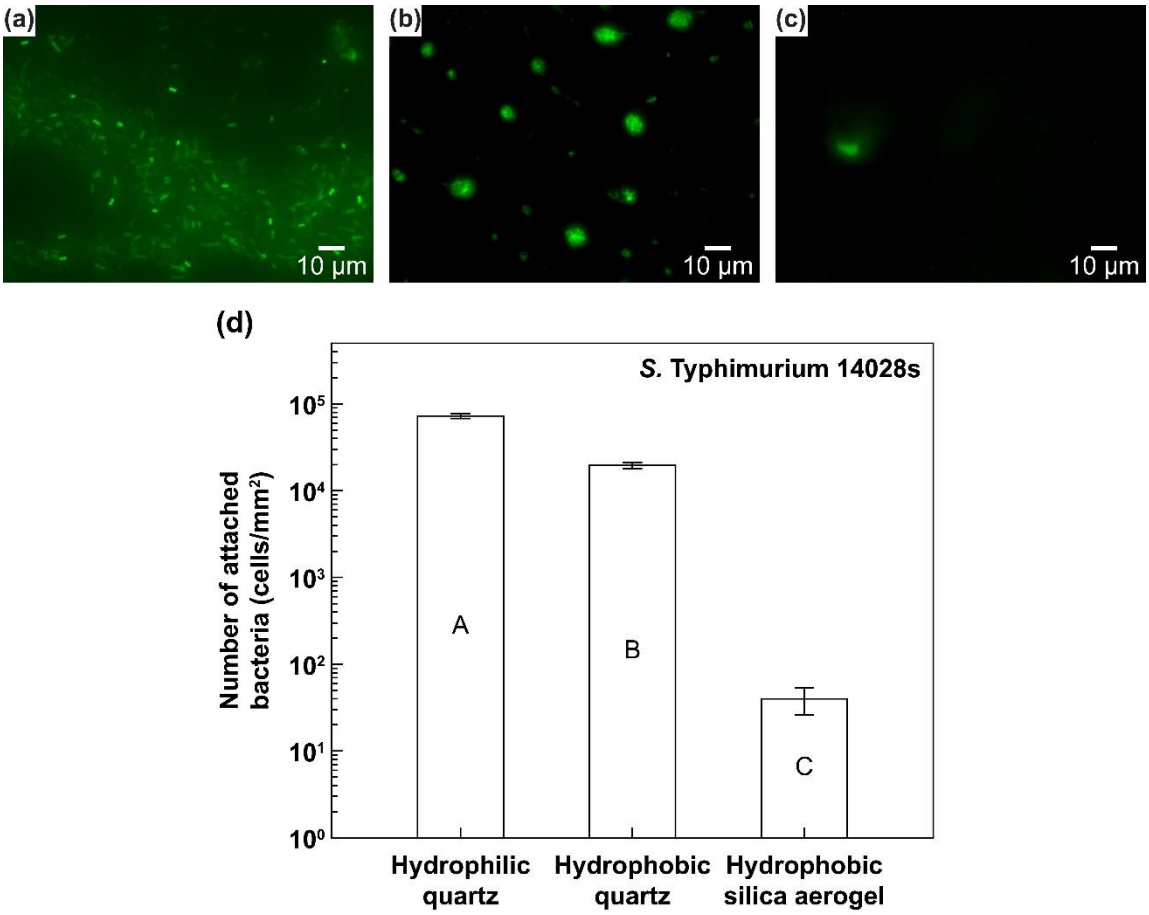

Figure 36. Fluorescent microscope micrographs of (a) hydrophilic quartz, (b) hydrophobic quartz, and (c) hydrophobic silica aerogel after inoculated by *S.* Typhimurium 14028s. (d) The number of bacteria per unit area (mm^2) remaining on surfaces (a logarithmic scale is chosen for the y-axis). The bacterial adhesion is statistically different between each surface ($p < 0.05$). Different letters indicate statistically significant difference.

aerobically without agitation at 37 °C for 24 h. After 24 h, a loopful of culture was transferred to fresh TSB containing 30 µg/mL erythromycin, and incubated aerobically for 24 h at 37 °C twice consecutively. First, pre-sterilized quartz, hydrophobic quartz, and hydrophobic silica aerogel substratum were immersed in 9.0 mL bacterial suspensions (8.2–8.8 1og CFU/mL) prepared as previously described for 4 h at room temperature

(23 °C). After 4 h, the substratum was gently removed from the bacterial suspension in a single vertical motion, and held vertically for five minutes to eliminate the remaining droplet so that drying effects were not superimposed on the adhesion effects. Finally, nitrogen (N_2) gas was gently blown on the substratum to further remove the thin liquid film. The treated surfaces were then isolated for counting attached bacterial cells. Fluorescent *S*. Typhimurium 14028s cell was determined by using an Axiovert 200M (Carl Zeiss, Thornwood, NY, USA) inverted fluorescent microscope. Micrographs obtained with fluorescent microscope were analyzed with Photoshop 6.0 (Adobe Systems Inc., San Jose, CA, USA) software to obtain fluorescent bacterial (*S.* Typhimurium 14028s) area coverage on each surface.

A3. Intermolecular Interactions between Silica Aerogel and Bacteria

Because tail groups of TMCS are methyl groups, acid-base, hydrogen-bond, and specific ligand-receptor types of interactions between TMCS and bacteria are non-existing. Therefore, van der Waals interactions are expected to primarily govern the thermodynamics of bacterial adhesion to TMCS-functionalized quartz and TMCS-functionalized silica aerogel surfaces. As a first approximation, van der Waals interaction energy between a bacteria and a surface can be approximated as an interaction between a sphere and flat surface, which is given as:

Equation 1.

$$E_{\mathrm{vdW}} = -\frac{A_{\mathrm{H}}}{6}\left[\frac{R}{d} + \frac{R}{2R+d} + ln\left(\frac{d}{2R+d}\right)\right]$$

where A_H is the Hamaker constant, R is radius of sphere (bacteria), and d is separation between bacteria and surface.[220] The Hamaker constant will be negative when the dielectric constant, ε, and refractive index, n, of the intervening medium is in between those of the substrate and adsorbate (e.g., particle and bacteria).[36] When the intervening medium is water, for which $\varepsilon_{water} = 80$ and $n_{water} = 1.33$, and the adsorbate is bacteria, for which $\varepsilon_{bacteria} = 60$ and $n_{bacteria} = 1.39$,[221,222] there is a repulsive van der Waals interactions between a surface and a bacteria as long as the refractive index and dielectric constant of the substrate is smaller than those of water. The index of refraction for nonporous silica materials is about 1.45–1.55 depending on the crystallinity and density. Therefore, the van der Waals interaction between nonporous silica and bacteria across water is attractive.[223] However, according to the Clausius-Mossotti equation, one obtains the effective index of refraction by averaging over the solid phase and the void phase.[224,225] Therefore, due to their highly porous nature, silica aerogel can have much lower refractive index and dielectric constants than water.[100] Thus, the dispersion interactions between bacteria and silica aerogel are repulsive assuming that water does not fill the pores of the hydrophobic silica aerogel. To check this assumption, we conducted ellipsometry experiments to measure the index of refraction of TMCS-functionalized silica aerogel under dry and wet conditions. These measurements showed that the index of refraction was 1.008 ± 0.001 under dry conditions while it was 1.013 ± 0.001 after immersing in bacterial suspension for 4 h. Here, it is important to mention that if the porosity of materials were large and allowed water to fill the pores, then the effective index of refraction for porous substrate would be larger than 1.33, leading to attractive van der Waals interactions and the

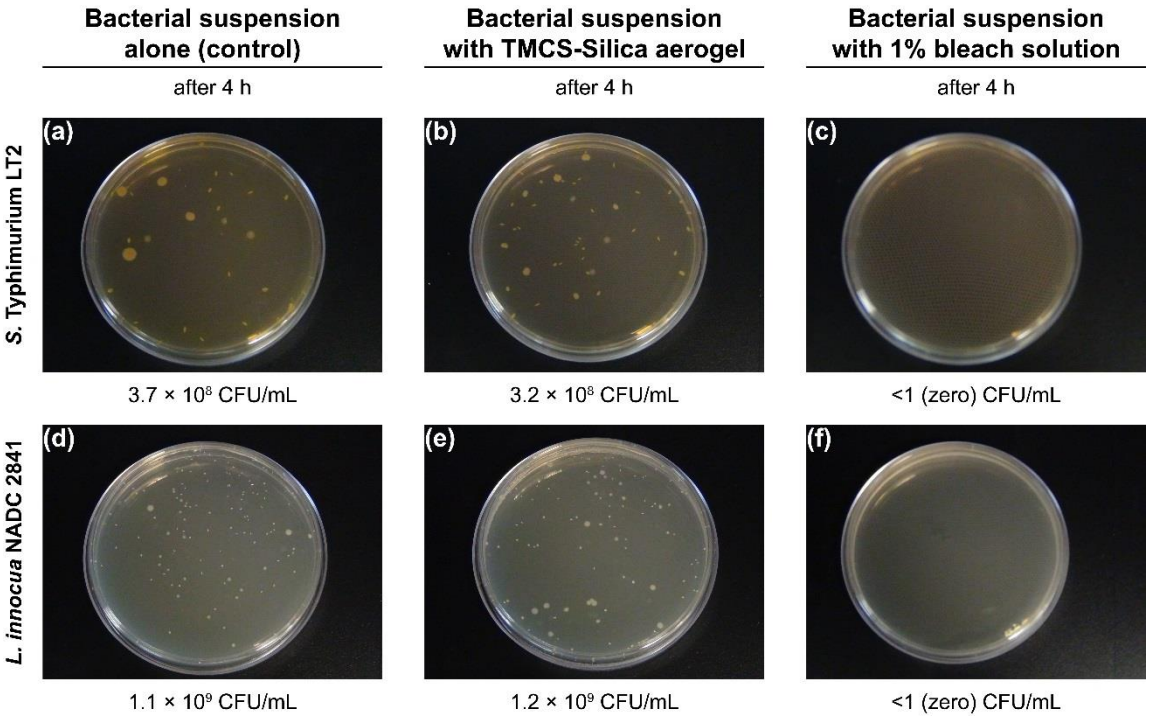

Figure 37. Comparison of bacterial (*S.* Typhimurium LT2 and *L. innocua* NADC 2841) proliferation behavior (a), (d) in the absence and (b), (e) in the presence of TMCS-Silica aerogel sample, and (c), (f) in the presence of 1% bleach solution. Significant reduction was only observed for 1% bleach solution.

promotion/facilitation of bacterial adhesion. Therefore, porosity is not often desired in food-contact surfaces. However, we showed that this is not true for materials with ultra-small, hydrophobic pores where water molecules cannot fill them.

APPENDIX B

SUPPLEMENTAL INFORMATION FOR CHAPTER IV

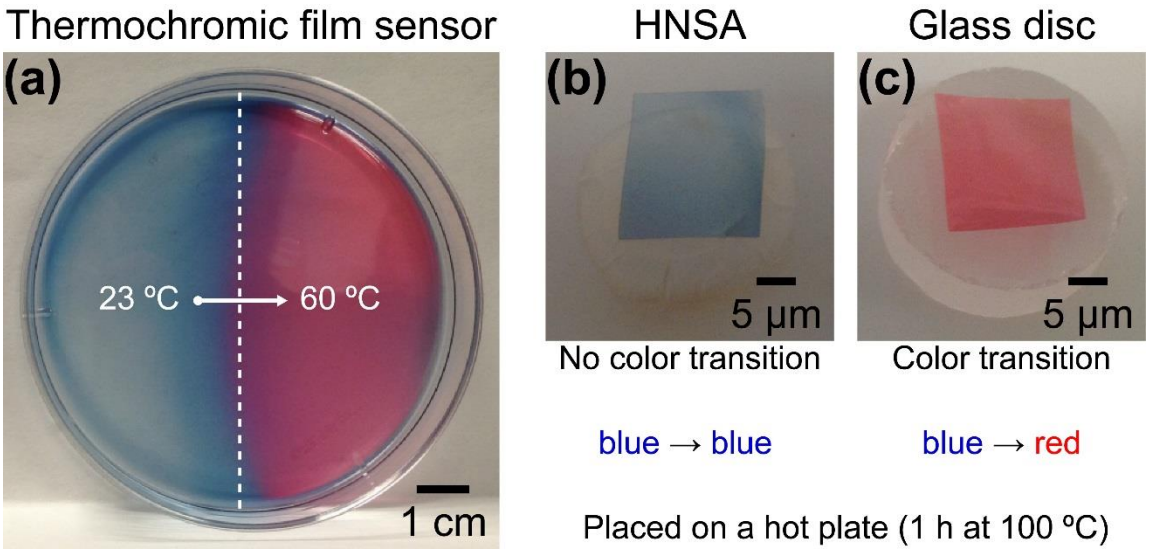

Figure 38. (a) A photograph showing the color transition of thermochromic film upon heating. Comparison of the thermal insulation properties of (b) HNSA and (c) glass disc were carried out by placing samples of the same thickness on a hot plate for 1 h at 100 °C. There was no color change in thermochromic film residing on HNSA surfaces while there was color change in thermochromic film residing on glass disc surfaces.

B1. Thermal Properties of Materials

A thermochromic film was used to compare the thermal insulation properties of the samples prepared (Figure 38). The thermochromic films were fabricated by dissolving 10, 12-pentacosadiynoic acid (PCDA; TCI America, Portland, OR, USA) in chloroform ($CHCl_3$; Sigma-Aldrich Co., St. Louis, MO, USA) to prepare polydiacetylene (PDA) vesicles.[226] After removing chloroform solvent by nitrogen gas purging, deionized (DI) water was added to make the final concentration of 1 mM. Subsequently, PDA was embedded in a poly(vinyl alcohol) (PVA, M_w = 89,000–98,000 g/mol; Sigma-Aldrich Co.,

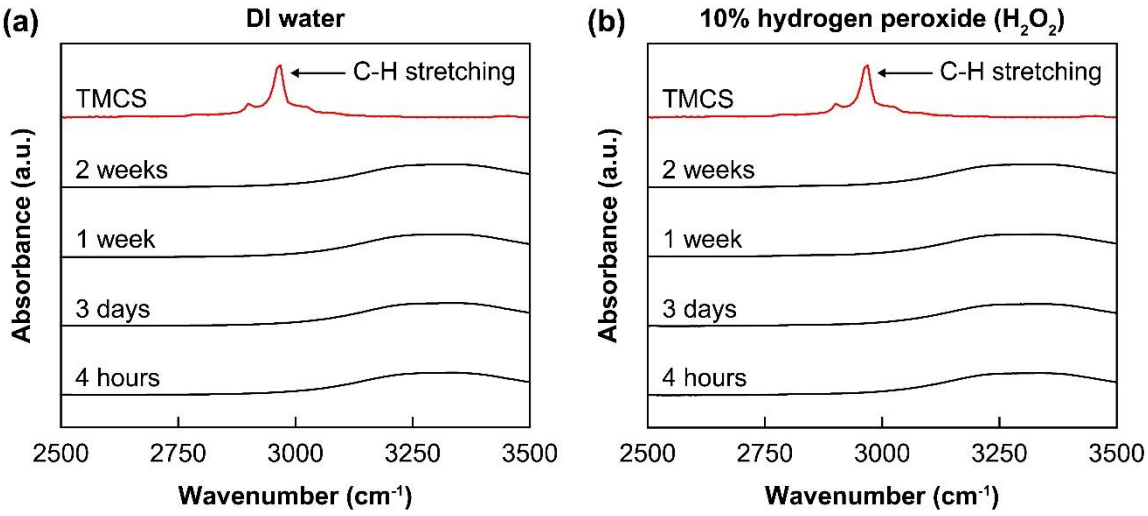

Figure 39. ATR-FTIR spectra of HNSA submerged in (a) DI water and (b) 10% hydrogen peroxide (H_2O_2). The data revealed that solutions containing HNSA has no chemical leaching within 2 weeks duration (detection limit of <1 ppm).

St. Louis, MO, USA) film by mixing PDA solution to 10wt% PVA solution. The PDA/PVA solution was poured into a mold and left to dry at room temperature (23 °C) for 3 days before peeling. The resultant thermochromic film changed its color from blue to red at temperatures 50 °C or above.

In addition, specific heat (C_p) value of sample (10 mg) was measured by differential scanning calorimetry (DSC, Q20; TA Instruments, New Castle, DE, USA) at heating rate of 10 °C/min to calculate thermal conductivity.

B2. Chemical Stability

To evaluate chemical stability of hydrophobic nanoporous silica aerogel (HNSA), samples were submerged in DI water and 10% hydrogen peroxide (H_2O_2, 30% solution; Avantor Performance Materials, Inc., Center Valley, PA, USA), a commonly used sanitizer in healthcare industry. Aliquots were collected from solutions at time points of 4

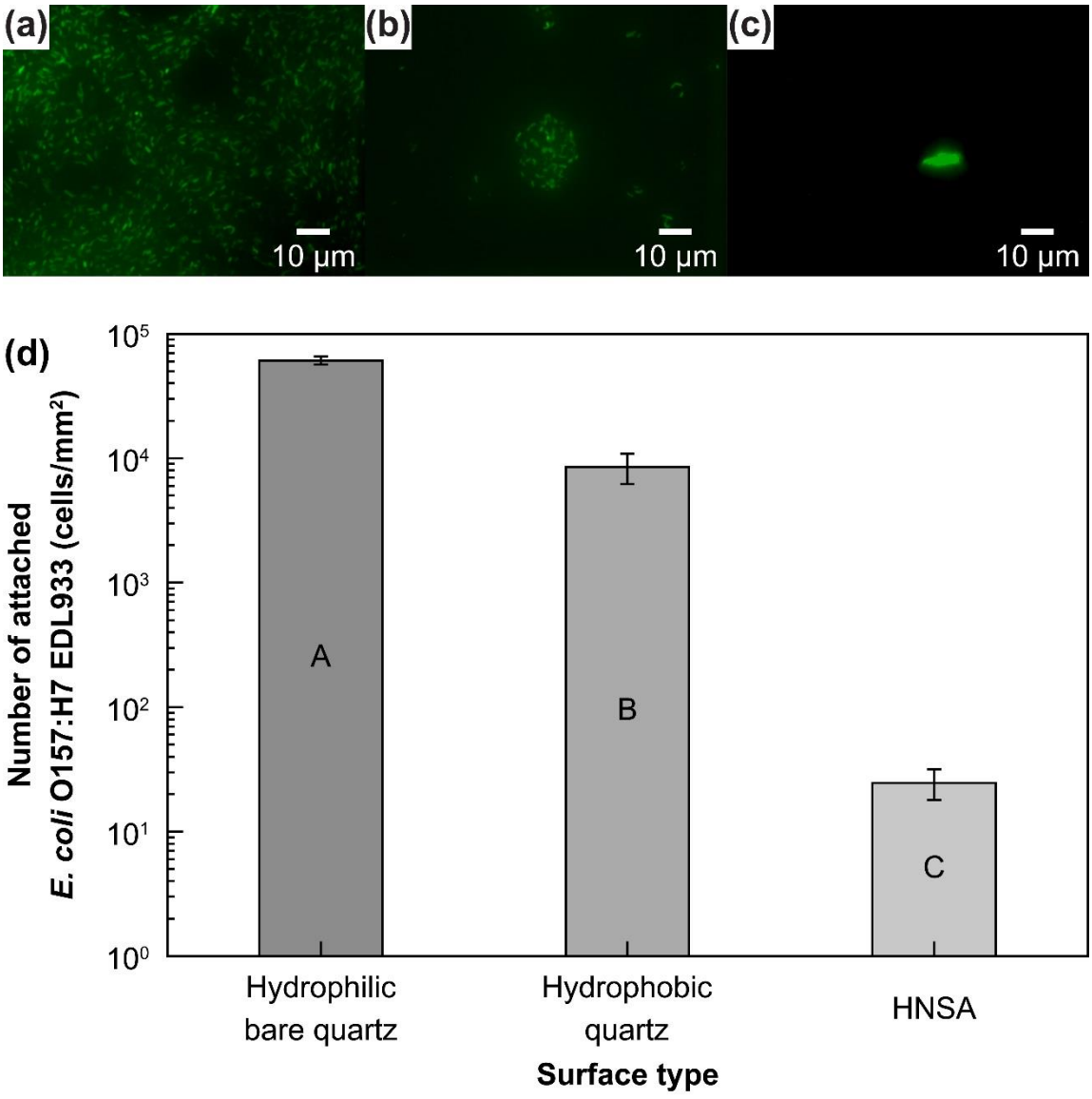

Figure 40. Fluorescent microscope micrographs of (a) hydrophilic bare quartz, (b) hydrophobic quartz, and (c) HNSA after inoculation with Gram-negative *E. coli* O157:H7 EDL933. (d) The average number of bacteria per unit area (mm^2) on different surfaces (y-axis has a logarithmic scale). Different letters (i.e., A, B, and C) indicate statistically significant difference ($p < 0.05$).

h, 3 days, 1 week, and 2 weeks to determine chemical leaching using ATR-FTIR spectroscopy.

B3. Preparation, Inoculation, and Enumeration of E. coli O157:H7 EDL933

To express green fluorescent, enterohemorrhagic *Escherichia coli* O157:H7 str. EDL933 (ATCC 43895) was transformed with a green fluorescent protein (GFP) expressing plasmid pCM18.[37] Working culture of *E. coli* O157:H7 EDL933 was obtained by transferring a loopful of culture from a Luria-Bertani (LB) agar plate (0.2% (w/v) glucose) to 9 mL of TSB containing 30 µg/mL erythromycin. The culture was incubated for 24 h at 37 °C. After 24 h, a loopful of culture was transferred twice to fresh TSB containing erythromycin every 24 h and reincubated at 37 °C.

For inoculation, hydrophilic bare quartz, hydrophobic quartz, and HNSA were submerged in 9 mL bacterial suspension (8.7 ± 0.1 1og CFU/mL) for 4 h at room temperature. The samples were gently removed from the bacterial suspensions in a single vertical motion after inoculation.

Fluorescent *E. coli* O157:H7 EDL933 was determined by using an Axiovert 200M (Carl Zeiss, Thornwood, NY, USA) inverted fluorescent microscope. Micrographs obtained with fluorescent microscope were analyzed with ImageJ (National Institutes of Health (NIH), Bethesda, MD, USA) software.

APPENDIX C

SUPPLEMENTAL INFORMATION FOR CHAPTER V

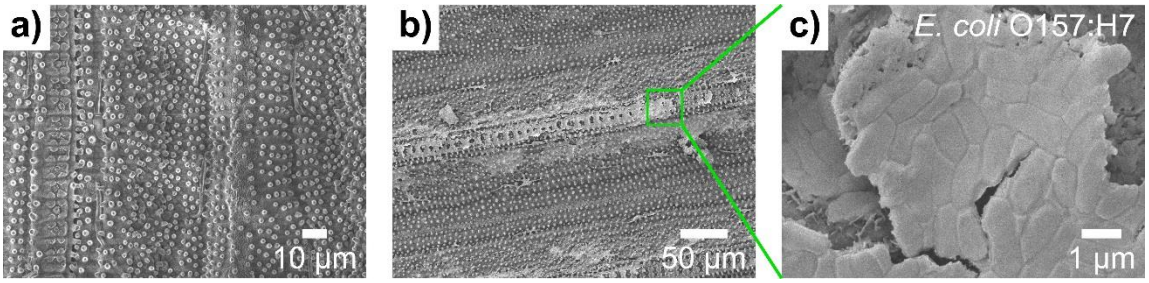

Figure 41. (a) SEM micrograph of *Oryza sativa* rice leaf surfaces. (b) SEM micrograph of rice leaf surfaces after inoculated in *E. coli* O157:H7 suspension for 4 h at room temperature (23 ºC). White regions indicate attached bacteria on rice leaf surfaces. (c) Detail view of *E. coli* O157:H7 biofilm formation on clover-shaped features of rice leaf surface.

C1. Photochemistry of Rice Leaf

Surface chemistry is an important factor to consider in the context of bacterial adhesion. Given the hydrophobic nature of leaf surfaces and the localization of the hollow structures on the leaves, these structures are leaf wax. Uchiyama and Okuyama[227] reported that rice leaf wax consists mainly of primary alcohols (20.4%), wax esters (27.8%), aldehydes (30.8%), and hydrocarbons (6.2%). However, in light of our overall conclusion that it is possible to prevent bacterial attachment by just mimicking the surface texture rather than the exact chemistry, we believe that wax chemistry plays a secondary role on the observed trends in this particular study.

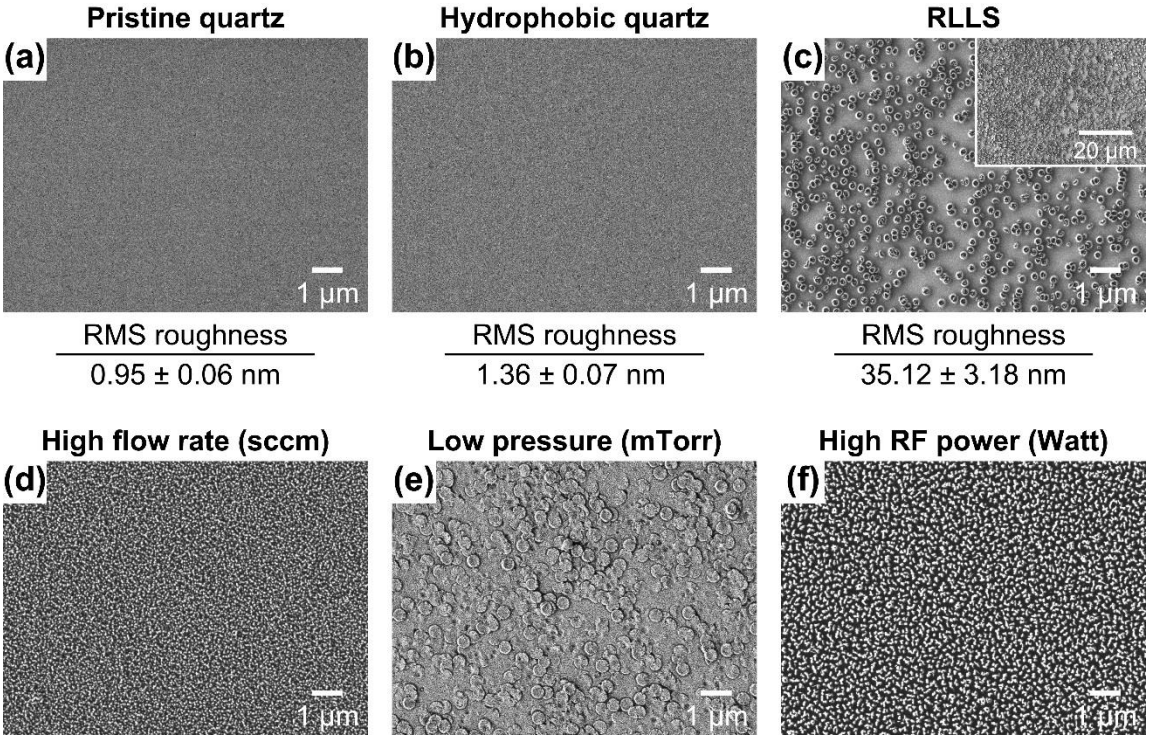

Figure 42. (a)–(c) SEM micrographs showing surface morphology of pristine quartz, hydrophobic quartz, and RLLS. SEM micrographs of results from different self-masking reactive-ion etching (SM-RIE) process conditions, (d) high oxygen (O_2) flow rate (5.0 sccm), (e) low pressure (100 mTorr), and (f) high radio frequency (RF) power (300 Watt), respectively.

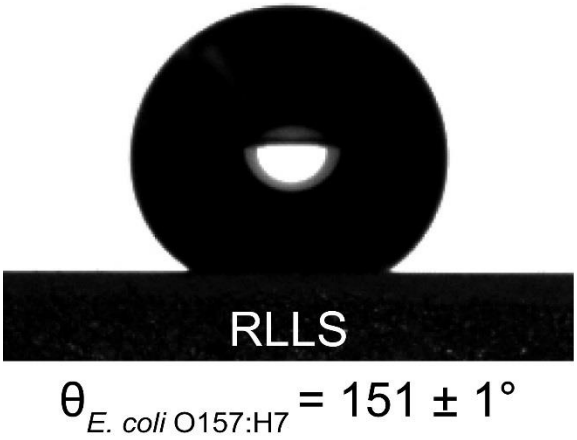

Figure 43. Contact angle measurement of *E. coli* O157:H7 suspension droplet (5 µL) on RLLS surfaces.

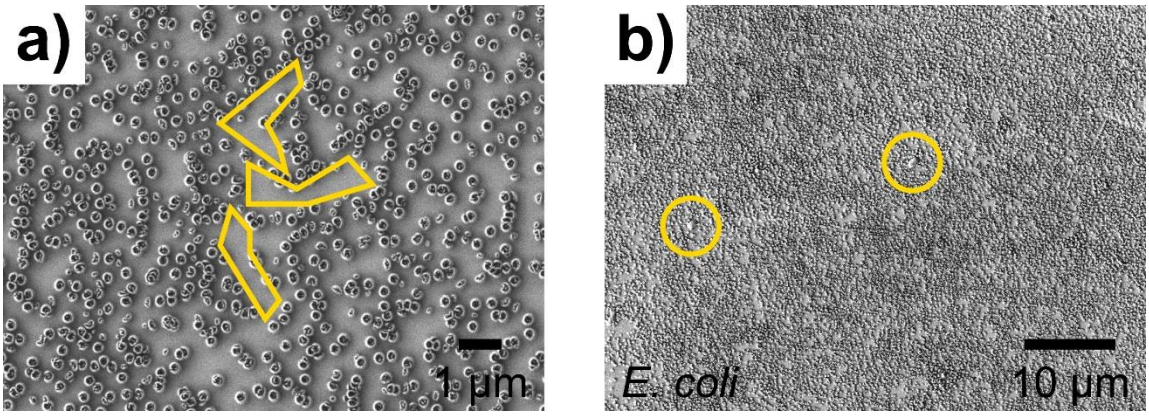

Figure 44. (a) The highlight of unpatterned regions (defects) arising during the preparation of RLLS and (b) the preferential attachment of bacteria on these regions.

Table 3. Comparison of the bacterial adhesion behavior on pristine quartz, methylated quartz, and RLLS surfaces for *E. coli* O157:H7 and *S. aureus* as a function of time.

	Pristine quartz		**Methylated quartz**		**RLLS**	
	E. coli O157:H7	*S. aureus*	*E. coli* O157:H7	*S. aureus*	*E. coli* O157:H7	*S. aureus*
10 min	17 ± 3	21 ± 3	3 ± 1	9 ± 4	1 ± 1	2 ± 1
20 min	35 ± 5	43 ± 3	10 ± 4	14 ± 2	1 ± 1	2 ± 2
40 min	53 ± 2	66 ± 5	15 ± 2	21 ± 5	1 ± 1	3 ± 2
60 min	97 ± 12	110 ± 9	21 ± 3	36 ± 4	1 ± 1	3 ± 2

Number of attached bacteria were expressed per unit area (25 μm × 25 μm)

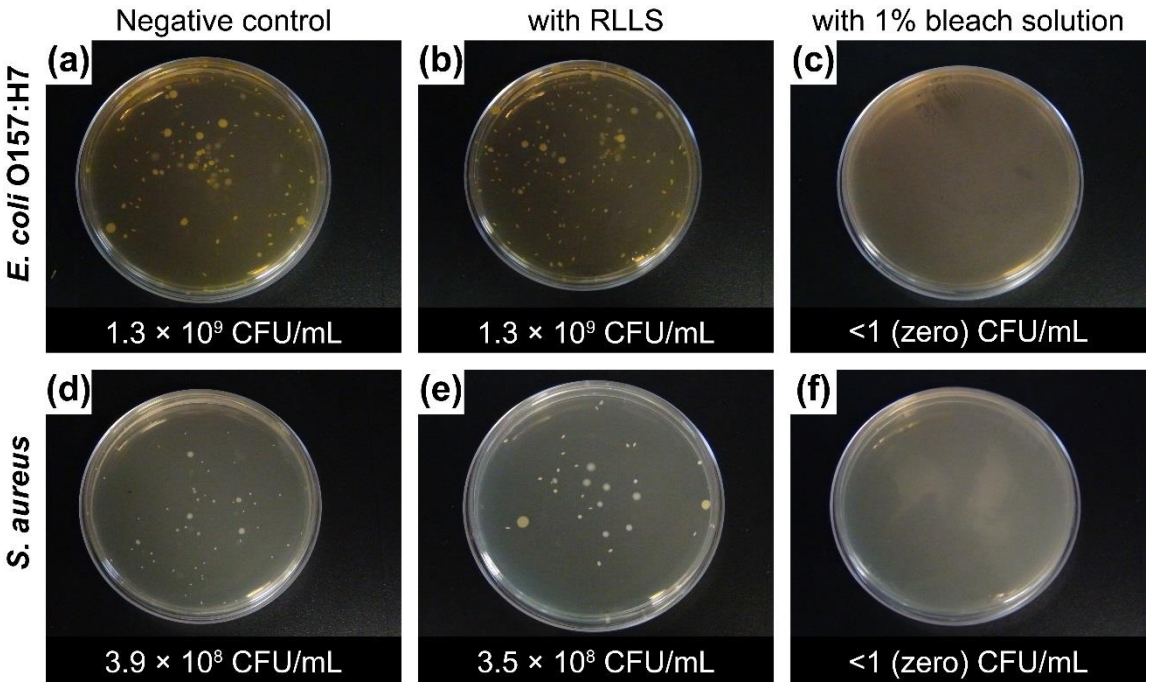

Figure 45. Comparison of (a)–(c) *E. coli* O157:H7 and (d)–(f) *S. aureus* growth in the absence of treatment or in the presence of RLLS and 1% bleach solution after 4 h cultured period by pour plating method. Only results from 1% bleach solution were statistically significant ($p < 0.05$).

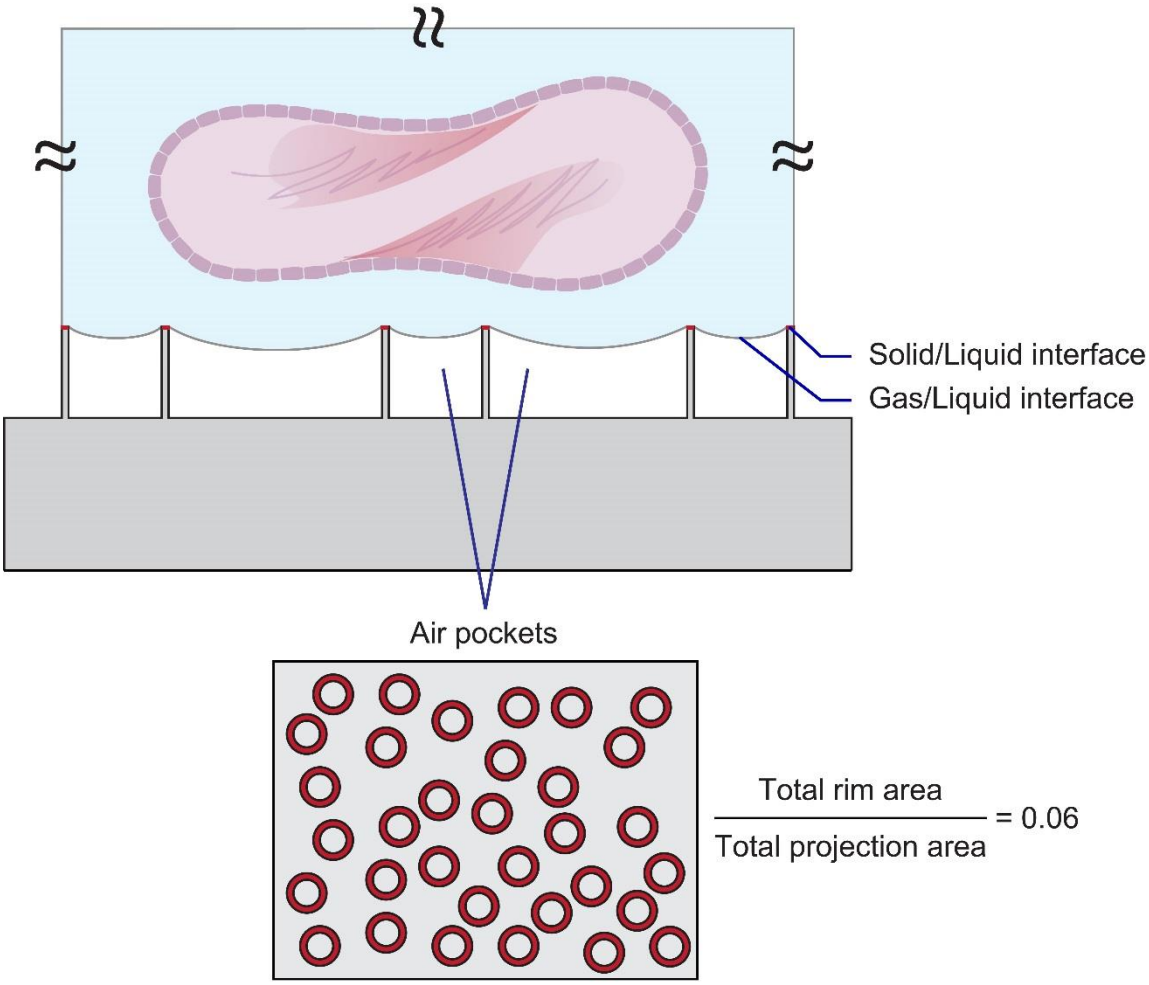

Figure 46. A schematic illustration of two key factors presumably responsible for desirable antiadhesion characteristics of RLLS.

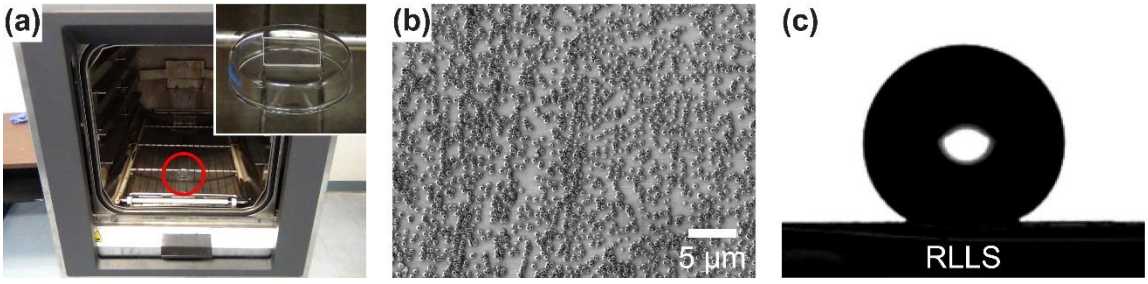

Figure 47. (a) RLLS (red circle) was tested under autoclave conditions (at 121 ºC and 20 psi for 20 min). Inset: photograph of RLLS placed inside chamber. (b) SEM micrograph of RLLS after autoclave treatment. No damage occurred on surfaces. (c) Contact angle measurement of water droplet (5 µL) on autoclaved RLLS surfaces showing that stable superhydrophobicity ($\theta > 150°$).

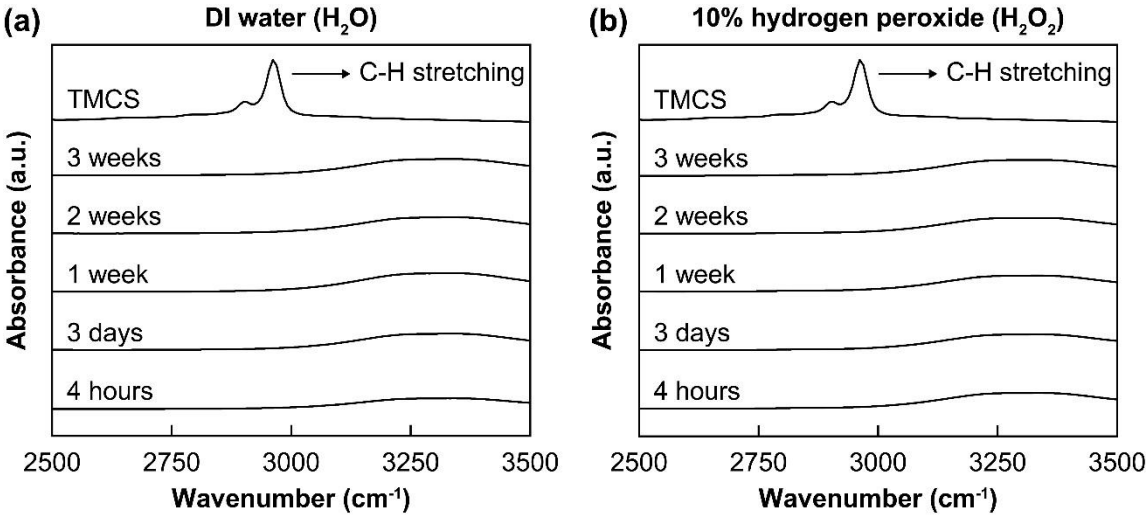

Figure 48. Chemical stability of RLLS immersed in (a) DI water (H_2O) and (b) 10% hydrogen peroxide (H_2O_2) were confirmed using ATR-FTIR spectroscopy. Samples do not have C–H stretching region (in detection limit of 1 ppm), which represents no unbound TMCS chemical from RLLS surfaces.

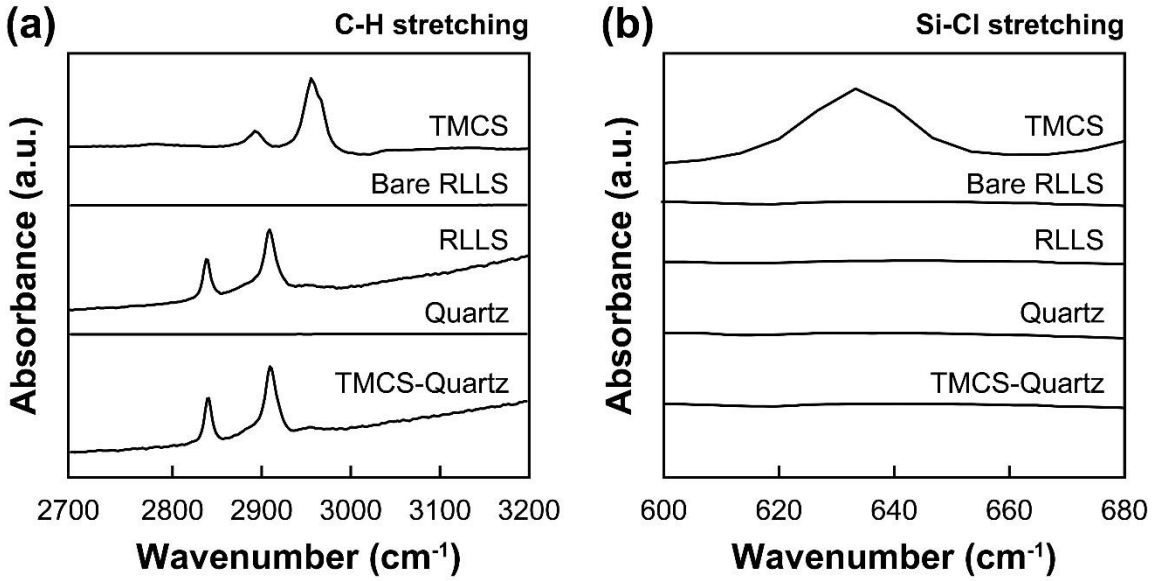

Figure 49. Successfully methyl (CH_3) functionalized RLLS and quartz surfaces were characterized by ATR-FTIR spectroscopy. (a) The presence of peaks are attributed to combination of symmetric and asymmetric C–H stretching from methyl groups formed upon the reaction of TMCS with silica surfaces. Peak shifts in C–H stretching region are due to the substitution of chlorine (Cl) atoms by oxygen (O) atoms during methylation reaction and because of the transformation from the liquid state to the crystalline state.[89] (b) Si–Cl stretching vibration region around ~620 cm^{-1} only existed for TMCS, provides evidence for the methylation reaction.[90]

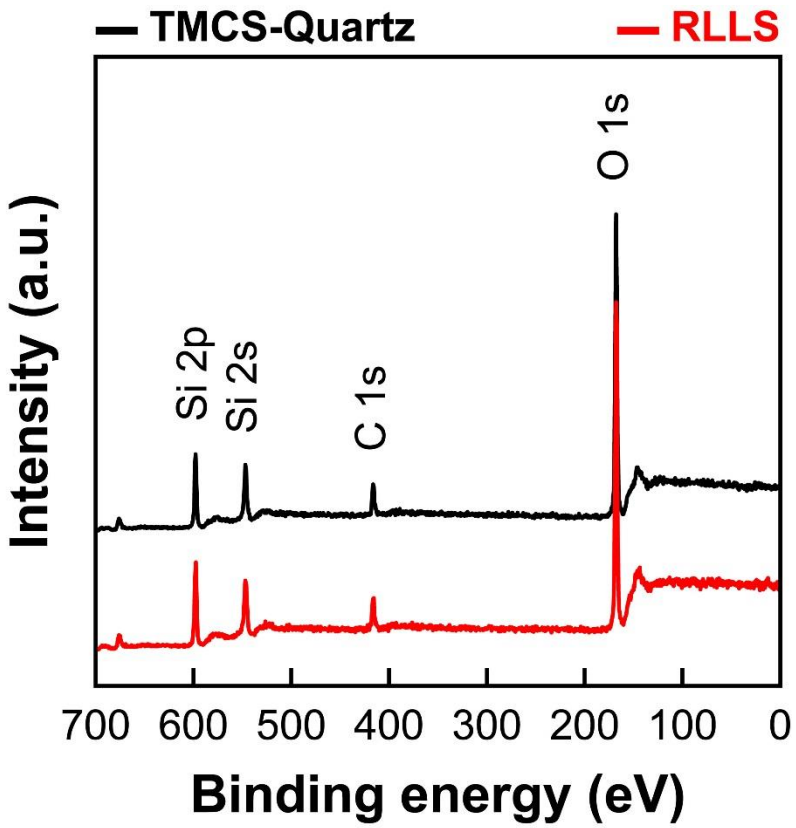

Figure 50. XPS spectra show that the atomic percentages for C, O, and Si were ~19%, 24%, and 57%, respectively, for hydrophobic quartz. While the atomic percentages for C, O, and Si were ~15%, 26%, and 59%, respectively, for RLLS. Therefore, these findings suggest that the degree of methylation for quartz and RLLS were very similar.